

Thesis presented to the Instituto Tecnológico de Aeronáutica, in partial fulfillment of the requirements for the degree of Doctor of Science in the Graduate Program of Physics, Field of Nuclear Physics.

Emanuel Vicente Chimanski

**EXTENSION OF THE QUANTUM FORMALISM
FOR MULTISTEP DIRECT NUCLEAR
REACTIONS**

Thesis approved in its final version by signatories below:

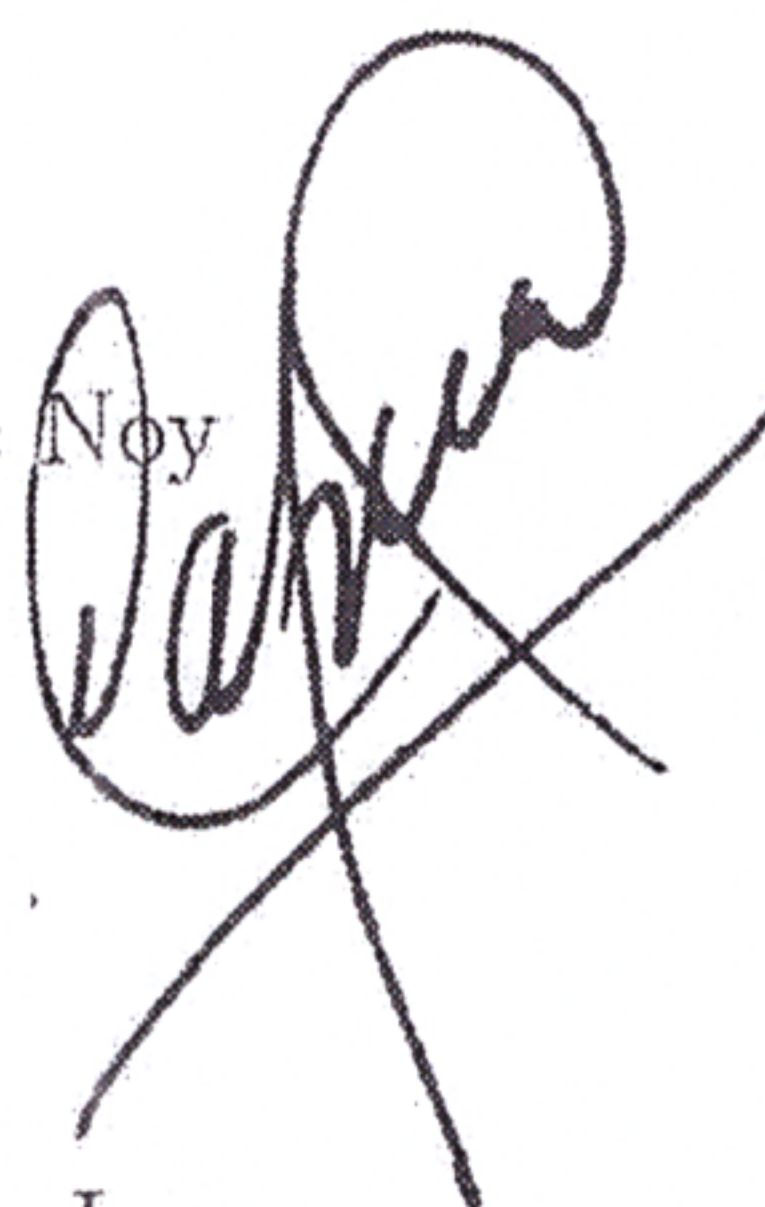


Prof. Dr. Brett Vern Carlson

Advisor

Dr. Roberto Capote Noy

Co-advisor



Prof. Dr. Pedro Teixeira Lacava

Dean for Graduate Education

Campo Montenegro
São José dos Campos, SP - Brazil
2019

Cataloging-in Publication Data
Documentation and Information Division

Chimanski, Emanuel Vicente

Extension of the Quantum Formalism for Multistep Direct Nuclear Reactions / Emanuel Vicente Chimanski.

São José dos Campos, 2019.

116f.

Thesis of Doctor of Science – Course of Physics. Area of Nuclear Physics – Instituto Tecnológico de Aeronáutica, 2019. Advisor: Prof. Dr. Brett Vern Carlson. Co-advisor: Dr. Roberto Capote Noy.

1. Reações nucleares. 2. Equilibrio. 3. Modelos nucleares. 4. Física nuclear. 5. Física. I. Instituto Tecnológico de Aeronáutica. II. Title.

BIBLIOGRAPHIC REFERENCE

CHIMANSKI, Emanuel Vicente. **Extension of the Quantum Formalism for Multistep Direct Nuclear Reactions**. 2019. 116f. Thesis of Doctor of Science – Instituto Tecnológico de Aeronáutica, São José dos Campos.

CESSION OF RIGHTS

AUTHOR'S NAME: Emanuel Vicente Chimanski

PUBLICATION TITLE: Extension of the Quantum Formalism for Multistep Direct Nuclear Reactions.

PUBLICATION KIND/YEAR: Thesis / 2019

It is granted to Instituto Tecnológico de Aeronáutica permission to reproduce copies of this thesis and to only loan or to sell copies for academic and scientific purposes. The author reserves other publication rights and no part of this thesis can be reproduced without the authorization of the author.

Emanuel Vicente Chimanski
Av. Dr. Nelson D'Avila, 1178
12.245-031 – São José dos Campos–SP

EXTENSION OF THE QUANTUM FORMALISM FOR MULTISTEP DIRECT NUCLEAR REACTIONS

Emanuel Vicente Chimanski

Thesis Committee Composition:

Prof. Dr.	Manuel Malheiro	Chairperson	-	ITA
Prof. Dr.	Brett Vern Carlson	Advisor	-	ITA
	Dr. Roberto Capote Noy	Co-advisor	-	IAEA
Prof. Dr.	Tobias Frederico	Committee Member	-	ITA
Prof. Dr.	Luiz Carlos Chamon	Committee Member	-	USP
Prof. Dr.	Leandro Gasques	Committee Member	-	USP
	Dr. Marc Dupuis	Committee Member	-	CEA

ITA

To my family.

Acknowledgments

My greatest and foremost gratitude to my advisor Professor Brett Vern Carlson for considerately mentoring me and guiding me in every step of this research. His vast and enviable knowledge of physics, math, computing, science, and infinite patience were critical to make this work possible. He was not only interested in helping me succeed in graduate school but also always willing to encourage my own interests. I feel a very privileged person for the opportunity to have Brett as my mentor. I have learned much more than physics with him.

I'm also very grateful to my co-advisor Roberto Capote for being patient and attentive and receiving me so well during my one year internship in the NAPC- Nuclear Data Section of the Atomic Energy Agency (IAEA) in Vienna - Austria. This was a life-change experience both professionally and personally.

To all my friends, and I am proud to have made many of them during the 4 years of this research. Their company have certainly made this process more enjoyable and less stressful.

I would like to thank God for somehow making me company when I felt alone. Also for the help in my studies, providing the perseverance to continue always when something got hard.

To my parents Isidio and Zelia and my brother Afonso, whose are my role models, for the unconditional support.

This study was financed in part by the Coordenação de Aperfeiçoamento de Pessoal de Nível Superior - Brasil (CAPES) - Finance Code 001.

My acknowledges to the financial support from grants 2016/07398-8 and 2017/13693-5 of the São Paulo Research Foundation (FAPESP). Also acknowledges to INCT-FNA project 464898/2014-5.

*“Take your time, don’t live too fast,
Troubles will come and they will pass.
Go find a woman and you’ll find love,
And don’t forget son,
There is someone up above.”*
— SIMPLE MAN- LYNYRD SKYNYRD

Resumo

Reações nucleares de pré-equilíbrio ocorrem em uma escala de tempo intermediária entre as rápidas reações diretas e as lentas reações de evaporação do núcleo composto. Com o aumento da energia do projétil, as reações de pré-equilíbrio se apresentam como uma componente cada vez mais destacada nos espectros e distribuições angulares de reações nucleares sendo de importância especial em aplicações utilizando feixes energéticos de nucleons tais como, por exemplo, em terapia com feixe de prótons ou “accelerator-driven systems”. Embora seu estudo iniciou-se há mais de 50 anos atrás, devido a sua complexidade, ainda não existe uma descrição bem fundamentada delas. Os modelos quânticos propostos se limitam a processos de emissão de apenas uma partícula. Estes também utilizam hipóteses estatísticas e aproximações dificilmente justificáveis. Analisamos as primeiras duas etapas de uma reação de pré-equilíbrio e propomos uma extensão para o formalismo quântico para incluir até duas partículas no contínuo após a primeira colisão e até três após a segunda colisão, os números máximos de partículas permitido fisicamente. Estudamos em detalhe a coerência/incoerência entre excitações de estados de partícula-buraco de natureza diferente. Para isto, utilizamos os estados excitados na aproximação conhecida como “Random Phase Approximation”. A contribuição de cada componente de partícula-buraco foi determinada como sendo bem representada por uma distribuição do tipo Breit-Wigner. Também determinamos um comportamento universal para a largura desta distribuição. Além disso, verificamos a validade da suposição de aleatoriedade para estados de energia alta.

Abstract

Pre-equilibrium nuclear reactions occur on a time scale intermediate between the fast direct reactions and the slow evaporation from the compound nucleus. With increasing projectile energy, the pre-equilibrium reaction component becomes more and more visible in the reaction spectra and angular distributions, being of special importance in applications using energetic beams of nucleons such as in proton radiotherapy or accelerator-driven systems (ADS). Although these reactions have been studied for over 50 years, due to their complexity, it has not yet been possible to obtain a fundamental description of them. The quantum models developed so far are limited to processes in which at most one particle is emitted. They also make use of statistical hypotheses and approximations that are, at best, difficult to justify. We have analyzed the first two steps of a pre-equilibrium reaction and provided an extension of the quantum formalism to include up to two particles in the continuum after the first interaction and up to three after the second interaction, the maximum number of continuum particles physically permitted. We have conducted a detailed study of the coherence/incoherence between excitations of particle-holes of different nature. For this, the excited states in the Random Phase Approximation (RPA) were analyzed. The contribution of each p-h mode was found to be of a Breit-Wigner function form. We have also determined a universal behavior for the spreading width. In addition, the validity of the randomness assumption was verified for higher energy states.

List of Figures

FIGURE 1.1 – Proton emission spectrum for 62 MeV protons incident on a ^{55}Fe target. Lower emission energies correspond to compound nuclear formation while the higher ones corresponds to direct nuclear reactions. The intermediate region corresponds to pre-equilibrium nuclear reactions (BERTRAND; PEELLE, 1973).	19
FIGURE 2.1 – Laboratory and CM system of reference.	22
FIGURE 2.2 – Schematic representation of the scattering process. Adapted from (KURT; TUNG-MOW, 2003).	25
FIGURE 2.3 – Two particle interaction picture with $R = R_1 + R_2$	30
FIGURE 2.4 – Quantum angular momentum associated to the scattering energy. For this, we take reduced mass of the system to be $\mu \approx 1$	31
FIGURE 2.5 – Diagram of eikonal approximation scattering, the straight-line trajectory is along the z-direction in a cylindrical coordinate system.	32
FIGURE 2.6 – Real (solid) and imaginary (dashed) parts of the T matrix for a Wood Saxon potential with: $V_0 = -10$ and $W_0 = 0$ MeV (a); $V_0 = 0$ and $W_0 = -10$ MeV (b); $V_0 = -30$ and $W_0 = -5$ MeV (c).	34
FIGURE 2.7 – Differential cross section convergence for different scattering angles considering the Wood Saxon potential with: $V_0 = -10$ and $W_0 = 0$ MeV (a); $V_0 = 0$ and $W_0 = -10$ MeV (b); $V_0 = -30$ and $W_0 = -5$ MeV (c).	35
FIGURE 2.8 – (a) Differential cross-section computed for $E_0 = 95$ MeV neutron induced elastic scattering in the eikonal approximation. The plus mark represent the experimental data taken from (MERMOD <i>et al.</i> , 2006). (b) Wood Saxon potential with $V_0 = -30$ MeV, $W_0 = -5$ MeV and $a = 0.65$ fm. The nuclear radius R_0 is shown as the the vertical solid gray line.	36

FIGURE 2.9 – Experimental cross sections for (p, n) , $(p, 2n)$ and (p, pn) involved in the ^{63}Zn compound nucleus formation. The scale of alpha particles were scaled with respect to proton energy to both correspond to the same excitation energy (GHOSHAL, 1950).	43
FIGURE 2.10 – Schematic representation of a general cross section distribution for preequilibrium reactions (topper panel) and angular distribution of each phase from (A) compound to (D) direct components (bottom panel). Adapted from (KONING; AKKERMANS, 1999).	44
FIGURE 2.11 – Average number of excitons at equilibrium, n_{eq} , and minimum number of excitons necessary to reach equilibrium within a configuration n_0 as a function of the product of the density of one particle density states and the excitation energy (gE). n_{10} curve is described in the text.	46
FIGURE 3.1 – Example of a graphical solution to the dispersion equation (3.36).	64
FIGURE 4.1 – Response function for 3^- RPA excited states of ^{56}Ni nucleus for low (left) and high (right) energetic p-h components. The vertical solid and doted lines represent the non-interacting p-h energy and the distribution mean for the Breit-Wigner fit.	66
FIGURE 4.2 – Single-particle strenght/response function for 3^- RPA excited states of ^{56}Ni nucleus.	67
FIGURE 4.3 – Spreading γ deponce on particle-hole energy components for ^{16}O (a) and ^{56}Ni (b).	67
FIGURE 4.4 – Spreading γ deponce on particle-hole energy components for ^{90}Zr (a) and ^{120}Sn (b).	67
FIGURE 4.5 – The distribution (4.6) for a low (a) and higher (b,c) energetic RPA basis components of 3^- states of ^{56}Ni . ΔE represents the energy bin where the amplitudes are averaged.	68
FIGURE 4.6 – (a) Averaged contribution of the RPA components from the diagonal (4.8) (solid dark lines) and off-diagonal (4.9) (dashed gray lines) terms of the for 3^- states of ^{56}Ni . (b) The number of states averaged within the bin of excitation energy interval ΔE	69
FIGURE 4.7 – Average energy of the fast (leading) and slow final particles in a nucleon-nucleon collision in nuclear matter as a function of the incident particle energy. The phase space final volume, in arbitrary units, is also shown as a function of initial energy.	70

- FIGURE 5.1 – Left panel: Optical potential for different nucleon induced reaction energies at ^{90}Zr . Right panel: The parameters for the $t\rho$ optical potential as a function of energy. 74
- FIGURE 5.2 – Differential cross section normalized to the Rutherford cross sections for $^{90}\text{Zr}(p,p)$ elastic scattering (with and without the Coulomb potential). The incident proton energy is $E = 185$ MeV. The parameters of WS function are $r_0 = 1.25$ fm and $a_0 = 0.65$ fm. The data filled circles represent the experimental values, see Table 5.3 for references. 75
- FIGURE 5.3 – Differential cross section normalized to the Rutherford cross sections for $^{90}\text{Zr}(p,p)$ at different energies. The experimental data are shown as symbols and the references are given in Table 5.3. The parameters of the potential are the same as Fig. 5.2. In order to present all cases, the cross sections were shifted by a constant factor starting from the bottom. 76
- FIGURE 5.4 – Proton elastic scattering cross section from a ^{208}Pb target for different incident energies. Experimental data are shown as symbols (see Table 5.3 for references). Both the data and the calculation at 800 MeV were shift. 76
- FIGURE 5.5 – Particle-hole mode contributions to the first 3^- excited state of ^{90}Zr . On the left two components are more pronounced but only contribute with 70 % of the strength. On the right panel, in log scale, many other modes make small contributions to complete the total strength. 87
- FIGURE 5.6 – Inelastic proton cross section for ^{90}Zr at 57.5 MeV (left panel) and 185 MeV (right panel). The dashed blue, red and gray lines represent the separate $E_{ph} = 3.1$ MeV, $E_{ph} = 3.8$ MeV particle hole contributions and the sum of these two components, respectively. The full dark solid line represent calculations performed with all p-h components. The dotted dark line is obtained with all p-h components of the RPA state with the single particle HF states employed. 88
- FIGURE 5.7 – Left panel: radial transition density δ_ν for the first excited energy 3^- state of ^{90}Zr . Right panel: Differential double cross section for proton scattering obtained with (5.58). Cross-section values of the right panel are shifted for visualization convenience. 90

FIGURE 5.8 – Differential double cross section of proton inelastic scattering at 3^- (left panel) and 2^+ (right panel) excited states of ^{208}Pb . The values are shifted for visualization convenience.	90
FIGURE 5.9 – Inelastic proton cross section from ^{90}Zr at different excitation energies for two incoming proton energies, 200 (left panel) and 160 MeV (right panel). Experimental data were taken from (RICHTER <i>et al.</i> , 1994).	92
FIGURE 5.10 – Spin distribution (5.62) for nucleon induced reaction on ^{90}Zr	93
FIGURE 5.11 – Scattering angle representation for two continuum particles.	95
FIGURE 5.12 – Angular distribution for two proton emission from ^{90}Zr target with proton projectiles of $E_i = 200$ MeV. One of the emitted particles is maintained fixed for the calculations (preliminary results).	97
FIGURE A.1 – The two options for z-axis definition: (a) z-axis is placed on incident particle momentum direction \vec{k} and (b) z-axis on the bisector of the scattering angle θ . Note that in the second case $\hat{z} \rightarrow \vec{k} + \vec{k}'$	101
FIGURE A.2 – Number of p-h proton states for ^{56}Ni . Only bound or quasi-bound (bellow Coulomb plus Centrifugal barrier, see Appendix A.5) states are taken as possible particle orbitals.	108

List of Tables

TABLE 5.1 – Parameters for nucleon-nucleon scattering necessary in the $t\rho$ potential approximation (RAY, 1979).	73
TABLE 5.2 – Lower energies parameters, averaged over pp and pn scattering, necessary in the $t\rho$ potential approximation (LENZI <i>et al.</i> , 1988).	74
TABLE 5.3 – Data sets for the proton elastic cross sections.	75
TABLE 5.4 – Data sets for the proton inelastic cross sections for specific J^π excited target states.	91
TABLE A.1 – Proton single particle energies for ^{16}O	107
TABLE A.2 – Proton single particle energies for ^{20}Ca	107

List of Abbreviations and Acronyms

CM	Center of Mass
MS	Multi-Step
MSC	Multi-Step Compound
MSD	Multi-Step Direct
WS	Wood Saxon
TDA	Tamm-Dancoff Approximation
RPA	Random Phase Approximation
HF	Hartree-Fock
QHO	Quantum Harmonic Oscillator
BW	Breit-Wigner

List of Symbols

a	Scalar
\mathbf{a}	Vector
a_x	First component of \mathbf{a}
$\delta_{i,j}$	Kronecker delta
$\text{Re}[\mathbf{z}]$	Real part of a complex number
$\text{Im}[\mathbf{z}]$	Imaginary part of a complex number

Contents

1	INTRODUCTION	18
2	QUANTUM SCATTERING AND NUCLEAR REACTIONS	21
2.1	Center of Mass and Laboratory Frames	21
2.2	The Two Body Quantum Elastic Scattering	23
2.2.1	The Distorted Wave Born Approximation – DWBA	25
2.2.2	Cross-Section	27
2.2.3	Partial Waves Expansion	28
2.2.4	The Eikonal Approximation	31
2.2.5	Scattering by the Coulomb Potential	37
2.2.6	Inelastic Scattering	40
2.3	Nuclear Reactions	41
2.3.1	Compound Nuclear Reactions	42
2.3.2	Direct Nuclear Reactions	42
2.4	Pre-equilibrium Mechanism	43
2.4.1	Semi-Classical Models	44
2.4.2	Quantum Models	48
2.4.3	Randomness Statistics	53
2.4.4	One-step Cross Section	54
2.4.5	Two-step Cross Section	55
3	QUANTUM MECHANICS – THE EIGEN-WORLD	58
3.1	Eigenvalue Problem	58
3.2	Strength Function	60

3.2.1	Collectivity	62
4	ANALYSIS OF THE ASSUMPTIONS	65
4.1	Single-Particle Contribution to the 1p-1h Response Function . . .	65
4.2	Analysis of Randomness Assumptions	68
4.3	Leading-Particle Analysis	70
5	EXTENSION OF THE QUANTUM FORMALISM	72
5.1	Elastic scattering	72
5.1.1	Proton Elastic Scattering	74
5.2	One-step inelastic scattering	77
5.3	Two-step inelastic scattering	79
5.4	Differential energy-angular distributions	82
5.5	One-step Cross Sections	84
5.5.1	One particle in continuum	84
5.5.2	Two particles in the continuum	94
5.5.3	No outgoing particle – absorption	96
6	CONCLUSION AND OUTLOOK	99
	APPENDIX A – TOOL BOX	101
A.1	Momentum Direction and System of Reference	101
A.2	Transition matrix elements	102
A.3	Single Particle Energy Model	106
A.4	Transition Density of States and Cross-Sections	108
A.5	Particle States Bellow Barrier	110
	BIBLIOGRAPHY	111

1 Introduction

Nuclei and their constituents form the basis of all visible matter in the Universe from microscopic to astrophysical objects. After the introduction of the Thompson model of atomic nucleus (1897) the modern view of internal structure of nuclei was first investigated in the Geiger and Marsden experiments in 1909 (GEIGER; MARSDEN, 1909). They worked on alpha particle scattering from foils of gold and silver, revealing particles deflected backward. Alpha particle would not be deflected by electrons of the atoms in the foil, due to their mass difference, which lead Rutherford in 1911 (RUTHERFORD, 1911) to turn to the idea of positive charges concentrated at the center of the atom. With his work, the discovery of the atomic nucleus was settled and confirmed by later experiments.

Processes of collisions/interactions involving nucleons (protons or neutrons) and/or nuclei are called nuclear reactions. Since the last century, bombarding particles with other particles and measuring the exit products has been a successful approach in the study of the action of the nuclear force and the proprieties of different nuclei. The density dependence of nuclear reactions is also important in the gravitational field of compact objects, e.g., neutron stars. In addition, nuclear reactions play also an important role in stellar evolution. Nowadays, nuclei with large ratios of neutrons to protons, the so called exotic nuclei, are being studied as well as highly deformed excited nuclei with high angular momenta. These systems are also used in the investigation of the limits of existing nuclei and new elements, the superheavy nuclei.

Nuclear reactions can basically be explained by three mechanisms: when the projectile-target interaction occurs rapidly, $10^{-20} - 10^{-21}$ seconds, the process is known as a direct nuclear reaction; for large time scales, $10^{-14} - 10^{-16}$ seconds, the projectile becomes indistinguishable after being captured by the target nucleus forming an excited state of a compound system (target plus projectile). This allows a large number of interactions and the emission process is called compound nuclear reaction. In between these two time scales are events that can not be classified either as direct or as compound reactions. They are called pre-equilibrium or pre-compound (usually in multi-step quantum models) nuclear reactions. Pre-equilibrium emissions take place after the first reaction stage but still before statistical equilibrium is reached in the compound system.

Fast (relatively high energy) particle energy spectra are evidence of pre-equilibrium nuclear reactions. Figure 1.1 shows the energy spectrum of protons emitted from the bombardment of a ^{55}Fe target by protons of 62 MeV of energy. Three different regions can be separated: on the left side, low energy particles are emitted from the nucleus with a compound nucleus evaporation like spectrum. This contrasts with the right side towards high energy emissions. There, the distribution corresponds to protons being emitted after a single interaction which usually excites collective states of the target nucleus. This component is associated with the direct reactions. Finally, pre-equilibrium processes are present in the intermediate region represented by an approximately constant spectrum. (BERTRAND; PEELLE, 1973; KAMAL, 2014).

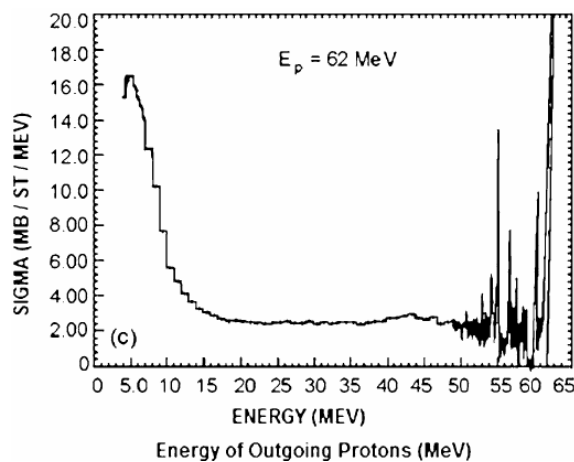


FIGURE 1.1 – Proton emission spectrum for 62 MeV protons incident on a ^{55}Fe target. Lower emission energies correspond to compound nuclear formation while the higher ones corresponds to direct nuclear reactions. The intermediate region corresponds to pre-equilibrium nuclear reactions (BERTRAND; PEELLE, 1973).

Direct reactions play an important role in basic nuclear physics, allowing the study of fundamental and low energy excited states of nuclei. They have been used to extend the knowledge from stable to exotic nuclei or even to nuclei found only as resonances. Compound nuclear reactions are of interest in the basic and applied areas of physics. These systems are examples of chaotic behavior in many body quantum systems (WEIDENMÜLLER; MITCHELL, 2009; MITCHELL *et al.*, 2010) and their cross sections are required for different applications such as: nuclear astrophysics, national security and nuclear energy. When it comes to the pre-equilibrium components, although fifty years have passed since the start of their study, these reactions are still not well described. Their relevance goes beyond fundamental studies, as they are very important for technical applications in many areas, e.g., fast nuclear reactors, accelerator-driven system (ADS) and proton therapy. The use of intensity modulated protons beams provide a better control of the concentration dose activity in patients, minimizing the effects on healthy nearby

tissues. The proton beam energy is associated with the maximum depth in tissue. For instance, to reach a penetration of about 32 cm, a 250 MeV proton beam is required (BORTFELD *et al.*, 2005), an energy at which pre-equilibrium processes are a dominant part of a reaction. Proton-induced reaction data are also necessary for planning the production of medical radionuclides for diagnostic and internal therapy purposes (QAIM, 2004; QAIM, 2017). Theoretical nuclear reaction models are very important for supplementing the existent data or even providing them, when practical or economic difficulties are faced. Therefore, pre-equilibrium nuclear reactions models are important tools in nuclear data evaluation.

In this work, we have extended the quantum formalism of pre-equilibrium reactions. To this end, we analyzed the spectral functions of the single-particle states obtained from the 1p-1h response function. One of our goals was to study the quantum description in comparison to the Blann and Chadwick semiclassical model. This helped us to extend the multistep direct reaction theory to include more than one unbound particle. We analyze the three components of a one-step nucleon-induced reaction where 0, 1 or 2 nucleons can be in the continuum. The second reaction step for which 0, 1, 2 or 3 nucleons can be in the continuum is also explored. The cross sections were computed in the eikonal approximation. These distorted waves were used to excite more particles to the continuum in the first two steps of the reaction.

This thesis is organized as follows: In the second chapter, an introduction to quantum scattering and nuclear reactions are presented. The concepts of semiclassical and the multi-step quantum models of pre-equilibrium nuclear reactions are introduced. In Chapters 4 and 5, an analysis of the statistical assumptions of quantum models is presented and the extension of the quantum model to include more than one particle in the continuum is given. The conclusions and discussions, as well as possible future developments, are presented in Chapter 6.

2 Quantum Scattering and Nuclear Reactions

Collision processes involving a projectile and a target are of great importance in the study of the properties of both objects involved, as well as possible different products formed after their interaction. This is the type of problem treated in this thesis, an incident particle interacts with a nucleus composed of many particles. In this case, the description of the collision becomes very complicated due to the number of particles involved – a many body problem. The next sections are devoted to an overview of the physics principles and mathematical methods to be used, a brief description of quantum scattering theory and a discussion of nuclear reaction mechanisms.

2.1 Center of Mass and Laboratory Frames

Throughout this thesis the subject of an incoming particle interacting with a target nucleus will be addressed. It is usually more convenient to study this problem in the center-of-mass frame rather than the laboratory frame. If we separate variables into center of mass (CM) and relative projectile-target coordinates, since the interactions do not depend on the position of the CM, the CM solutions contribute with a constant energy and momentum (the CM motion is a trivial plane wave function)¹. In this way, the two-body problem is reduced to one-body system, and the efforts are concentrated on calculations in the relative space of coordinates.

As the uniform movement of the CM does not affect the collision dynamics, the total energy of the relative motion of system is also conserved. The transformation to the CM frame and back to the laboratory frame is depicted in Fig.2.1.

Assuming the Hamiltonian for a collision between a projectile a and a target A to be

$$\mathcal{H} = H_a + H_A + V(|\vec{r}_a - \vec{r}_A|), \quad (2.1)$$

¹We also assume that if the incident beam is turned on and maintained for a while, the system might reach a steady state and therefore results are time independent.

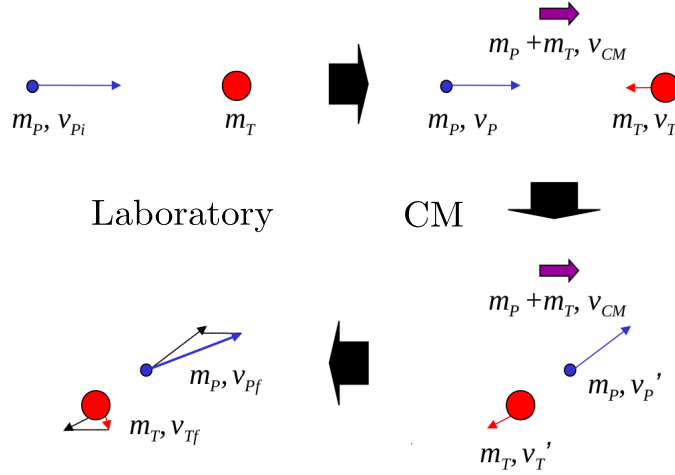


FIGURE 2.1 – Laboratory and CM system of reference.

where $H_{a,A} = p_{a,A}^2/2m_{a,A}$ represents the individual kinematic energies and V the two body interaction as a function of the particles separation distance. The individual, stationary, noninteracting wave functions can be written as

$$\psi_a = a_0 \exp \left[i\vec{k}_a \cdot \vec{r} \right], \quad \psi_A = A_0 \exp \left[i\vec{k}_A \cdot \vec{r}_A \right],$$

where the normalization constants correspond to the a_0 incident and A_0 target particles per unit volume. We assume $A_a = 1$ (one target particle per unit volume) and $a_0 = \sqrt{I_a/v_a}$ for the incident projectile, where I_a is the incident flux in units of particles per unit area per unit time and v_a the their incident velocity.

The total and relative momenta are defined by

$$\vec{K} = \vec{k}_a + \vec{k}_A, \quad \vec{k} = \frac{m_A \vec{k}_a - m_a \vec{k}_A}{m_a + m_A},$$

and the relative and the CM coordinates

$$\vec{r} = \vec{r}_a - \vec{r}_A, \quad \vec{R} = \frac{m_a \vec{r}_a + m_A \vec{r}_A}{m_a + m_A}.$$

These variables can be inverted

$$\vec{k}_a = \frac{m_a}{m_a + m_A} \vec{K} + \vec{k}, \quad \vec{r}_a = \vec{R} + \frac{m_A}{m_a + m_A} \vec{r},$$

and

$$\vec{k}_A = \frac{m_A}{m_a + m_A} \vec{K} - \vec{k}, \quad \vec{r}_A = \vec{R} - \frac{m_a}{m_a + m_A} \vec{r},$$

to result in an Hamiltonian

$$\mathcal{H} = \frac{1}{m_a + m_A} K^2 + H. \quad (2.2)$$

The solution for the center of mass motion is a trivial free wave

$$\exp \left[i \vec{K} \cdot \vec{R} \right],$$

due to the conservation of the total momentum.

One is then left with the last term in (2.2) which represents only the relative motion

$$H = \frac{1}{2\mu} p^2 + V(r), \quad H\psi = E\psi \quad (2.3)$$

with the reduced mass of the system given by

$$\mu = \frac{m_a m_A}{m_a + m_A}. \quad (2.4)$$

A more detailed description of both projectile and target internal states takes into account their respective internal Hamiltonians H_a and H_A

$$H_a \psi_a = E_a \psi_a, \quad H_A \psi_A = E_A \psi_A. \quad (2.5)$$

The final Hamiltonian becomes then the sum of these two and the relative motion given above

$$H_T = H_a + H_A + H, \quad (2.6)$$

with

$$H_T \Psi = E_T \Psi, \quad (2.7)$$

where E_T is the total relative energy of the system and the total wave function is

$$\Psi = \psi_a \psi_A \psi. \quad (2.8)$$

The internal details will be included in the discussion later on in this thesis when the multi-step nuclear reaction formalism is presented.

2.2 The Two Body Quantum Elastic Scattering

Let the relative motion of the incident particle be represented by a plane wave with energy

$$E = \frac{\hbar^2 k^2}{2\mu}, \quad (2.9)$$

where $k = |\mathbf{k}|$, represents the modulus of the propagation momentum vector in the three-dimensional Euclidean space with an orthonormal basis $(\mathbf{e}_x, \mathbf{e}_y, \mathbf{e}_z)$. Assuming the particle to be deflected by a static potential $V(\mathbf{r})$, the Schrödinger equation

$$(\nabla^2 + k^2) \psi(\mathbf{r}) = \frac{2\mu}{\hbar^2} V(\mathbf{r}) \psi(\mathbf{r}) \quad (2.10)$$

has to be solved. \mathbf{r} and μ , represent the incident particle-target distance and the reduced mass of the system, respectively.

Associated with (2.10) is the Green's function $G(\mathbf{r}, \mathbf{r}')$, solution of the inhomogeneous wave equation

$$(\nabla^2 + k^2) G(\mathbf{r}, \mathbf{r}') = \frac{2\mu}{\hbar^2} \delta(\mathbf{r} - \mathbf{r}'). \quad (2.11)$$

The solution of this Poisson-like equation is very known and corresponds to the amplitude of the outgoing radiation at \mathbf{r} from a source at \mathbf{r}'

$$G(\mathbf{r}, \mathbf{r}') = -\frac{2\mu}{4\pi\hbar^2} \frac{e^{ik|\mathbf{r}-\mathbf{r}'|}}{|\mathbf{r} - \mathbf{r}'|}. \quad (2.12)$$

The wave function scattered by the potential V , $\psi^{(+)}(\mathbf{r})$ ², is given by

$$\psi^{(+)}(\mathbf{r}) = e^{i\mathbf{k}\cdot\mathbf{r}} + \int G(\mathbf{r}, \mathbf{r}') V(\mathbf{r}') \psi(\mathbf{r}') d\mathbf{r}'. \quad (2.13)$$

The asymptotic form of (2.13) can be obtained by expanding with the assumption of $(r'/r \ll 1)$ ($|\mathbf{r}| = r$)

$$\begin{aligned} |\mathbf{r} - \mathbf{r}'| &= \sqrt{r^2 + (r')^2 - 2\mathbf{r} \cdot \mathbf{r}'} = r \left(1 + \frac{1}{2} \left(-2\frac{1}{r^2} \mathbf{r} \cdot \mathbf{r}' \right) + O(r^{-2}) \right) \\ &\rightarrow r - \hat{\mathbf{r}} \cdot \mathbf{r}'. \end{aligned}$$

Now, one may define

$$\mathbf{k}' \equiv |\mathbf{k}| \hat{\mathbf{r}} = k \frac{\mathbf{r}}{r}, \quad (2.14)$$

as the vector of magnitude k pointing from the origin toward \mathbf{r} . The waves represented by \mathbf{k}' are elastically scattered particles in the direction of \mathbf{r} . The scattering angle θ , see Figure 2.2, relating both the initial and final momenta can be written as

$$\mathbf{k} \cdot \mathbf{k}' = k^2 \cos \theta. \quad (2.15)$$

²Since waves represent relative motion with velocity of the pair given by $v = \hbar k/\mu$, the + and - are the incoming and outgoing waves, which stand for the pair approaching and departing from each other, respectively.

Apart from a constant, the asymptotic $r \rightarrow \infty$ wave function becomes

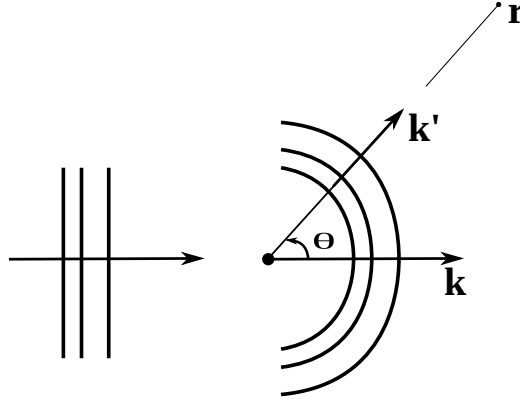


FIGURE 2.2 – Schematic representation of the scattering process. Adapted from (KURT; TUNG-MOW, 2003).

$$\psi_{\mathbf{k}}^{(+)}(\mathbf{r}) \rightarrow e^{i\mathbf{k}\cdot\mathbf{r}} - \frac{2\mu}{4\pi\hbar^2} \frac{e^{ik}}{r} \int e^{-i\mathbf{k}'\cdot\mathbf{r}'} V(\mathbf{r}') \psi(\mathbf{r}') d\mathbf{r}'. \quad (2.16)$$

This expression is often written as

$$\psi_{\mathbf{k}}^{(+)}(\mathbf{r}) \rightarrow e^{i\mathbf{k}\cdot\mathbf{r}} + f(\mathbf{k}', \mathbf{k}) \frac{e^{ikr}}{r}, \quad (2.17)$$

where the second term represents a spherical wave weighted by the scattering amplitude

$$f(\mathbf{k}', \mathbf{k}) = -\frac{2\mu}{4\pi\hbar^2} \int e^{-i\mathbf{k}'\cdot\mathbf{r}} V(\mathbf{r}) \psi_{\mathbf{k}}^{(+)}(\mathbf{r}) d\mathbf{r}. \quad (2.18)$$

The symbol $f(\mathbf{k}', \mathbf{k})$ stands for the amplitude of scattering from direction \mathbf{k} to \mathbf{k}' , and can also be represented by $f(\theta, k)$, where θ is the angle between both propagating vectors ($k = |\mathbf{k}| = |\mathbf{k}'|$).

2.2.1 The Distorted Wave Born Approximation – DWBA

A first approximation to compute (2.18) is to consider a weak interaction V so that

$$\psi_{\mathbf{k}}^{(+)}(\mathbf{r}) = \psi_{\mathbf{k}}(\mathbf{r}) = e^{i\mathbf{k}\cdot\mathbf{r}}. \quad (2.19)$$

This is the so-called Born Approximation and allows the elastic scattering amplitude to have a form of a Fourier transform

$$f(\mathbf{q}) = -\frac{2\mu}{4\pi\hbar^2} \int e^{i\mathbf{q}\cdot\mathbf{r}} V(\mathbf{r}) d\mathbf{r} \quad (2.20)$$

with the transferred momentum given by $\mathbf{q} = \mathbf{k} - \mathbf{k}'$.

A more sophisticated solution can be obtained by splitting the interaction $V = V_1 + V_2$. Having the solution ψ_1 for V_1 one might deal with two waves: a plane wave summed to a outgoing scattered wave we denote by $\psi_1^{(+)}$, and another plane wave plus an incoming wave named $\psi_1^{(-)}$. These two are related by

$$\psi_1^{(+)}(\mathbf{k}, \mathbf{r}) = \psi_1^{(-)}(-\mathbf{k}, \mathbf{r})^*.$$

The asymptotic wave becomes

$$\psi^{(+)}(\mathbf{k}, \mathbf{r}) \rightarrow \psi_1^{(+)}(\mathbf{k}, \mathbf{r}) - \frac{\exp(ikr)}{r} \int \psi_1^{(-)}(\mathbf{k}', \mathbf{r}')^* V_2(\mathbf{r}') \psi^{(+)}(\mathbf{k}, \mathbf{r}) d\mathbf{r}', \quad (2.21)$$

note that this is a wave with $\psi_1^{(+)}$ as initial condition plus its distortion due to the second part of the interaction V_2 . The full scattering amplitude is obtained by the sum of f_1 (ψ_1 from potential V_1) and the second term of the expression above (due to V_2)

$$f(\mathbf{k}, \mathbf{k}') = f_1(\mathbf{k}, \mathbf{k}') - \frac{1}{4\pi} \int \psi_1^{(-)}(\mathbf{k}', \mathbf{r}')^* V_2(\mathbf{r}') \psi^{(+)}(\mathbf{k}, \mathbf{r}) d\mathbf{r}'. \quad (2.22)$$

Finally, if V_2 is weak compared to V_1 we use a Born-like expansion (first order in V_2) for $\psi^{(+)}(\mathbf{k}, \mathbf{r})$ to obtain

$$f_{\text{DWBA}}(\mathbf{k}, \mathbf{k}') = f_1(\mathbf{k}, \mathbf{k}') - \frac{1}{4\pi} \int \psi_1^{(-)}(\mathbf{k}', \mathbf{r}')^* V_2(\mathbf{r}') \psi^{(+)}(\mathbf{k}, \mathbf{r}) d\mathbf{r}'. \quad (2.23)$$

This expression is generalized to inelastic scattering with f_1 and V_1 describing the elastic part and V_2 the inelastic components. The validity of it relies on the more important contribution coming from the elastic component while the inelastic is treated as a perturbation term. The very general formula for an inelastic amplitude is

$$f_{\text{DWBA}}(\mathbf{k}, \mathbf{k}') = -\frac{1}{4\pi} \int \psi_{\beta}^{(-)}(\mathbf{k}_{\beta}, \mathbf{r}_{\beta})^* \langle b, B | V_2 | A, a \rangle \psi_{\alpha}^{(+)}(\mathbf{k}_{\alpha}, \mathbf{r}_{\alpha}) d\mathbf{r}_{\beta} d\mathbf{r}_{\alpha}, \quad (2.24)$$

where the potential V_2 is responsible for inelastic transitions and the distorted wave functions ψ^{\pm} describes the elastic scattering in the entrance channel ($\alpha = a + A$) with an optical potential V_{α} and elastic component for the exit channel ($\beta = b + B$) with V_{β} optical potential.

2.2.2 Cross-Section

One may ask for the angular distribution of particles scattered by the potential $V(\mathbf{r})$. The concept of probability current

$$\mathbf{j} = \frac{\hbar}{m} \text{Im}(\psi^* \nabla \psi), \quad (2.25)$$

is useful to define the particle flux through the experiment, the detected particles. For the incident plane wave,

$$j_i = \frac{\hbar}{m} \text{Im} \left(e^{-ikz} \frac{d}{dz} e^{ikz} \right) = \frac{\hbar k}{m} = v \quad (2.26)$$

and for the emergent spherical wave

$$j_e = \frac{\hbar}{m} \text{Im} \left[f^*(\theta, k) \frac{e^{-ikr}}{r} \frac{\partial}{\partial r} \left(f(\theta, k) \frac{e^{ikr}}{r} \right) \right] = \frac{\hbar k}{r^2 m} |f(\theta, k)|^2 = \frac{v}{r^2} |f(\theta, k)|^2. \quad (2.27)$$

The number of particles scattered per unit time into an element of area subtending the solid angle located at a target distance r can be written as

$$d\dot{N} = j_e dA = v |f(\theta, k)|^2 d\Omega, \quad (2.28)$$

where $dA = r^2 \sin \theta d\theta d\phi$ in spherical coordinates.

The differential cross section (angular dependent) for elastic scattering is defined as

$$d\sigma_{\text{el}} = \frac{\text{Flux through the solid angle}}{\text{Incident Flux}}, \quad (2.29)$$

which corresponds to

$$\frac{d\sigma_{\text{el}}}{d\Omega} = \frac{d\dot{N}/d\Omega}{j_i}, \quad (2.30)$$

which after substitution gives,

$$\frac{d\sigma}{d\Omega} = |f(\theta, k)|^2. \quad (2.31)$$

The total scattering cross section is obtained by integrating (2.31)

$$\sigma = \int \frac{d\sigma}{d\Omega} d\Omega = 2\pi \int_{-1}^{+1} |f(\theta, k)|^2 d(\cos \theta), \quad (2.32)$$

and refers to the number of events per target per unit time with respect to the incident flux.

2.2.3 Partial Waves Expansion

When dealing with a central scattering potential, the solutions of Eq.(2.10) can be conveniently expanded in a linear combination of the product of radial and angular parts

$$\psi = \sum_{lm} a_{lm} \frac{u_l(r)}{r} Y_l^m(\theta, \phi), \quad (2.33)$$

where the radial function must satisfy

$$\frac{d^2 u_l}{dr^2} + \frac{2\mu}{\hbar^2} \left[E - V(r) - \frac{\hbar^2 l(l+1)}{2m r^2} \right] u_l = 0, \quad (2.34)$$

with $u_l(0) = 0$, as the boundary condition.

For a plane ($V = 0$) wave,

$$\psi = e^{ikz} = e^{ikr \cos \theta} = \sum_l^{\infty} (2l+1) i^l j_l(kr) P_l(\cos \theta), \quad (2.35)$$

where $j_l(x)$ are the spherical Bessel functions and the $P_l(\cos \theta)$ the Legendre polynomials. The scattering amplitude can be obtained using the asymptotic form of the above expansion, reading

$$f(\theta) = \frac{1}{2ik} \sum_l (2l+1)(C_l - 1) P_l(\cos \theta), \quad (2.36)$$

where

$$C_l = e^{2i\delta_l} \quad (2.37)$$

have absolute value unity for purely real potentials $V(r)$. In this case the number of particles is conserved (Optical Theorem). The δ_l are the phases shifts of the partial wave due to the scattering processes.

If the potential is complex, δ_l is also. When $\text{Im}[V(r)] < 0$ (absorptive potential), the values of

$$|C_l|^2 < 1, \quad \text{Im}[\delta_l] > 0$$

imply a loss of particle flux due to the target absorption. These, can be verified writing

$$\psi_{\mathbf{k}'}^* \nabla^2 \psi_{\mathbf{k}} - \psi_{\mathbf{k}'} \nabla^2 \psi_{\mathbf{k}}^* = \frac{4\mu i}{\hbar^2} \text{Im}[V(\mathbf{r})] \psi_{\mathbf{k}'}^* \psi_{\mathbf{k}}, \quad (2.38)$$

where integration of the asymptotic form of wave functions in a large sphere (GLAUBER, 1959), gives

$$\frac{1}{2i} \{f(\mathbf{k}', \mathbf{k}) - f^*(\mathbf{k}', \mathbf{k})\} = \frac{k}{4\pi} \int f^*(\mathbf{k}_r, \mathbf{k}') f(\mathbf{k}_r, \mathbf{k}') d\Omega_r - \frac{\mu}{2\pi\hbar^2} \int \text{Im}[V(\mathbf{r})] \psi_{\mathbf{k}'}^* \psi_{\mathbf{k}} d\mathbf{r}. \quad (2.39)$$

In the case of a complex potential with regions where

$$\text{Im}[V(\mathbf{r})] < 0,$$

particles are removed from the incident flux with a probability density rate ³,

$$\nabla \cdot \mathbf{j} = \frac{2}{\hbar} \text{Im}[V(\mathbf{r})] |\Psi_{\mathbf{k}}|^2. \quad (2.40)$$

The absorption cross section can be obtained from the total rate of captured particles $v\sigma_{\text{abs}}$

$$v\sigma_{\text{abs}} = - \int \nabla \cdot \mathbf{j} d\mathbf{r} = -\frac{2}{\pi} \int \text{Im}[V(\mathbf{r})] |\Psi_{\mathbf{k}}|^2 d\mathbf{r}. \quad (2.41)$$

For scattering with zero angular deflection ($\theta = 0$, or $\mathbf{k}' = \mathbf{k}$) (2.39) becomes the so called generalized Optical Theorem,

$$\text{Im}[f(\theta = 0)] = \frac{k}{4\pi} (\sigma_{\text{sca}} + \sigma_{\text{abs}}) = \frac{k}{4\pi} \sigma_{\text{tot}}. \quad (2.42)$$

It is clear from (2.40) that for pure real potentials, a divergence free current implies particle number conservation, i.e. σ_{abs} vanishes. This automatically implies

$$\sigma_{\text{sca}} = \sigma_{\text{tot}}.$$

³ Let the Schrödinger equation be

$$\nabla^2 \psi + \frac{2m}{\hbar} (E + V_0 + iW_0) \psi = 0.$$

If we multiply it by ψ^* and subtract the complex conjugated version of same Schrödinger equation multiplied by ψ , one obtains

$$\psi^* \nabla^2 \psi - \psi \nabla^2 \psi^* = \frac{4miW_0}{\hbar^2} |\psi|^2.$$

The divergence of $\mathbf{j} = \frac{\hbar}{2im} (\psi^* \nabla \psi - \psi \nabla \psi^*)$ is then,

$$\nabla \cdot \mathbf{j} = \frac{\hbar}{2im} \psi^* \nabla^2 \psi - \psi \nabla^2 \psi^* = \frac{2}{\hbar} W_0 |\psi|^2.$$

The scattering cross section can be obtained by integrating the scattering amplitude

$$\sigma_{\text{sca}} = \frac{\pi}{k^2} \sum_l (2l + 1) |C_l - 1|^2, \quad (2.43)$$

and the total cross section is obtained from the generalized optical theorem

$$\sigma_{\text{tot}} = \frac{4\pi}{k} \text{Im} [f(\theta = 0)] = \frac{2\pi}{k^2} \sum_l (2l + 1) (1 - \text{Re} [C_l]). \quad (2.44)$$

Having both the scattering and total cross sections, one can also compute the total absorption cross section (also called reaction cross section) as

$$\sigma_{\text{abs}} = \sigma_{\text{tot}} - \sigma_{\text{sca}}. \quad (2.45)$$

Considering the tools presented in this section, the task is resumed to find the scattering amplitude. One may note that with the increase of the energy involved, more angular momenta are necessary in the expansion, which makes the above formulation difficult to be implemented. For instance, consider the case where two particles with radii R_1 and R_2 collide. Their relative momentum is $\mathbf{p} = \hbar\mathbf{k}$, with an associated angular momentum $l\hbar = pb$, or

$$l = kb, \quad (2.46)$$

where b is the impact parameter. If we assume a simple case where the two particles only interact within a distance $R < R_1 + R_2$, as depicted in Fig.2.3, one has

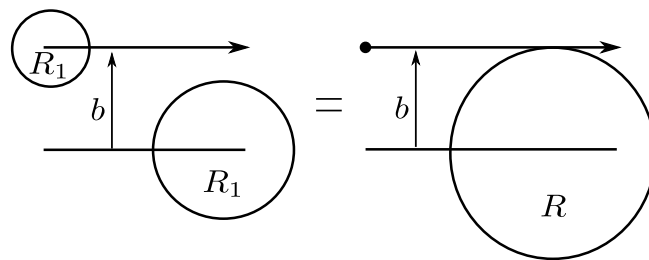


FIGURE 2.3 – Two particle interaction picture with $R = R_1 + R_2$.

$$l \leq kR,$$

which gives a rough upper limit for the quantum angular momentum l that contributes to the partial wave expansion. The distance R varying from a few fms to about 20 fm, furnishes up to 60 terms in the expansion at 200 MeV for the extreme seen in Fig.2.4. Even more components are required for higher energy particles, making this expansion

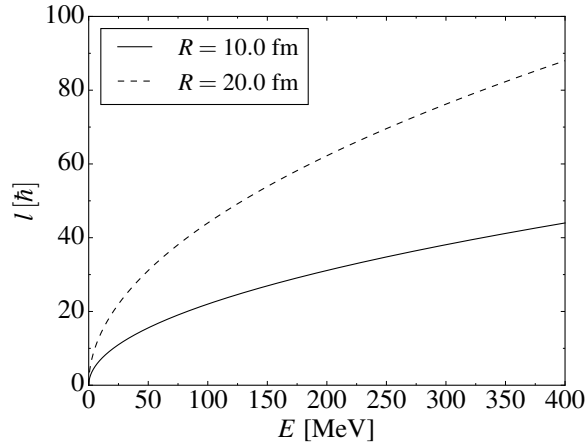


FIGURE 2.4 – Quantum angular momentum associated to the scattering energy. For this, we take reduced mass of the system to be $\mu \approx 1$.

very time-consuming when many fast particle interactions are involved. The next section is devoted to a convenient approximation to high energy scattering, the eikonal approximation also known as the Glauber theory is presented.

2.2.4 The Eikonal Approximation

Consider a scattering wave-function of almost plane wave form

$$\psi(\mathbf{r}) = S(\mathbf{r}) \exp[i\mathbf{k} \cdot \mathbf{r}], \quad (2.47)$$

where S is a slowly varying function.

Substituting in the Schrödinger equation (2.10), one finds

$$2ik \frac{\partial S}{\partial z} + \nabla^2 S - \frac{2\mu}{\hbar^2} V S = 0. \quad (2.48)$$

Defining the wave number k such that

$$E = \frac{\hbar^2}{2\mu} k^2 \quad (2.49)$$

and neglecting the second derivative term, $|\nabla^2 S| \ll k|\nabla S|$, one has

$$\hat{k} \cdot \nabla S = -\frac{1}{v} V(\mathbf{r}), \quad (2.50)$$

with $v = \hbar k / \mu$.

Assuming that $\hat{k} = \hat{z}$, the wave function with an incoming-wave boundary condition

becomes

$$\psi_k^{(+)}(z, \mathbf{b}) = \exp \left[i\mathbf{k} \cdot (\mathbf{b} + z\hat{\mathbf{z}}) - \frac{i}{\hbar v} \int_{-\infty}^z V(z', \mathbf{b}) dz' \right] \quad (2.51)$$

while that with an outgoing-wave boundary condition

$$\psi_k^{(-)}(z, \mathbf{b}) = \exp \left[i\mathbf{k} \cdot (\mathbf{b} + z\hat{\mathbf{z}}) + \frac{i}{\hbar v} \int_z^{\infty} V(z', \mathbf{b})^* dz' \right]. \quad (2.52)$$

The Green's function takes the form

$$G^{(+)}(z, \mathbf{b}; z', \mathbf{b}') = \frac{-i}{\hbar v} \exp \left[i\mathbf{k} \cdot (\mathbf{r} - \mathbf{r}') - \frac{i}{\hbar v} \int_{z'}^z V(z'', \mathbf{b}) dz'' \right] \theta(z - z') \delta(\mathbf{b} - \mathbf{b}'). \quad (2.53)$$

The wave functions (2.51-2.52), represent the propagation in the scattering process along a straight-line trajectory along the z -direction. This situation is depicted in Figure 2.5. If the potential is centered at the origin, the distance b can be interpreted as the impact parameter.

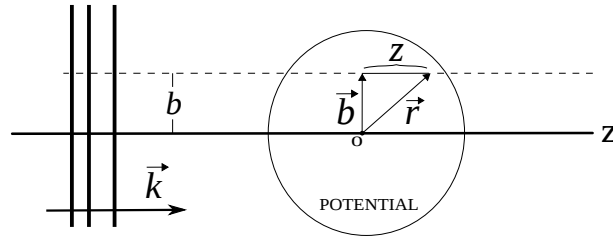


FIGURE 2.5 – Diagram of eikonal approximation scattering, the straight-line trajectory is along the z -direction in a cylindrical coordinate system.

Defining the transfer momentum as

$$\mathbf{q} \equiv \mathbf{k} - \mathbf{k}', \quad (2.54)$$

inserting expression (2.51) in the scattering amplitude (2.18), and introducing cylindrical coordinates $\mathbf{x} \rightarrow \mathbf{b} + z\hat{\mathbf{z}}$ and $d^3r = d^2b dz$, one finds

$$\begin{aligned} f(\mathbf{k}', \mathbf{k}) &= -\frac{1}{4\pi} \frac{2m}{\hbar^2} \int d^2b dz e^{i\mathbf{q} \cdot \mathbf{b}} V(\sqrt{b^2 + z^2}) \\ &\times \exp \left[iq_z z - \frac{im}{\hbar^2 k} \int_{-\infty}^z V(\sqrt{b^2 + z'^2}) dz' \right]. \end{aligned} \quad (2.55)$$

We now have to define the momentum directions and the reference coordinate system. Two options (a) and (b) are discussed in Appendix A.1. If we consider for this elastic scattering case (b), then for small angle deflection ($\theta \sim 0$)

$$(k - k' \cos \theta) = 0.$$

For case (a) we can perform the z integration analytically

$$\int_{-\infty}^{\infty} dz V \exp \left[-\frac{i\mu}{\hbar^2 k} \int_{-\infty}^z V dz' \right] = \frac{i\hbar^2 k}{\mu} \exp \left[-\frac{i\mu}{\hbar^2 k} \int_{-\infty}^z V dz' \right] \Big|_{z=-\infty}^{z=+\infty} \quad (2.56)$$

where the contribution from $z = -\infty$ on the r.h.s of (2.56) vanishes in the exponent. The scattering amplitude becomes

$$f(\mathbf{k}', \mathbf{k}) = -i \frac{k}{2\pi} \int d^2 b e^{i\mathbf{q} \cdot \mathbf{b}} (e^{i\delta(\mathbf{b})} - 1) \quad (2.57)$$

After angular integration of the polar coordinate ϕ^4 , the scattering amplitude becomes

$$f(k, \theta) = -ik \int_0^{\infty} db b J_0(|q_x|b) (e^{2i\delta(b)} - 1) \quad (2.59)$$

where

$$\delta(b) \equiv \frac{-\mu}{2k\hbar^2} \int_{-\infty}^{+\infty} V(\sqrt{b^2 + z^2}) dz. \quad (2.60)$$

In (2.60) the impact parameter b is fixed and the expressions integrated along the straight-line path z . Note that there is no contribution from the term between brackets in (2.59) if b is greater than the range of V .

If we choose, for instance, the z -axis position to be the case (b) of App. A.1, then

$$f(k, \theta) = -ik \int_0^{\infty} db b J_0(2k \sin(\theta/2) b) (e^{2i\delta(b)} - 1) \quad (2.61)$$

The total cross section given by optical theorem is

$$\sigma_{\text{tot}} = 2 \int d^2 b (1 - \text{Re} [e^{2i\delta(b)}]), \quad (2.62)$$

and by carrying out the angular integration of (2.61)

$$\sigma_{\text{sca}} = \int d^2 b |e^{2i\delta(b)} - 1|^2. \quad (2.63)$$

Subtracting the two expressions, one finds for the absorption cross section

$$\sigma_{\text{abs}} = \int d^2 b (1 - |e^{2i\delta(b)}|^2). \quad (2.64)$$

In the absence of absorption, i.e $\delta(b)$ real, the scattering and the total cross sections are

4

$$\int_0^{2\pi} d\phi e^{-ix \cos(\phi)} = 2\pi J_0(x) \quad (2.58)$$

equal.

2.2.4.1 Eikonal approach for $O^{16}(n, n)$ elastic scattering data at 95 MeV

As an example of the use of the eikonal approximation, the $O^{16}(n, n)$ elastic scattering data at 95 MeV (MERMOD *et al.*, 2006) is studied. A complex Wood Saxon (WS) potential is used for the nuclear interaction,

$$V(r) = \frac{V_0 + iW_0}{1 + \exp\left[\frac{(r-R_0)}{a_0}\right]}, \quad (2.65)$$

where

$$R_0 = r_0 A^{1/3}, \quad (2.66)$$

is the nuclear radius with $r_0 = 1.3$ fm and $a_0 = 0.65$ fm the diffuseness of the nuclear surface.

Figure 2.6 shows the real and imaginary part of the T -matrix (term between brackets of 2.61) for a pure real, pure imaginary and complex Wood Saxon potential. All T -matrices are sensible to values of the impact parameter up to a potential range ≈ 6 fm. One may note that with an imaginary potential, see Fig.2.6(b), $\text{Im}[T]$ vanishes, representing a pure absorptive process.

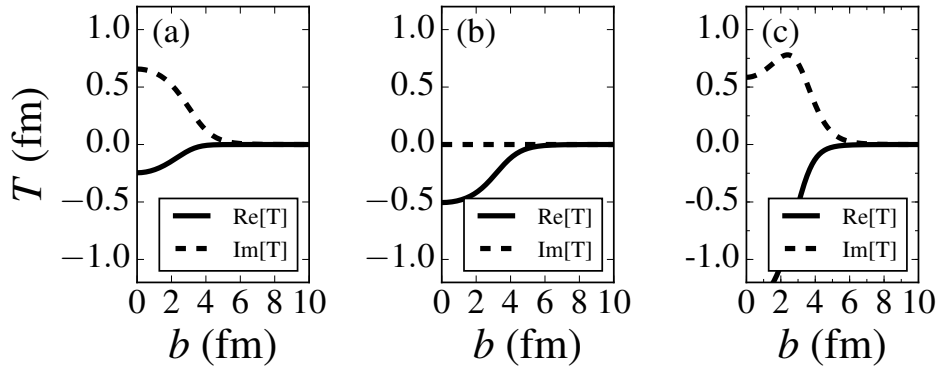


FIGURE 2.6 – Real (solid) and imaginary (dashed) parts of the T matrix for a Wood Saxon potential with: $V_0 = -10$ and $W_0 = 0$ MeV (a); $V_0 = 0$ and $W_0 = -10$ MeV (b); $V_0 = -30$ and $W_0 = -5$ MeV (c).

For the same WS potential parameters, we show the convergence of the differential cross section for different scattering angles in Figure 2.7. The convergence is associated with the range of the interaction of ≈ 6 fm. Beyond this value the T -matrix tends to zero and the cross section value is stable. Thus, the numerical integration can be usually stopped at a radius slightly larger than the potential range.

A better reproduction of the neutron elastic scattering data is obtained using a small weak absorptive potential, see Figure 2.8, with $V_0 = -30$ MeV for the real part and

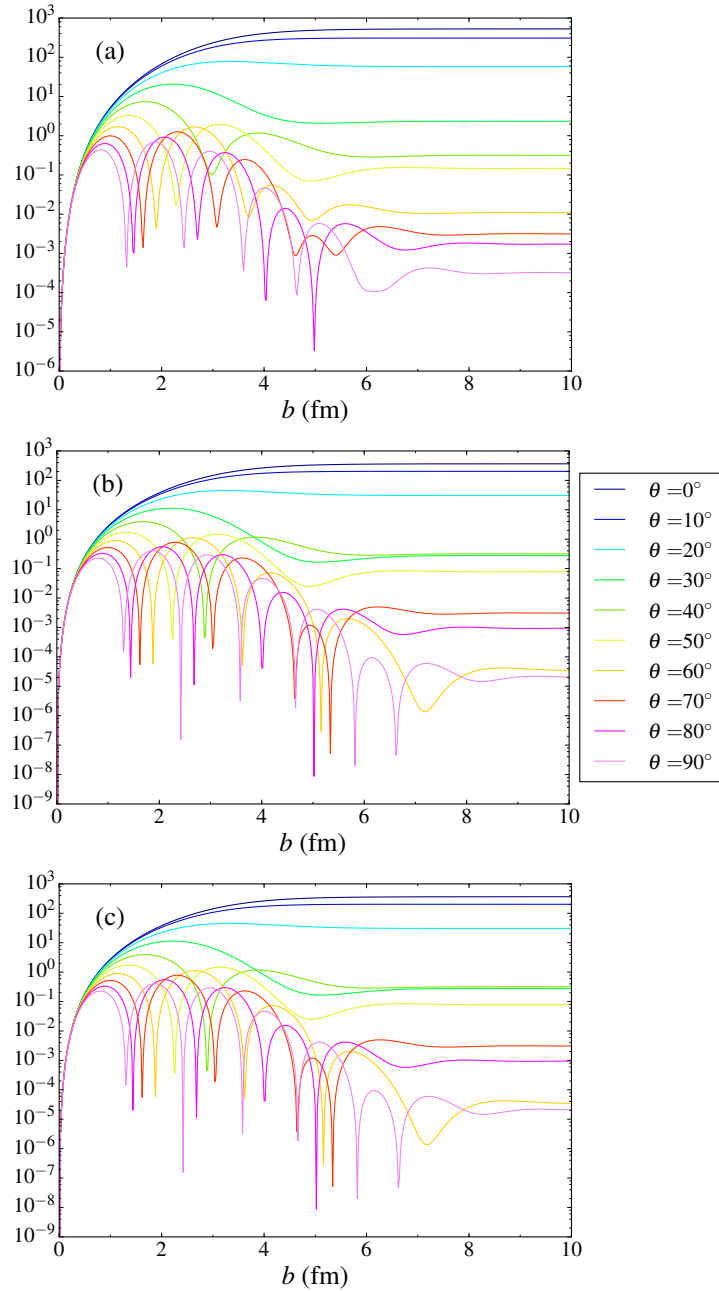


FIGURE 2.7 – Differential cross section convergence for different scattering angles considering the Wood Saxon potential with: $V_0 = -10$ and $W_0 = 0$ MeV (a); $V_0 = 0$ and $W_0 = -10$ MeV (b); $V_0 = -30$ and $W_0 = -5$ MeV (c).

$W_0 = -5$ MeV for the imaginary part of the Wood Saxon potential (Fig.2.8(b)). This is an attempt to study surface scattering characteristics. Apart from the oscillating cross-section behavior, our results show reasonable agreement with the data, as can be seen in Fig.2.8(a).

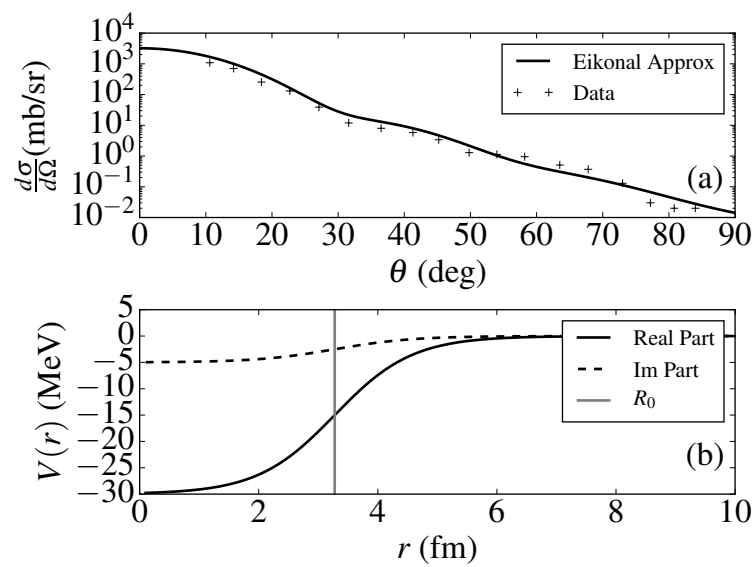


FIGURE 2.8 – (a) Differential cross-section computed for $E_0 = 95$ MeV neutron induced elastic scattering in the eikonal approximation. The plus mark represent the experimental data taken from (MERMOD *et al.*, 2006). (b) Wood Saxon potential with $V_0 = -30$ MeV, $W_0 = -5$ MeV and $a = 0.65$ fm. The nuclear radius R_0 is shown as the the vertical solid gray line.

2.2.4.2 Validity of the Eikonal Approximation

In the derivation of the eikonal wave functions, the V and S functions were assumed to vary slowly within a wave length. The resulting wave function

$$\psi(x) = e^{ikx - \frac{i}{\hbar v} \int_{-\infty}^x V(x') dx'}, \quad (2.67)$$

contains a correction to the free wave. The condition on V requires that $ka \gg 1$, where a stands for the length scale on which the potential varies. The second assumption requires that $k \gg V/\hbar v$, or

$$1 \gg \frac{V}{E}. \quad (2.68)$$

One may note that there is no restriction on the product of both

$$ka \frac{V}{E} = 2 \frac{Va}{\hbar v},$$

which makes the approximation valid for arbitrary values of

$$Va/\hbar v. \quad (2.69)$$

The eikonal approximation is very accurate for higher energy scattering, Buuck and Miller (BUUCK; MILLER, 2014) have shown that precision of about ten percent can be reached if the theory is taken beyond the first-order term. More recently, C. Hebborn and P. Capel (HEBBORN; CAPEL, 2017), have studied corrections in more detail. They addressed Wallace's corrections (further orders terms in the Taylor expansion of T matrix) and also a better way to account for the closest projectile-target approach. The eikonal approach usually provides larger values for the cross section at backward angles when compared to experimental data. A consequence of the assumption that the incident particles cross the target nucleus with only a small deflection. In (HEBBORN; CAPEL, 2017), a complex distance of maximum approach b'' is introduced, which produces accurate results up to 25° at 20 MeV/nucleon and up to 20° at 10 MeV/nucleon.

2.2.5 Scattering by the Coulomb Potential

When the Coulomb interaction

$$V(r) = \frac{Ze^2}{r} \quad (2.70)$$

is present in the potential, a difficulty appears in the calculation of (2.60) due to the logarithmic divergence at both extremes of the integration range,

$$2\delta(b) = \frac{-mZe^2}{\hbar^2k} \int_{-\infty}^{\infty} \frac{dz}{\sqrt{b^2 + z^2}}. \quad (2.71)$$

In nuclear scattering experiments it is possible to say that the Coulomb interaction takes place in a limited target region (atomic radius). This region is small compared to laboratory dimensions but large compared to particle wavelengths. The field felt by the particles fall off rapidly enough with distance to permit an approximated method of regularization. Differential cross-sections are difficult to be measured for small angle deflections due to incident beam's finite width. This leads to an upper limit on the impact parameter values. In addition, forward scattered particles ($\theta = 0$) are difficult to be distinguished from the incident beam.

The incident particles experience a target nucleus potential screened by surrounding electrons. The screened Coulomb potential can be written as

$$V(r) = \frac{Ze^2}{r} F(r) \quad (2.72)$$

where the regularization function $F(r) \rightarrow 0$ as $r \rightarrow 0$. This ensures the convergence of the integral.

If $F(r) = e^{-r/a}$ is used, the Yukawa potential is recovered. The simplest choice for $F(r)$ is

$$F(r) = \begin{cases} 0 & \text{if } r > a \\ 1 & \text{if } r < a \end{cases}$$

which leads to ($r = a = \sqrt{b^2 + z^2}$, so $z = \sqrt{a^2 - b^2}$)

$$2\delta(b) = \frac{-mZe^2}{\hbar^2k} \int_{-\sqrt{a^2-b^2}}^{\sqrt{a^2-b^2}} \frac{dz}{\sqrt{b^2 + z^2}} = \frac{-mZe^2}{2\hbar^2k} \int_{-\tan^{-1}\left(\frac{\sqrt{a^2-b^2}}{b}\right)}^{\tan^{-1}\left(\frac{\sqrt{a^2-b^2}}{b}\right)} \sec \theta d\theta$$

where $z = b \tan \theta$ and $\sec^2 \theta = \sqrt{1 + \tan^2 \theta}$ were used. Performing this integral and using again the $\sec^2 \theta$ relation

$$\begin{aligned}
2\delta(b) &= \ln |\sec \theta + \tan \theta| \Big|_{-\tan^{-1}\left(\frac{\sqrt{a^2-b^2}}{b}\right)}^{\tan^{-1}\left(\frac{\sqrt{a^2-b^2}}{b}\right)} = \ln \left| \frac{\sqrt{1 + \left(\frac{\sqrt{a^2-b^2}}{b}\right)^2} + \left(\frac{\sqrt{a^2-b^2}}{b}\right)}{\sqrt{1 + \left(\frac{\sqrt{a^2-b^2}}{b}\right)^2} - \left(\frac{\sqrt{a^2-b^2}}{b}\right)} \right| \\
&= \ln \left| \frac{\sqrt{b^2 + (\sqrt{a^2-b^2})^2} + \sqrt{a^2-b^2}}{\sqrt{b^2 + (\sqrt{a^2-b^2})^2} - \sqrt{a^2-b^2}} \right| = \ln \left| \frac{\sqrt{b^2 + (a^2-b^2)} + \sqrt{a^2-b^2}}{\sqrt{b^2 + (a^2-b^2)} - \sqrt{a^2-b^2}} \right| \\
&= \ln \left| \frac{a + \sqrt{a^2-b^2}}{a - \sqrt{a^2-b^2}} \right| = \ln \left| \frac{(a + \sqrt{a^2-b^2}) \times (a + \sqrt{a^2-b^2})(a - \sqrt{a^2-b^2})}{(a - \sqrt{a^2-b^2}) \times (a + \sqrt{a^2-b^2})(a - \sqrt{a^2-b^2})} \right| \\
&= \ln \left(\frac{a + \sqrt{a^2-b^2}}{b} \right)^2 = 2 \ln \left(\frac{a + \sqrt{a^2-b^2}}{b} \right)
\end{aligned}$$

Finally,

$$2\delta_C(b) = \begin{cases} 0 & \text{if } b > a \\ -\frac{2mZe^2}{\hbar^2 k} \ln \left(\frac{a + \sqrt{a^2-b^2}}{b} \right) & \text{if } b < a \end{cases} \quad (2.73)$$

Taking $a \rightarrow \infty$ in (2.73), gives

$$\delta_C(b) = 2\eta \ln(kb), \quad (2.74)$$

where

$$\eta = \frac{Ze^2\mu}{\hbar^2 k}. \quad (2.75)$$

The eikonal phase can be written as a sum of nuclear and Coulomb contributions as

$$e^{2i\delta(b)} = e^{i(2\delta_{\text{Nucl}}(b) + 2\delta_C(b))}. \quad (2.76)$$

One may rewrite (2.76) as

$$e^{2i\delta(b)} = [e^{2i\delta_C(b)} (e^{2i\delta_{\text{Nucl}}(b)} - 1) + e^{2i\delta_C(b)}], \quad (2.77)$$

and inserting it in the elastic scattering amplitude (2.61) produces

$$f_{\text{el}}(\theta, k) = -ik \int b db J_0(qb) [e^{2i\delta_C(b)} (e^{2i\delta_{\text{Nucl}}(b)} - 1) + e^{2i\delta_C(b)} - 1]. \quad (2.78)$$

The last two terms can be separated as a Coulomb amplitude defined by

$$f_C(\theta, k) = -ik \int b db J_0(qb) [e^{2i\delta_C(b)} - 1], \quad (2.79)$$

which after integration gives

$$f_C(\theta, k) = \frac{\eta}{2k \sin^2(\theta/2)} \exp[-i2\eta \ln(\sin(\theta/2)) + i\pi + 2i\phi_0], \quad (2.80)$$

where $\phi_0 = \arg \Gamma(1 + i\eta)$. The phase ϕ_0 can be computed using the following identity (ABRAMOWITZ; STEGUN, 1964)

$$\arg \Gamma(x + iy) = y\xi(x) + \sum_{j=0}^{\infty} \left(\frac{y}{j+x} - \arctan \frac{y}{j+x} \right), \quad (2.81)$$

where $\xi(z) = \Gamma'(z)/\Gamma(z)$. This gives, with $\Gamma'(1) = -e$ and $\Gamma(1) = 1$,

$$\phi_0 = -\eta e + \sum_{j=0}^{\infty} \left(\frac{\eta}{j+1} - \arctan \frac{\eta}{j+1} \right). \quad (2.82)$$

The final elastic scattering amplitude becomes

$$f_{el}(k, \theta) = f_C(\theta) - ik \int b db J_0(qb) [e^{2i\delta_C(b)} (e^{2i\delta_{\text{Nuc}}(b)} - 1)]. \quad (2.83)$$

This formula has the advantage that the term $(e^{i\delta_{\text{Nuc}}(b)} - 1)$ goes to zero rapidly for impact parameters b larger than the nucleus radius. This, dominates the Coulomb part $e^{i\delta_C(b)}$, ensuring numerical convergence of the integral.

2.2.6 Inelastic Scattering

For events where the energy of the incident projectile differs from that of the outgoing particle, we generalize the transition rate between states of well defined energy, which is proportional to

$$|T_{fi}|^2 \delta(E_i - E_f),$$

to one that describes transitions in the interval E_f and $E_f + dE_f$, proportional to

$$|T_{fi}|^2 \rho_f, \quad (2.84)$$

where $\rho_f = d^3k_f/dE_f$ is the density of final states per unit of energy (with only one particle being emitted (KURT; TUNG-MOW, 2003)). This is a generalization of the Golden Rule. The cross-section can now be obtained from the transition rate divided by the incident

flux, reading

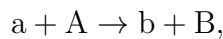
$$\frac{d\sigma}{d\Omega_f} = \frac{\mu_i \mu_f}{(2\pi\hbar^2)^2} \frac{k_i}{k_f} |T_{fi}|^2, \quad (2.85)$$

where $T_{fi} = \langle \psi_f | V | \psi_i^{(+)} \rangle$.

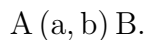
2.3 Nuclear Reactions

Nuclear reactions are collisions involving nuclei in which final states can be differentiated from the initial projectile and target ones.

Let a be an incident projectile and A a target nucleus. Their collision resulting in the products, b and B , is represented by



or



It is very common to have a particle or light nuclei for a and b and for A , B a heavy nucleus. An experiment usually measures b with different energies and scattering angle θ in the laboratory frame. These reactions can involve complex interactions which makes them examples of quantum chaotic behavior as well as a prime area to apply quantum physics, statistical mechanics and many-body techniques.

The mechanism of a nuclear reaction can be roughly divided into three types – the compound, direct and preequilibrium components. The projectile can be scattered by the target or initiate a chain of internal collisions. The fast processes are responsible for direct emissions. If the collisions continue until equilibration of the system is reached – when initial energy is equally distributed among the nucleons, a compound nucleus is formed. Particles and radiation are later emitted from the hot (compound) nucleus. Processes of emission occurring before equilibrium are named pre-equilibrium or pre-compound reactions. Although the energy range in which they occur is difficult to define, direct reactions generally prevail over compound nucleus formation at high energies while at low energies compound nucleus formation dominates. In what follows, some basic information on both compound and direct reactions is presented. A subsequent entire chapter is devoted to the preequilibrium mechanism.

2.3.1 Compound Nuclear Reactions

Compound reactions can be represented by



where the star represents an excited state of the compound nucleus. These are slow reactions of about $10^{-14} - 10^{-16}$ seconds, where the incident particle is captured becoming indistinguishable within the target nucleus. The decaying of C^* happens via evaporation (emission) of one or more particles, and even more emissions can occur if the excitation energy is sufficient. The number of possible emitted particles increases with the excitation energy. Gamma ray emission dominates the evaporation process for very small values of energy of the compound nucleus. The time scale involved is so large that the way in which the compound nucleus is formed becomes irrelevant, i.e., the system does not have memory of its formation. This implies that the emissions depend only on the conserved quantities – energy, parity and angular momentum of the compound nucleus.

The compound nucleus $^{64}\text{Zn}^*$ can be formed in different ways, for example in $p+^{63}\text{Cu}$ or $\alpha+^{60}\text{Ni}$ reactions. Independently of how the excited state of Zn was formed, its decay process can produce different products (exit channels), e.g., $^{63}\text{Zn} + n$, $^{62}\text{Zn} + 2n$ or $^{62}\text{Cu} + n + p$ (GHOSHAL, 1950). The independence of the cross section from initial channel is presented in Figure 2.9. One notes that the curves are similar and the distributions only depends on the exit channels. Another experimentally verified characteristic of such reactions is the isotropic distribution (in the CM) of the differential cross section of fragments, with the exception of small deviations for heavy ion projectile where large angular momentum transfer takes place. The angular distribution is symmetric about 90° due to parity conservation.

2.3.2 Direct Nuclear Reactions

At high energy of the incident particle, reactions tends to occur in which a single hit interaction takes place without compound nuclei formation. The projectile-target interaction time is short, $10^{-20} - 10^{-21}$ seconds, compared to the time for compound nucleus formation. This roughly the time needed for the particle to cross the target nucleus. These events present different processes, such as stripping and pick-up reactions (with transfer of nucleons), as well as elastic and inelastic scattering. They are called direct nuclear reactions.

A knock-out reaction, happens when the projectile removes, in general, one particle from the target nucleus, resulting in three reaction products $A(a,bc)B$, e.g., $^5\text{Li}(p, 2p)$. These are commonly used to study deep single-particle states and also to excite target collec-

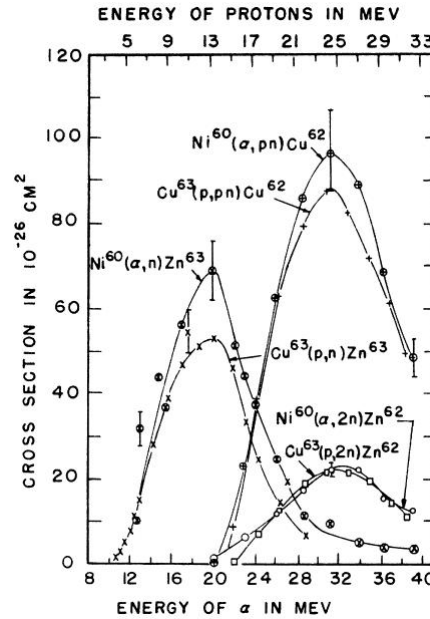


FIGURE 2.9 – Experimental cross sections for (p, n) , $(p, 2n)$ and (p, pn) involved in the ^{63}Zn compound nucleus formation. The scale of alpha particles were scaled with respect to proton energy to both correspond to the same excitation energy (GHOSHAL, 1950).

tive states. In a stripping reaction, the projectile nucleons are transferred to the target nucleus, e.g., (d, p) and $^{32}\text{S}(^{14}\text{N}, ^{13}\text{N})^{33}\text{S}$. These reactions present a diffraction like angular distribution with higher values for forward angle scattering.

In general, the mechanism acting in a reaction is not restricted to a certain incident projectile energy and neither are the products of nuclear reactions. They can partly formed by compound formation and partly by direct reactions.

2.4 Pre-equilibrium Mechanism

At intermediate time scales, there are events occurring after the first stage of the direct component. They happen with a relatively few number of collisions if compared to compound nucleus formation. They are called pre-equilibrium reactions. The evidence for such a mechanism relies on the distribution in energy of emitted particles at the high energy part of the spectrum.

Griffin in 1966 (GRIFFIN, 1966) proposed the first theory to explain preequilibrium emissions, the semi-classical exciton model. Over the years, extensions to his model as well as quantum models have been developed. Figure 2.10 present in the top panel the typical energy spectra of preequilibrium reactions, the bottom panel shows the associated angular distribution transition from isotropic compound (A) to direct components (D). The exciton model treats the region between both of them, while the quantum description

can be separated in two contributions in the Multi-Step reaction framework. The region (B) stands for the multi-step compound (MSC) formalism and on the right side (C) the multi-step direct (MSD) reactions take place.

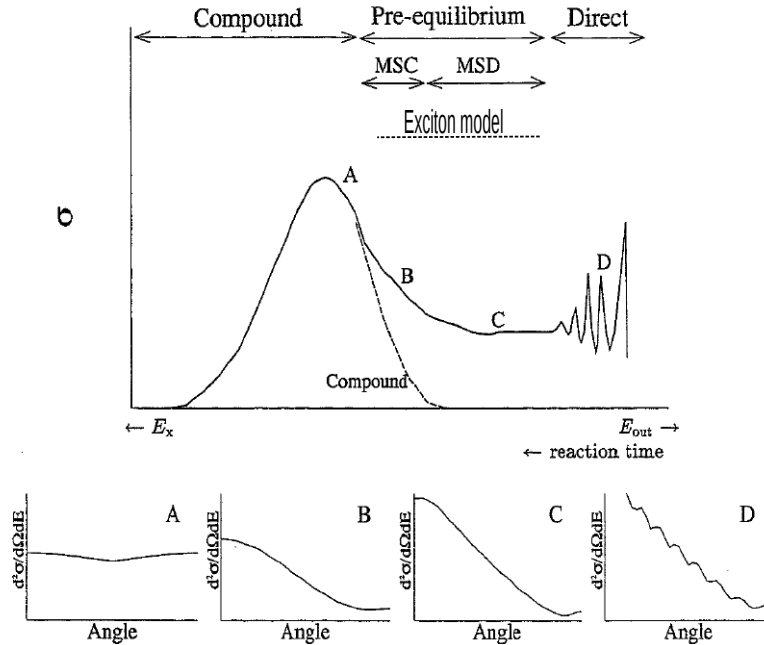


FIGURE 2.10 – Schematic representation of a general cross section distribution for pre-equilibrium reactions (topper panel) and angular distribution of each phase from (A) compound to (D) direct components (bottom panel). Adapted from (KONING; AKKERMANS, 1999).

The next sections are devoted to present both classical and especially, the quantum mechanical models.

2.4.1 Semi-Classical Models

The exciton emission model was proposed by Griffin (GRIFFIN, 1966) to explain the observed excess of high energy neutrons in (p, n) proton-neutron reactions (HOLBROW; BARSCHALL, 1963; WOOD *et al.*, 1965; BORCHERS *et al.*, 1966) relative to the compound nucleus decay.

In a proton induced reaction, the projectile-target collision creates initially a two-particle one-hole state (2p-1h). This happens via an interaction between the incident proton with a nucleon of the target nucleus. For energies below 200 MeV, the nucleon wave length is larger than 2 fm and the nucleon-nucleus interaction produces excitations composed by a linear combination of particle-hole states instead of just an individual configuration of this kind. This makes the identification of a particle-hole (p-h) pair of occupied or unoccupied single particle states difficult, as only their global characteristics, such as excitation energies, total angular or total total linear momenta are determined. Subsequent

interactions caused by a nucleon of the nucleus can create, spread or destroy p-h pairs. The classical exciton model classifies states according to the number of particles p and the number of holes h and also assume that all states with same number of particle and holes are equally populated. Since the total particle number is conserved the difference between particle and holes $p - h$ is constant during the reaction. The quantity called exciton number n is defined by the sum of all particle and holes $n = p + h$. For low n configurations, the particle emission is more energetic and more forwardly distributed when compared to compound nucleus evaporation.

A time-dependent master equation was proposed by Cline and Blann, where the competition between transitions to different exciton configuration with particle emissions can be treated, taking into account energy but no angular momentum conservation (CLINE; BLANN, 1971). The model is taken as the time evolution for the cross section fraction $P(n)$ of the n exciton configuration

$$\frac{dP(n)}{dt} = \lambda_-(n+2)P(n+2) + \lambda_0(n)P(n) + \lambda_+(n-2)P(n-2) - \lambda(n)P(n) \quad (2.86)$$

where $\lambda(n)$ is the total rate of transitions out of an n -exciton configuration,

$$\lambda(n) = \lambda_-(n) + \lambda_0(n) + \lambda_+(n) + \lambda_e(n),$$

with $\lambda_e(n)$ being the total particle emission rate from the n -exciton configuration. $\lambda_-(n)$, $\lambda_0(n)$, and $\lambda_+(n)$ represent averages of transition rates from the n to $n-2$, n and $n+2$ exciton configuration, respectively. At each transition, a new p-h pair is created and all transitions must be related to a ± 2 changes in the exciton number. The exciton transition rate $\lambda_0(n)$ cancels and does not contribute to the time evolution.

Fermi's golden rule can be used to compute the internal transition rates as a summation over all squared residual interaction matrix elements corresponding to the transition from initial to final configurations. This sum can be approximate by the product of the value of the mean squared matrix element of the residual interaction $|M|^2$ with the density of available states. For transitions changing the exciton number, the density of available states corresponds to the average number of ways in which an initial exciton configuration can be converted into three excitons (or that three excitons could be converted into one), assuming that those transitions are equally probable. In the case of exciton number conservation the density counts the number of ways, in average, any pair of excitons may scatter from one another with the same probability. Expressions for these densities were obtained by Williams (WILLIAMS, 1970) and later corrected by Cline (CLINE, 1972) with the use Pauli exclusion principle.

The hybrid model (BLANN, 1971; BLANN, 1972; BLANN, 1973) uses state densities

from the exciton model to determine the probability that a particle or hole has a given energy. Then the corresponding transition and emission rates can be determined. Exciton model results, where the integrated transition and emission rates are used to determine the competition between scattering and emission, can be reproduced by a modification of the total transition rate magnitude.

Blann and Vonach showed that the hypothesis of equal occupation of all states is reasonably satisfied for the initial transitions to the 2p-1h exciton configuration of a nucleon induced reaction (BLANN; VONACH, 1983). Bisplinghoff has shown that this is not the case for more complex transitions (BISPLINGHOFF, 1986). The hypothesis would still be reasonable if the transition rate $\lambda_0(n)$ became very large compared to those that modify the exciton configuration $\lambda_{\pm}(n)$. Although this would allow the equilibrium to be reached between transitions, this is rarely the case, with

$$\lambda_+(n) > \lambda_0(n) > \lambda_-(n) \quad (2.87)$$

for small exciton number n , with the exception of extremely low excitation energy where the pre-equilibrium emission is suppressed. The reason is that when n is small the density of $n+2$ exciton configuration states is relatively large compared to the density of n exciton states. Fig.2.11 shows the exciton number of the configuration defining equilibrium n_{eq}

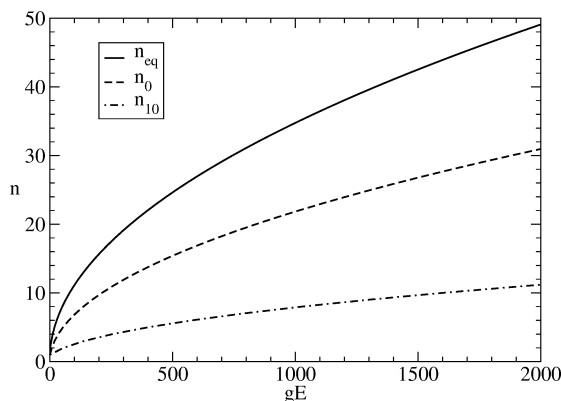


FIGURE 2.11 – Average number of excitons at equilibrium, n_{eq} , and minimum number of excitons necessary to reach equilibrium within a configuration n_0 as a function of the product of the density of one particle density states and the excitation energy (gE). n_{10} curve is described in the text.

$$\lambda_+(n_{eq}) = \lambda_-(n_{eq}), \quad (2.88)$$

as a function of the product of the density of one particle states $g \approx A/13 \text{ MeV}^{-1}$ and the excitation energy E . Also shown is the minimum number of excitons needed to reach

equilibrium within a configuration between subsequent transitions, n_0 , defined by

$$\lambda_+(n_0) = \lambda_0(n_0). \quad (2.89)$$

For Fig.2.11 it was assumed that the average matrix element that induces the configuration changing transitions is equal to that among states of the same configuration. The n_{10} curve represent the exciton number for equilibration within a configuration when the average squared transition matrix elements among the states of a configuration is ten times bigger than that of the transitions between configurations. This could be the case for low excitation energies (SATO; YOSHIDA, 1987) where the hole-hole transitions dominate $\lambda_0(n)$. For higher excitation energies, however, the p-h and p-p matrix elements dominates in the transition rates, resulting in average matrix elements that are similar in magnitude (POMPEIA *et al.*, 2007).

Equilibrium for the 3p-2h ($n = 5$) configuration can be reached for values of gE below 50 MeV, see Fig.2.11, corresponding to excitation energies of about 17 MeV and 3 MeV in ^{40}Ca and ^{208}Pb , respectively. The minimum number of excitons necessary for equilibrium increases as $n_0 \approx \sqrt{0.4gE}$ and the exciton number for global equilibrium as $n_{eq} \approx \sqrt{gE}$. Thus, at low excitation energy the good agreement of the hybrid and exciton model with pre-equilibrium spectra is justified, but more complex configurations are occupied as E increases and the hypothesis of equally occupied configurations of the exciton and hybrid model fails.

This problem was overcome by the Blann hybrid Monte Carlo simulation model (BLANN, 1996), later improved with Chadwick (BLANN; CHADWICK, 1998) to a model of double differential pre-equilibrium spectra. This model computes the transition rates as a function of energy – like the hybrid model, and uses the transition rates to 2p-1h and 1p-2h configurations corresponding to the individual particles and holes. A Monte Carlo selection from the 2p-1h and 1p-1h distributions is then used to determine the energies of the particles and holes after collisions. This is similar to an intranuclear cascade performed in an energy-angle space rather than phase space. This is justified by the relatively low nucleon kinetic energy of this type of reaction (below 200 MeV), where the indistinguishability of nucleons in the nucleus is still present due to the large wave length at these energies. These models don't completely describe the high energy component of spectra, where collective effects are important nor backward angles scattering in which quantum coherence effects are present. This would require a quantum mechanics model of pre-equilibrium reactions.

Before turning to the quantum mechanical formalism, an overview of the weaknesses of the semi-classical models are convenient. Although the exciton and hybrid model do not take into account transition rates of states within the same configuration, $\lambda_0(n)$, their equal occupancy hypothesis is consistent with strong transition rates among states within

the same configuration, if equilibrium is always reached before another configuration is occupied. In contrast, the hybrid Monte Carlo model takes $\lambda_0(n) = 0$ neglecting completely these transition rates. Pompeia et al (POMPEIA; CARLSON, 2006) studied which of the models reflects best the physical case. They included all transition rates in a Monte Carlo extension of the Blann and Chadwick model. The transition rate among states of the same configuration is found to be negligible when all average matrix elements are equal, which is believed to be close to the physical case. The exciton model result was reproduced only after an extreme increase (a factor of 1000) of the average matrix elements between states of the same configuration. This suggests that the hybrid Monte Carlo simulation provides a better semi-classical description of pre-equilibrium emission process.

2.4.2 Quantum Models

An advantage of pre-equilibrium quantum models is the possibility of distinguishing between bound and continuum states, which is not possible in semi-classical approaches. The exciton idea is still used here as a tool to define a continuum P and bound Q state space decomposition. With the emphasis on nucleon-induced reactions the decomposition can be write as

$$\begin{aligned} P &= P_1 + P_3 + P_5 + P_7 + \dots, \\ Q &= Q_3 + Q_5 + Q_7 + \dots \end{aligned} \tag{2.90}$$

Reactions occurring in P space are called multistep direct (MSD) reactions. These contain the elastic component P_1 and a series of components increasing in exciton number where it is assumed that only one of the nucleons involved is in the continuum. The continuum nucleon-target interaction provides the progression along the stages of the P chain, although interactions within the target could also do this.

The chain of bound Q space states start with an exciton configuration $n = 3 \rightarrow Q_3$, since the incident nucleon must collide with at least one target nucleon in order to form a 2p-1h configuration of the nucleus. Reactions in the compound space Q are known as multistep compound (MSC) reactions.

The pioneers in the multistep direct reaction formalism were: Feshbach, Kerman e Koonin (the so-called FKK model) (FESHBACH *et al.*, 1980); Tamura, Udagawa e Lenske (TAMURA *et al.*, 1982) and were followed later by Nishioka, Weidenmüller e Yoshida (NISHIOKA *et al.*, 1988). The first model of multistep compound nuclear reactions was developed by Agassi, Weidenmüller and Mantzouranis (AGASSI *et al.*, 1975). This model was derived again in a more rigorous way a decade later (NISHIOKA *et al.*, 1986).

2.4.2.1 Multistep Compound Nuclear Reaction

In this model, only bound states are included in the densities of states and levels. Thus, it turns out to be similar to an exciton model restricted to transitions between bound single particle states (STANKIEWICZ *et al.*, 1985; OBLOŽINSKÝ, 1986). In the MSC model the energy of the incident particle needs to be reduced by a value of a bound state in the absorption process. Unlike the exciton model, one needs an interaction to occur in order to have particle emission from the compound system. With the internal transition factors, $\lambda_{\pm}(n)$ and $\lambda_0(n)$, the elements that describe emission can change the number of exciton by two $Y_{c\pm}(n)$ or zero $Y_{c0}(n)$ units (taking into account the particle in the continuum). One particle to two-particle configuration transitions don't contribute to emission rates due to the restrictions of no bound states in the initial configuration. A more detailed discussion of the multistep compound theory can be found in (BONETTI *et al.*, 1991).

The MSC model has the same conceptual problem as the exciton and hybrid ones: the equally occupation of configuration states with more than three excitons can not be justified. This problem still exists when the energy becomes higher and MSD reaction takes place before forming the MSC states, because the minimum number of excitons necessary for equilibration within a configuration also increases with energy.

2.4.2.2 Multistep Direct Nuclear Reaction

The expressions of the MSD reaction model are obtained analyzing the P chain, presuming excitations large in number but individually weak. The main objective of this thesis is the study of reactions in the continuum state space. Thus, a detailed description of the MSD model is required. For this, we follow (NISHIOKA *et al.*, 1988; KONING; AKKERMANS, 1991; BONETTI *et al.*, 1994).

Let the total Hamiltonian be

$$H = H_{\text{res}} + H_{\text{rel}} + V \quad (2.91)$$

where H_{res} represents the target nucleus, H_{rel} the relative motion of the leading particle in the mean field of the target nucleus and V a perturbation term accounting for the residual interaction of the leading particle with the target nucleus.

The $|n\rangle$ states are eigenstates of eigenvalue E_n of

$$H_{\text{res}} |n\rangle = E_n |n\rangle. \quad (2.92)$$

The above Hamiltonian is composed of the sum, $H_{\text{res}} = H_0 + H_1$, of a shell model Hamil-

tonian H_0

$$H_0 = \sum_{i=1}^{A-1} [K(i) + U(i)], \quad (2.93)$$

where K and U are the kinetic energy and the shell model potential, respectively, and residual interaction of the target nucleus H_1

$$H_1 = \sum_{i<j}^{A-1} v(i, j) - \sum_i^{A-1} U(i), \quad (2.94)$$

where v is the two body nucleon interaction.

We let the complete set of p-h states generated by H_0 be

$$H_0 |m\mu\rangle = E_{m\mu} |m\mu\rangle, \quad (2.95)$$

where m represent the number of particle and holes (mp - mh – exciton class) for each p-h configuration μ .

The eigenstates of (2.92) can be expanded in a linear combination of $|m\mu\rangle$ states caused by the residual interaction H_1 as

$$|n\rangle = \sum_{m\mu} a_{m\mu}^n |m\mu\rangle. \quad (2.96)$$

The second term, H_{rel} , of the total Hamiltonian (2.91), depends on the incident nucleon kinetic energy and the optical potential representing the relative motion between the projectile and the target. The dynamics is represented by a distorted wave $|\chi^{(+)}(\mathbf{k})\rangle$

$$H_{\text{rel}} |\chi^{(+)}(\mathbf{k})\rangle = E_k |\chi^{(+)}(\mathbf{k})\rangle, \quad (2.97)$$

where E_k is the relative kinetic energy and the $(+)$ designates the outgoing solution. The $|\chi^{(+)}(\mathbf{k})\rangle$ wave functions alone don't form an orthonormal and complete basis due to the complex part of the H_{rel} operator (SATCHLER, 1983). The use of their bi-orthogonally conjugated counterparts $|\hat{\chi}^{(+)}(\mathbf{k})\rangle$ is required with

$$H_{\text{rel}}^* |\hat{\chi}^{(+)}(\mathbf{k})\rangle = E_k |\hat{\chi}^{(+)}(\mathbf{k})\rangle. \quad (2.98)$$

The orthonormality and completeness relations are

$$\langle \hat{\chi}^{(+)}(\mathbf{k}') | \chi^{(+)}(\mathbf{k}) \rangle = \langle \chi^{(+)}(\mathbf{k}) | \hat{\chi}^{(+)}(\mathbf{k}') \rangle = \delta(\mathbf{k} - \mathbf{k}'), \quad (2.99)$$

$$\int d\mathbf{k} |\chi^{(+)}(\mathbf{k})\rangle \langle \hat{\chi}^{(+)}(\mathbf{k})| = 1. \quad (2.100)$$

The interaction V is responsible for transitions between states of the projectile-plus-

target system. These transition elements are represented by the T -matrix computed in the Born-like expansion

$$\begin{aligned} T_{f\leftarrow 0} &= \langle \chi^{(-)}(\mathbf{k}) | \langle f | V + VGV + VGVGV + \dots | 0 \rangle | \chi^{(+)}(\mathbf{k}_0) \rangle \\ &= \sum_{i=1}^{\infty} T_{f\leftarrow 0}^i, \end{aligned} \quad (2.101)$$

where $|0\rangle | \chi^{(+)}(\mathbf{k}_0) \rangle$ and $\langle f | \langle \chi^{(-)}(\mathbf{k}) |$ stands for the initial (nucleus in its ground state) and final state, respectively. The propagator G in (2.101) is given by

$$G = \sum_n \int d\mathbf{k}_1 \frac{|n\rangle | \chi^{(+)}(\mathbf{k}_1) \rangle \langle \hat{\chi}^{(+)}(\mathbf{k}_1) | \langle n |}{E - E_n - E_{k_1} + i\epsilon}. \quad (2.102)$$

The \mathbf{k}_1 integral of (2.102) runs over positive (above binding energy) values of the leading particle momentum. This defines the P space corresponding to the multistep Born series. If the energy of the leading particle lies below the binding energy, the present formalism loses its validity and, instead, bound configurations would play a role in the multistep compound reaction description.

Transitions amplitudes can be used to calculate double differential cross sections as

$$\frac{d^2\sigma}{d\Omega dE_k} = \frac{m^2}{(2\pi\hbar^2)^2} \frac{k}{k_0} \sum_f |T_{f\leftarrow 0}|^2 \delta(E_f - E_x) \quad (2.103)$$

where E_x is the target excitation energy. This distribution is introduced for the purposed of later averaging over the many continuum states. The standard cross-section formula is recovered for discrete transitions when it is integrated over a small energy region around one particular state.

A simplification arises when averaging over a small excitation energy interval. Any cross terms should cancel out, e.g.,

$$\overline{\langle \chi^{(-)}(\mathbf{k}) | \langle f | V | 0 \rangle | \chi^{(+)}(\mathbf{k}_0) \rangle} \times \overline{\langle \chi^{(-)}(\mathbf{k}) | \langle f | VGV | 0 \rangle | \chi^{(+)}(\mathbf{k}_0) \rangle}, \quad (2.104)$$

due to incoherence of the amplitudes of the states involved when (2.101) is inserted in the double differential cross section equation (2.103).

This reduces the cross section to a sum of one-step and multi-steps terms (dropping bars)

$$\begin{aligned} \frac{d^2\sigma}{d\Omega dE_k} &= \frac{m^2}{(2\pi\hbar^2)^2} \frac{k}{k_0} \times \left[|\langle \chi^{(-)}(\mathbf{k}) | \langle f | V | 0 \rangle | \chi^{(+)}(\mathbf{k}_0) \rangle|^2 \right. \\ &\quad + |\langle \chi^{(-)}(\mathbf{k}) | \langle f | VGV | 0 \rangle | \chi^{(+)}(\mathbf{k}_0) \rangle|^2 \\ &\quad \left. + |\langle \chi^{(-)}(\mathbf{k}) | \langle f | VGVGV | 0 \rangle | \chi^{(+)}(\mathbf{k}_0) \rangle|^2 \dots \right] \\ \frac{d^2\sigma}{d\Omega dE_k} &= \sum_{n=1}^{\infty} \frac{d^2\sigma^n}{d\Omega dE_k}. \end{aligned} \quad (2.105)$$

Further simplification of the above equation requires other statistical assumptions that will be discussed in Sec. 2.4.3.

In the FKK model the use of an average residual interaction with exciton configuration densities is claimed to be sufficient to reduce the n-step cross section to a single step convolution like cross section. For instance, the two-step cross section is reduced to the convolution of two one-step cross sections as

$$\frac{d^2\sigma^{(2)}}{dEd\Omega}(\mathbf{k}, \mathbf{k}_0) = \int \frac{d\mathbf{k}'}{2\pi^3} \frac{d^2\sigma^{(1)}}{dEd\Omega}(\mathbf{k}, \mathbf{k}') \frac{d^2\sigma^{(1)}}{dEd\Omega}(\mathbf{k}', \mathbf{k}_0) \quad (2.106)$$

This model was compared to experimental data (BONETTI *et al.*, 1994) and used up to fourth order in including charge exchange reactions (KONING; CHADWICK, 1997). Although the model has shown to be efficient, the reduction to the convolution form requires the substitution in the intermediate propagators of

$$|\chi^{(-)}(\mathbf{k})\rangle \rightarrow |\hat{\chi}^{(+)}(\mathbf{k})\rangle, \quad (2.107)$$

to obtain the DWBA matrix elements. This elements differs from the normal DWBA matrix elements because $|\hat{\chi}^{(+)}(\mathbf{k}_1)\rangle$ is an eigenstate of the Hamiltonian with the complex conjugated optical potential and, secondly, has different boundary condition (BONETTI *et al.*, 1994).

Tamura, Udagwa and Lenske (TAMURA *et al.*, 1982; RAMSTRÖM *et al.*, 2004) developed an alternative approach using physical structures of the excitations but limited to two step reactions. Their approach uses a 1p-1h response function obtained by diagonalizing the target nucleus Hamiltonian in the 1p-1h expansion. Single-step calculation have been more rigorously performed in this model producing excellent agreement with data in the appropriate energy region (DUPUIS, 2006; DUPUIS *et al.*, 2011; DUPUIS, 2017).

For higher incident particle energy, more terms in the multistep direct reaction formalism become necessary. Tamura, Udagawa and Lenske extended the one-step response

function a two-step one by arguing that the microscopic structure of the intermediate states are incoherent on the average. With this assumption, they performed a convolution of the 1p-1h response function with itself to obtain a 2p-2h response function. However, they considered the correct boundary conditions of the intermediate propagator in the two-step cross section. The intermediate state statistics was claimed to be insufficient even for averages over microscopic structure by Nishioka, Weidenmüller and Yoshida, who claimed that a coherent 2p-2h response function should be used instead in order to obtain the two-step cross section. Their arguments in Ref.(NISHIOKA *et al.*, 1988) can be used in a general analysis of the hypotheses normally used to simplify the description of the multi-step direct reactions.

2.4.3 Randomness Statistics

The cross section equation (2.105) is still too difficult to be used due to the complicated large level density of excited states of the nucleus and quantum interference effects. The complexity of the coupled states leads to randomness assumptions that can be taken into account via energy averaging statistics. The two different types of randomness assumptions are discussed in what follows. For this, the final target states are represent as linear combination of particle-hole excitations

$$|f\rangle = \sum_{\mu} a_{\mu}^f |\mu\rangle, \quad (2.108)$$

where μ represents different p-h components.

2.4.3.1 Residual-System Statistics

The residual-system statistics related to random configuration mixing is associate with the residual nucleus alone and underlies in the basis of Tamura, Udagwa and Lenske model (TAMURA *et al.*, 1982; RAMSTRÖM *et al.*, 2004). The distribution of a_{μ}^f coefficients in the linear expansion (2.108 or 2.96) are assumed to be random and an energy averaging should be sufficient to eliminate non-diagonal coupling elements. The description of an one-step process becomes

$$\sum_f \langle 0|V|f\rangle \langle f|V|0\rangle = \sum_f \sum_{\mu\nu} a_{\mu}^f a_{\nu}^f \langle 0|V|\mu\rangle \langle \nu|V|0\rangle \delta(E_f - E_x), \quad (2.109)$$

which, when averaged over a small range of residual excitation energy gives

$$\overline{\sum_f \langle 0|V|f\rangle \langle f|V|0\rangle} = \overline{\sum_f \sum_{\mu} |a_{\mu}^f|^2 \langle 0|V|\mu\rangle \langle \mu|V|0\rangle} \delta(E_f - E_x). \quad (2.110)$$

In a more general expression, the approximation uses a Kronecker delta to select the excitations of the particle-hole index

$$\overline{\sum_f a_\mu^f a_\nu^f \delta(E_f - E_x)} = \delta_{\mu\nu} \overline{\sum_f |a_\mu^f|^2 \delta(E_f - E_x)}. \quad (2.111)$$

In this way, the relative contribution from p-h components to the real E_x level is represented by the distribution

$$\rho_\mu(E_x) = \sum_f |a_\mu^f|^2 \delta(E_f - E_x), \quad (2.112)$$

usually modeled as a Gaussian or a Lorentzian (Breit-Wigner) function. The magnitude of the residual interaction can be associated with the width of the distribution.

2.4.3.2 Leading-Particle Statistics

In leading-particle statistics the projectile-nucleus interaction V furnishes the randomness. This has been used in the convolution form of the FKK model (KONING; AKKERMANS, 1991). In this approach it is believed that V randomly connects a given nuclear state $|n\rangle$ to many other nuclear states and the energy averaging cancels cross products of matrix elements. The formalism can be represented as

$$\begin{aligned} & \overline{\langle \chi^{(+)}(\mathbf{k}_0) | \langle 0 | V | \nu \rangle | \chi^{(-)}(\mathbf{k}) \rangle \langle \chi^{(-)}(\mathbf{k}) | \langle \mu | V | 0 \rangle | \chi^{(+)}(\mathbf{k}_0) \rangle} \\ & = \delta_{\nu\mu} \overline{|\langle \chi^{(-)}(\mathbf{k}) | \langle \mu | V | 0 \rangle | \chi^{(+)}(\mathbf{k}_0) \rangle|^2}, \end{aligned} \quad (2.113)$$

where the bars represent the residual excitation energy E_x average over a small interval with sufficiently accessible states.

2.4.4 One-step Cross Section

In the one-step cross section, either by the use of residual-system or leading-particle statistics, the resulting expression (dropping bars) is the same

$$\frac{d^2\sigma^{(1)}}{d\Omega dE_k} \propto \sum_\mu \hat{\rho}_\mu(E_x) |\langle \chi^{(-)}(\mathbf{k}) | \langle \mu | V | 0 \rangle | \chi^{(+)}(\mathbf{k}_0) \rangle|^2, \quad (2.114)$$

where the effective density of particle-hole contributions is defined by

$$\hat{\rho}_\mu(E_x) = \sum_f |a_\mu^f|^2 \delta(E_f - E_x). \quad (2.115)$$

2.4.5 Two-step Cross Section

We employ the usual never-come-back assumption by supposing that the dominant process is that in which the leading particle always creates a new particle-hole pair, leaving the rest of the nucleons as spectators:

$$\langle f|V|n\rangle = \sum_{\nu} a_{1\nu,n}^f \langle 1\nu, n|V|n\rangle \quad (2.116)$$

and remarking that for two body forces the nuclear state can be expanded as a linear combination of p-h configurations

$$|n\rangle = \sum_{1\mu} a_{1\mu}^n |1\mu\rangle \quad (2.117)$$

so that,

$$\langle n|V|0\rangle = \sum_{1\mu} a_{1\mu}^n \langle 1\mu|V|0\rangle \quad (2.118)$$

The transition amplitude for the two-step cross section is

$$T_{f\leftarrow 0}^{(2)} = \langle \chi^{(-)}(\mathbf{k}) | \langle f|VGV|0\rangle | \chi^{(+)}(\mathbf{k}_0) \rangle, \quad (2.119)$$

where

$$G = \sum_n \int d\mathbf{k}_1 \frac{|n\rangle \langle \chi^{(+)}(\mathbf{k}_1) | \langle \hat{\chi}^{(+)}(\mathbf{k}_1) | \langle n|}{E - E_n - E_{k_1} + i\epsilon}. \quad (2.120)$$

Inserting (2.120) and (2.116) into (2.119) reads

$$\begin{aligned} T_{f\leftarrow 0}^{(2)} &= \langle \chi^{(-)}(\mathbf{k}) | \sum_n \int d\mathbf{k}_1 \sum_{\nu} a_{1\nu,n}^f \langle 1\nu, n|V|n\rangle \frac{| \chi^{(+)}(\mathbf{k}_1) \rangle \langle \hat{\chi}^{(+)}(\mathbf{k}_1) |}{E - E_n - E_{k_1} + i\epsilon} \\ &\quad \times \sum_{\mu} a_{1\mu}^n \langle 1\mu|V|0\rangle | \chi^{(+)}(\mathbf{k}_0) \rangle. \end{aligned} \quad (2.121)$$

Computing its squared modulus and summing over final states

$$\begin{aligned} \sum_f |T_{f\leftarrow 0}^{(2)}|^2 &= \sum_f \sum_{\mu} \sum_{\mu'} \sum_{\nu} \sum_{\nu'} \sum_n \sum_{n'} \int d\mathbf{k}_1 \int d\mathbf{k}'_1 a_{1\nu,n}^f a_{1\mu}^n a_{1\nu',n'}^f a_{1\mu'}^{n'} \\ &\quad \times \langle \chi^{(+)}(\mathbf{k}_0) | \langle 0|V|\mu'\rangle \langle \hat{\chi}^{(+)}(\mathbf{k}'_1) | \\ &\quad \times \frac{1}{E - E_{n'} - E_{k'_1} + i\epsilon} \langle \chi^{(+)}(\mathbf{k}'_1) | \langle n'|V|\nu', n'\rangle | \chi^{(-)}(\mathbf{k}) \rangle \\ &\quad \times \langle \chi^{(-)}(\mathbf{k}) | \langle \nu, n|V|n\rangle | \chi^{(+)}(\mathbf{k}_1) \rangle \\ &\quad \times \frac{1}{E - E_n - E_{k_1} + i\epsilon} \langle \hat{\chi}^{(+)}(\mathbf{k}_1) | \langle \mu|V|0\rangle | \chi^{(+)}(\mathbf{k}_0) \rangle \delta(E_f - E_x) \end{aligned} \quad (2.122)$$

Now, we apply leading-particle statistics to the second step matrix elements first. The non-diagonal elements in n, V , and \mathbf{k}_1 , then vanish upon energy averaging, yielding

$$\begin{aligned} \sum_f |T_{f \leftarrow 0}^{(2)}|^2 &= \sum_{\mu} \sum_{\mu'} \sum_{\nu} \sum_n \int d\mathbf{k}_1 a_{\mu}^n a_{\mu'}^n \hat{\rho}_{\nu, n}(E_x) \\ &\quad \times |\langle \chi^{(-)}(\mathbf{k}) | \langle \nu | V | n \rangle | \chi^{(+)}(\mathbf{k}_1) \rangle|^2 \\ &\quad \times \langle \chi^{(+)}(\mathbf{k}_0) | \langle 0 | V | \mu' \rangle | \hat{\chi}^{(+)}(\mathbf{k}_1) \rangle \left| \frac{1}{E - E_n - E_{k_1} + i\epsilon} \right|^2 \\ &\quad \times \langle \hat{\chi}^{(+)}(\mathbf{k}_1) | \langle \mu | V | 0 \rangle | \chi^{(+)}(\mathbf{k}_0) \rangle, \end{aligned} \quad (2.123)$$

where

$$\hat{\rho}_{\nu, n}(E_x) = \sum_f \overline{|a_{\nu, n}^f|^2} \delta(E_f - E_x). \quad (2.124)$$

A further approximation can be made by noting that the matrix element $\langle \nu, n | V | n \rangle = \langle \nu | V | 0 \rangle$ as a consequence of the two-body nature of V . Now, we assume $\hat{\rho}_{\nu, n}(E_x) \rightarrow \hat{\rho}_{\nu}(E'_x)$, where $E'_x = E_{k_1} - E_k$ is the energy transferred in the second step, giving

$$\begin{aligned} \sum_f |T_{f \leftarrow 0}^{(2)}|^2 &= \sum_{\mu} \sum_{\mu'} \sum_{\nu} \sum_n \int d\mathbf{k}_1 a_{\mu}^n a_{\mu'}^n \hat{\rho}_{1\nu}(E'_x) \\ &\quad \times |\langle \chi^{(-)}(\mathbf{k}) | \langle \nu | V | 0 \rangle | \chi^{(+)}(\mathbf{k}_1) \rangle|^2 \\ &\quad \times \langle \chi^{(+)}(\mathbf{k}_0) | \langle 0 | V | \mu' \rangle | \hat{\chi}^{(+)}(\mathbf{k}_1) \rangle \left| \frac{1}{E - E_n - E_{k_1} + i\epsilon} \right|^2 \\ &\quad \times \langle \hat{\chi}^{(+)}(\mathbf{k}_1) | \langle 1\mu | V | 0 \rangle | \chi^{(+)}(\mathbf{k}_0) \rangle. \end{aligned} \quad (2.125)$$

An equivalent expression is obtained inserting $\delta(E_n - E'_x)$ and taking the corresponding integral over the intermediate excitation energy $E'_x = E_{k_0} - E_{k_1}$

$$\begin{aligned} \sum_f |T_{f \leftarrow 0}^{(2)}|^2 &= \sum_{\mu} \sum_{\mu'} \sum_{\nu} \sum_n \int d\mathbf{k}_1 \int dE'_x a_{1\mu}^n a_{1\mu'}^n \hat{\rho}_{1\nu}(E'_x) \\ &\quad \times |\langle \chi^{(-)}(\mathbf{k}) | \langle 1\nu | V | 0 \rangle | \chi^{(+)}(\mathbf{k}_1) \rangle|^2 \\ &\quad \times \langle \chi^{(+)}(\mathbf{k}_0) | \langle 0 | V | 1\mu' \rangle | \hat{\chi}^{(+)}(\mathbf{k}_1) \rangle \left| \frac{1}{E - E'_x - E_{k_1} + i\epsilon} \right|^2 \\ &\quad \times \langle \hat{\chi}^{(+)}(\mathbf{k}_1) | \langle 1\mu | V | 0 \rangle | \chi^{(+)}(\mathbf{k}_0) \rangle \delta(E_n - E'_x), \end{aligned} \quad (2.126)$$

where the delta function accounts for the replacement of E_n , by E'_x in the denominator of the Green function.

The leading-particle statistics can now be applied again removing the non-diagonal terms

in μ' , which yields

$$\begin{aligned} \sum_f |T_{f \leftarrow 0}^{(2)}|^2 &= \sum_\mu \sum_\nu \int dE'_x \hat{\rho}_{1\mu}(E'_x) \hat{\rho}_{1\nu}(E''_x) \int d\mathbf{k}_1 \\ &\times \left| \langle \chi^{(-)}(\mathbf{k}) | \langle 1\nu | V | 0 \rangle | \chi^{(+)}(\mathbf{k}_1) \rangle \right. \\ &\times \left. \frac{1}{E - E'_x - E_{k_1} + i\epsilon} \langle \hat{\chi}^{(+)}(\mathbf{k}_1) | \langle 1\mu | V | 0 \rangle | \chi^{(+)}(\mathbf{k}_0) \rangle \right|^2 \quad (2.127) \end{aligned}$$

We have made use of the leading particle statistics. A similar expression is obtained but keeping the coherency in the integral over the intermediate propagating particle $d\mathbf{k}_1$, i.e. inside the modules when residual system statistics are used. Also, an interesting limit for both the one and two-step formula, is the independent-particle approximation, $H_1 \rightarrow 0$ or $a_\mu^n \rightarrow \delta_{\mu,n}$. This simplifies the p-h coupling giving rise to a leading-particle model with independent particle excitations.

3 Quantum Mechanics – The Eigen-World

This is perhaps the simplest chapter of this thesis and one of the most interesting at the same time. Eigenvectors and eigenvalues form the basis of any daily calculation in many areas of physics. Here a brief introduction to this widely used subject together with several simple but instructive examples is presented.

3.1 Eigenvalue Problem

Suppose a general time-independent Hamiltonian

$$H = H_0 + V,$$

where H_0 is the kinematic operator and V represents the interaction involved. As usual, we look for the eigenvalues (energies) and eigenvectors (wave functions) giving

$$H\Psi_i = E_i\Psi_i. \tag{3.1}$$

Unfortunately, it is rarely the case when (3.1) can be solved analytically, as for example, the infinite well or quantum harmonic oscillator (QHO) interactions. It is more likely to have very complex and complicated operators and interactions to deal with. For these cases, one of the approaches is to expand Ψ (expansion method) in a linear combination of a defined basis.

$$\Psi_i = \sum_m c_m^i \psi_m, \tag{3.2}$$

where ψ_m form a complete set of orthogonal basis and could (not necessarily) be the solution of the non interacting case

$$H_0\psi_m = e_m\psi_m. \tag{3.3}$$

This is an interesting way to study the system, since the new solutions are a composition of functions that we already have knowledge about ¹. It is convenient to denote by ψ the wave functions of the unperturbed basis and by Ψ the perturbed wave functions.

Substituting (3.2) into Eq. (3.1) and multiplying from left by ψ_n one obtains:

$$\sum_m (H_{nm} - E_i \delta_{nm}) c_m^i = 0, \quad (3.4)$$

where

$$H_{nm} = \int \psi_n(x) H \psi_m(x) dx. \quad (3.5)$$

One can evaluate H_{nm} to obtain

$$H_{nm} = e_m \delta_{nm} + V_{nm}, \quad (3.6)$$

where

$$V_{nm} = \int dx \psi_n(x) V \psi_m(x), \quad (3.7)$$

with dx representing the space of coordinates where basis function and operators are defined.

The task now is to construct a matrix (3.6) and with the use of your preferred numerical method obtain the eigenvalues and eigenvectors of the H_{nm} matrix. Numerically, the eigenvector c^i for each eigenvalue E_i will be a set numbers $[c_1^i, c_2^i, \dots, c_N^i]$ that provides the contribution of each of the basis-states ψ_n in the expansion (3.2). The wave function Ψ_i can be obtained in the same coordinate space of ψ straightforwardly by multiplying the linear coefficients from the eigenvector and the defined initial unperturbed basis. In a very simple example and small basis ($N = 3$)

$$\begin{pmatrix} H_{11} & H_{12} & H_{13} \\ H_{21} & H_{22} & H_{23} \\ H_{31} & H_{32} & H_{33} \end{pmatrix} \begin{pmatrix} c_1^i \\ c_2^i \\ c_3^i \end{pmatrix} = E_i \begin{pmatrix} c_1^i \\ c_2^i \\ c_3^i \end{pmatrix}, \quad (3.8)$$

reads

$$\Psi^i(x) = \sum_{m=1}^3 c_m^i \psi_m(x). \quad (3.9)$$

For an eigenvalue E^i of the matrix H_{nm} , we use the eigenvector components c_m^i , assuming they are normalized

$$\sum_m^3 |c_m^i|^2 = 1,$$

¹It is very common to find deep in many complicated physical problems expansions in the free-wave or QHO basis.

and (3.9) to give

$$\Psi^i(x) = c_1^i \psi_1(x) + c_2^i \psi_2(x) + c_3^i \psi_3(x). \quad (3.10)$$

3.2 Strength Function

Having solved the problem one may ask for the contribution of each unperturbed mode along the the spectra of eigenvalues. This is the definition of the strength function. In what follows an introduction and an important example where this function can be obtained analytically are given. For this section, we follow Appx 2D of (BOHR; MOTTELSON, 1998).

Assume the following Hamiltonian

$$H = H_0 + V, \quad (3.11)$$

where the non-interacting case can be splitted as

$$H_0 |n\rangle = E_n |n\rangle \quad (3.12)$$

$$H_0 |m\rangle = E_m |m\rangle \quad (3.13)$$

where m represents all other base states with the exception of state n .

Defining a simplified interaction such that

$$\langle n|V|n\rangle = \langle m|V|m\rangle = 0, \quad \langle n|V|m\rangle = \langle m|V|n\rangle, \quad (3.14)$$

the total eigenvalue problem (3.11) reads

$$H |i\rangle = E_i |i\rangle, \quad (3.15)$$

where

$$|i\rangle = c_n^i |n\rangle + \sum_m c_m^i |m\rangle. \quad (3.16)$$

We can study the coupling of the state n if we multiply Eq(3.15) from the left by $|n\rangle$ to give

$$(E_n - E_i)c_n^i = - \sum_m V_{nm} c_m^i. \quad (3.17)$$

If we do the same but now multiplying by $|m\rangle$, we have

$$c_m^i = \frac{-V_{mn}}{(E_m - E_i)} c_n^i. \quad (3.18)$$

Inserting (3.18) in (3.17) gives

$$E_n - E_i = \sum_m \frac{V_{nm}^2}{E_m - E_i}, \quad (3.19)$$

the eigenvalue equation.

The sum of squared linear components c , if normalized, gives

$$(c_n^i)^2 + \sum_m (c_m^i)^2 = 1, \quad (3.20)$$

we can eliminate c_m^i using (3.18),

$$c_n^i = \left(1 + \sum_m \frac{V_{nm}^2}{(E_m - E_i)^2} \right)^{-1/2}. \quad (3.21)$$

The amplitudes c_n^i represent the contribution of state n over the new spectrum i . We define a continuous strength function $P_n(E)$ to represent the strength per unit energy – and average over the states i around a small energy interval dE .

An analytical expression can be obtained for an equidistantly spaced energy basis

$$E_m = mD, \quad m = 0, \pm 1, \pm 2, \quad (3.22)$$

and constant coupling matrix elements,

$$V_{nm} = v. \quad (3.23)$$

This simple model gives,

$$E_m - E_i = -\frac{\pi v^2}{D} \cot \frac{\pi E_i}{D}, \quad (3.24)$$

and

$$c_n^i = \left[1 + \left(\frac{\pi v}{D} \right)^2 + \frac{(E_n - E_i)^2}{v^2} \right]^{-1/2}. \quad (3.25)$$

The probability, strength function, of the state n per unit energy interval of the spectrum is then²

$$P_n(E) = \frac{c_n^2(E \approx E_i)}{D} = \frac{1}{2\pi} \frac{\Gamma}{(E_n - E)^2 + (\Gamma/2)^2}, \quad (3.26)$$

the Breit-Wigner distribution, with width

$$\Gamma = 2\pi \frac{v^2}{D}. \quad (3.27)$$

² $v > D$ neglecting the first term in the brackets.

3.2.1 Collectivity

Eigenvalue problems usually have non trivial solutions in most cases. The study of the shape of the strength functions and their spreading width are very important when statistics are involved, since both quantities can be used to obtain survival probabilities and decay times of different wave functions and excited states. A complicated linear coupling of the basis can be obtained depending on the amplitudes of the off diagonal elements in relation to the diagonal ones. For instance, a new ground state energy i.e. smaller than the lowest energy state of the unperturbed basis can appear. This can be seen in the following simplified way.

Assuming an unperturbed basis to have zero eigenvalues $e_m = 0$ and using a constant coupling $v_{nm} = -v$ we can write

$$H = -v \begin{pmatrix} 1 & 1 & 1 \\ 1 & 1 & 1 \\ 1 & 1 & 1 \end{pmatrix}.$$

The eigenvalues are $E_1 = -3v$, $E_2 = E_3 = 0$. We can immediately see that two of the basis energies were not changed, but one eigenvalue was pushed down (if the interaction was positive the eigenvalue would be pushed up). This shift, can be generalized to $E_1 = -Nv$, where N is the dimension of the basis (matrix). Any unperturbed mode contribute coherently to the eigenvector of the shift eigenvalue. This state, represents an example of a collective state and it is interpreted as a rhythmic motion of the modes involved. In this context, the two-particle excited states of ^{18}O can be written as (COHEN, 1971)

$$\psi_1 = 0.557(d_{5/2})^2 + 0.557(s_{1/2})^2 + 0.557(d_{3/2})^2, \quad (3.28)$$

$$\psi_2 = -0.707(s_{1/2})^2 + 0.707(d_{3/2})^2, \quad (3.29)$$

$$\psi_3 = 0.816(d_{5/2})^2 - 0.408(s_{1/2})^2 - 0.408(d_{3/2})^2 \quad (3.30)$$

where the states between brackets represent the single particle basis functions. ψ_1 is the collective state in which all unperturbed modes contribute with the same sign.

Another way of visualizing this effect in connection with the excited states of a nucleus is by means of a graphical solution of the dispersion equation in terms of the particle-hole excitations. Again take our simple case $H = H_0 + V$ expanded in the basis of the unperturbed Hamiltonian H_0 .

Rewrite (3.4) as

$$c_n^i = \frac{1}{E^i - E_n} \sum_m V_{nm} c_m^i, \quad (3.31)$$

where the unperturbed basis E_n represent the single particle energies obtained from a mean field solution H_0 . Assuming a simple model for the case of one-body creation

operator acting on the ground state obtained with H_0 ,

$$|n\rangle = q_n^\dagger |0\rangle, \quad (3.32)$$

with $E_n = E_p - E_h$ being the unperturbed particle hole energies ($E_p > 0$ and $E_h < 0$ if we set $E_F = 0$). In this picture, the interaction is related to destroying one particle-hole state at m and creating another one at n . The interaction can be written in a general form as ³

$$V_{nm} = v q_n q_m, \quad (3.33)$$

where $q_m = \langle k | q^\dagger | 0 \rangle$.

Now, the problem can be solved up to a normalization constant A^i ,

$$c_n^i = \frac{q_n}{E^i - E_n} A^i, \quad A^i = v \sum_m q_m c_m^i. \quad (3.34)$$

We can change the index of the first expression and insert it into the second one to give

$$A^i = v \sum_m \frac{q_m^2}{E^i - E_m} A^i. \quad (3.35)$$

The trivial solution for this equation $A^i = 0$ gives eigenvalues equal to the unperturbed particle hole energies $E^i = E_n$. For non-zero values of A^i , collective and non-collective solutions appear. They are obtained solving the dispersion relation, sometimes called the secular or characteristic, equation

$$\sum_m \frac{q_m^2}{E^i - E_m} = \frac{1}{v}. \quad (3.36)$$

The roots of (3.36), determine the eigenvalues (excited energies) E^i . The l.h.s of (3.36) has poles at every energy E_n of the basis. The graphical plot of the l.h.s as a function of energy E provides a very instructive view of the effect of v on the eigenvalues.

In Fig.3.1, a graphical solution is shown. The intersection points of the dashed and solid lines represent the eigenvalues E^i . For negative values of v (bottom quadrant) the energy of the ground state is lower compared to the lowest basis state E_1 value. For positive interaction (upper quadrant), the largest state is pushed up compared to the upper bound of the basis E_6 . This displacement in energy is a characteristic of collective states that are likely to appear in both Tamm-Dancoff Approximation (TDA) or Random Phase Approximation (RPA) excitations. A more detailed description of this phenomena is found in (COHEN, 1971; ROWE, 2010; ZELEVINSKY; VOLYA, 2017).

³Assume $q^\dagger = q$ so that the amplitudes c_n^i are real numbers.

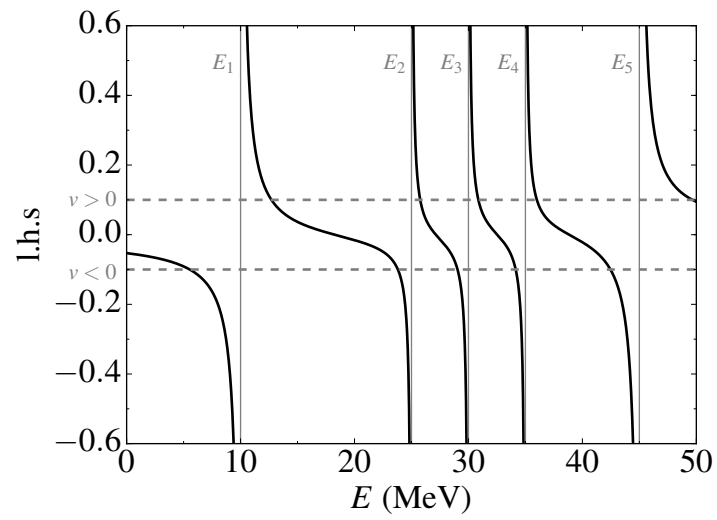


FIGURE 3.1 – Example of a graphical solution to the dispersion equation (3.36).

4 Analysis of the Assumptions

In this section, the strength function for the p-h excitation is analyzed and the statistical assumptions involved in the MSC calculation are studied. The results presented here were published in Physical Review C (CHIMANSKI *et al.*, 2019).

4.1 Single-Particle Contribution to the 1p-1h Response Function

We analyze the energy distribution of the 1p-1h states that contribute to the response function. For this, we add one more step of complexity replacing the non interacting p-h μ states by RPA (Random Phase Approximation) excited states. To this end, we have made use of the RPA code by Colò (COLÒ *et al.*, 2013). The Hartree-Fock (HF) problem is solved self-consistently and the necessary unoccupied states are obtained using the self-consistent mean field. Then, the RPA problem is solved for a given value of total angular momentum and parity J^π . The excited states and energies are obtained by diagonalization of the RPA eigenvalue problem

$$\begin{pmatrix} A & B \\ -B & -A \end{pmatrix} \begin{pmatrix} X^\mu \\ Y^\mu \end{pmatrix} = E_\mu \begin{pmatrix} X^\mu \\ Y^\mu \end{pmatrix} \quad (4.1)$$

where the matrix elements are given by

$$A_{mi,nj} = (E_m - E_i)\delta_{mn}\delta_{ij} + \langle mj|V|in\rangle \quad (4.2)$$

$$B_{mi,nj} = \langle mn|V|ij\rangle \quad (4.3)$$

where the indices $m, n(i, j)$ represent HF single-particle states with energies above (below) the Fermi level. The Tamm–Dancoff approximation (TDA) can easily be recovered by setting $B = 0$. The Skyrme interaction Sly5 (CHABANAT *et al.*, 1998a; CHABANAT *et al.*, 1998b), is used for all results shown in this analysis.

Figure 4.1 presents histograms of the contribution of the p-h energy components to the eigenvalue spectra (strength function) for the 3^- states of ^{56}Ni . For the low energy com-

ponents (left-panel) the collectivity of the excited states generates a broader distribution when compared to the more high energetic ones (right-panel) of the right panel. We have found the states towards high energy, above 20 MeV, to be composed of a dominant and strong peak very close to the non-interacting p-h energy E_{ph} , which is represented by the vertical solid line. These distributions have a long tail in common, bringing on important contribution from distant states. We attempt to fit the histogram with a Breit-Wigner distribution,

$$\text{BW}(E_x) = \frac{1}{\pi} \frac{\gamma}{(E_x - \bar{E})^2 + \left(\frac{\gamma}{2}\right)^2}, \quad (4.4)$$

with width γ and mean value \bar{E} representing the spreading of the p-h modes and the noninteracting component energy, respectively. We also computed the single particle

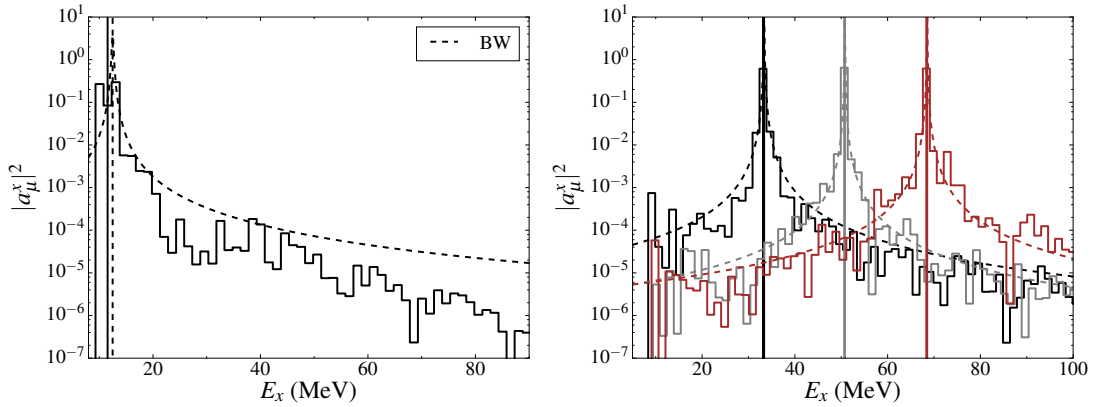


FIGURE 4.1 – Response function for 3^- RPA excited states of ^{56}Ni nucleus for low (left) and high (right) energetic p-h components. The vertical solid and dotted lines represent the non-interacting p-h energy and the distribution mean for the Breit-Wigner fit.

contribution to the excited states by removing from the eigenvalue the energy of all coupled holes $E'_m = E_x - \sum E_h$. We show this in Fig. 4.2. The distribution is very narrow and a Breit-Wigner curve is nicely adjusted for the high energy states. Figures (4.3-4.4), present the spreading γ of the Breit-Wigner fit dependence on the entire p-h energy basis. Wider distributions are found for the low energy components. At energies beyond 20 MeV, γ decreases rapidly representing very narrow strength functions. This, seems to be a universal behavior found in different nuclei, for instance ^{16}O , ^{56}Ni , ^{90}Zr , ^{120}Sn .

Although many states make small contributions to the low-energy collective states, the energy distribution of the high-energy states is concentrated around the energies of the non-interacting p-h states. The width can be used a measure of the residual interaction providing the particle hole mixing in the excited states of the target.

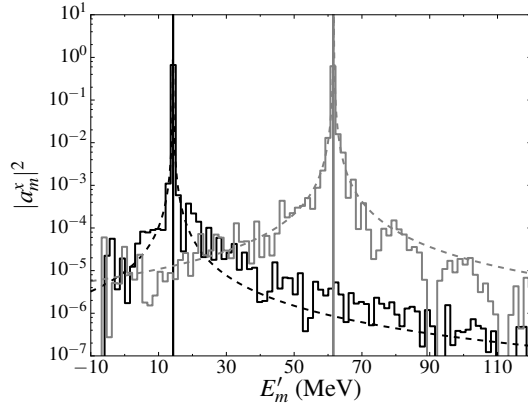


FIGURE 4.2 – Single-particle strength/response function for 3^- RPA excited states of ^{56}Ni nucleus.

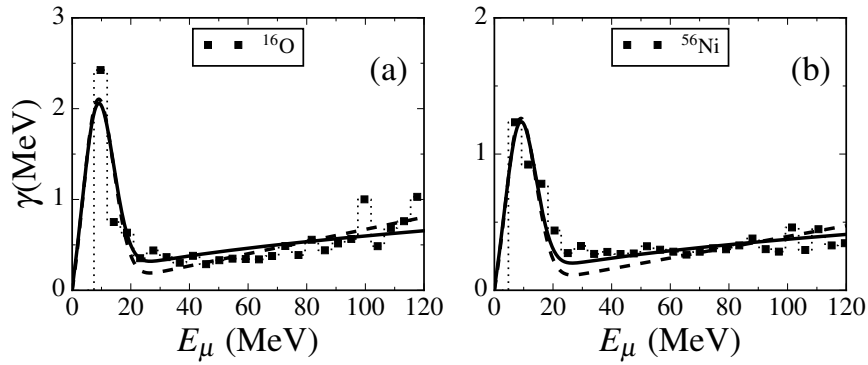


FIGURE 4.3 – Spreading γ dependence on particle-hole energy components for ^{16}O (a) and ^{56}Ni (b).

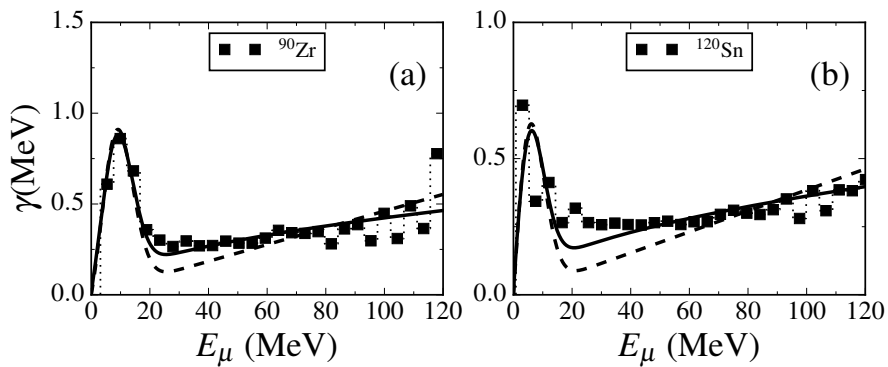


FIGURE 4.4 – Spreading γ dependence on particle-hole energy components for ^{90}Zr (a) and ^{120}Sn (b).

4.2 Analysis of Randomness Assumptions

We also performed a study of randomness assumptions discussed in Sec.(2.4.3). There, it was stated that the off-diagonal elements of the matrix elements should satisfy

$$\overline{\sum_{f \in \Delta E} a_\mu^f a_\nu^f} = \overline{|a_\mu^f|^2} \delta_{\mu\nu}. \quad (4.5)$$

In order to verify this assumption, we define a distribution representing the contribution of the RPA modes to the transition amplitude necessary for the cross-section calculation

$$P_\mu(E_{\mu'}) = \sum_{E_x \in \Delta E} a_{\mu'}^x a_\mu^x, \quad (4.6)$$

where a_μ^x denotes the component μ of the final RPA eigenvector $f \rightarrow x$. The assumptions of randomness implies

$$P_\mu(E_{\mu'}) \rightarrow \delta(E_{\mu'} - E_\mu), \quad (4.7)$$

for an energy average over a a bin of excitation energy.

Figure 4.5 shows (4.6) for three different components of the RPA state. On the left, a low energy mode does not satisfy (4.7) due to the lack of a sufficient number of states in the average and the sign fluctuation. For the other two more energetic components, the randomness assumption is verified for energy averages of $\Delta = 1$ MeV. This is due to the fact that these states have an incoherent sign pattern for their components, which vanish when averaged.

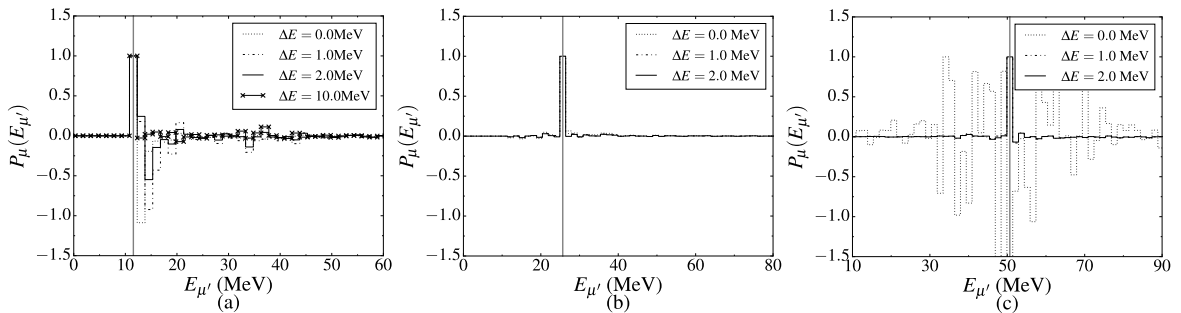


FIGURE 4.5 – The distribution (4.6) for a low (a) and higher (b,c) energetic RPA basis components of 3^- states of ^{56}Ni . ΔE represents the energy bin where the amplitudes are averaged.

We obtained the contribution of all non-diagonal and diagonal terms by defining the following quantities:

$$\sum_{\text{diag}} = \frac{1}{N} \sum_{E_x \in \Delta E} \sum_{\mu} a_{\mu}^x a_{\mu}^x, \quad (4.8)$$

for the diagonal terms and

$$\sum_{\text{off}} = \frac{1}{N} \sum_{E_x \in \Delta E} \sum_{\mu} \sum_{\mu' \neq \mu} a_{\mu}^x a_{\mu'}^x, \quad (4.9)$$

for the off-diagonal terms. N is the number of states within the bin energy ΔE .

We show in Fig.4.6 the relative contribution of diagonal and off diagonal terms together with the number of states used in the average calculation. The contributions from off diagonal terms rapidly vanish for more energetic unperturbed components. The discreteness of the low-energy collective states does not permit enough states for a randomness assumption to be valid. We estimate that at least $N > 10$ is necessary.

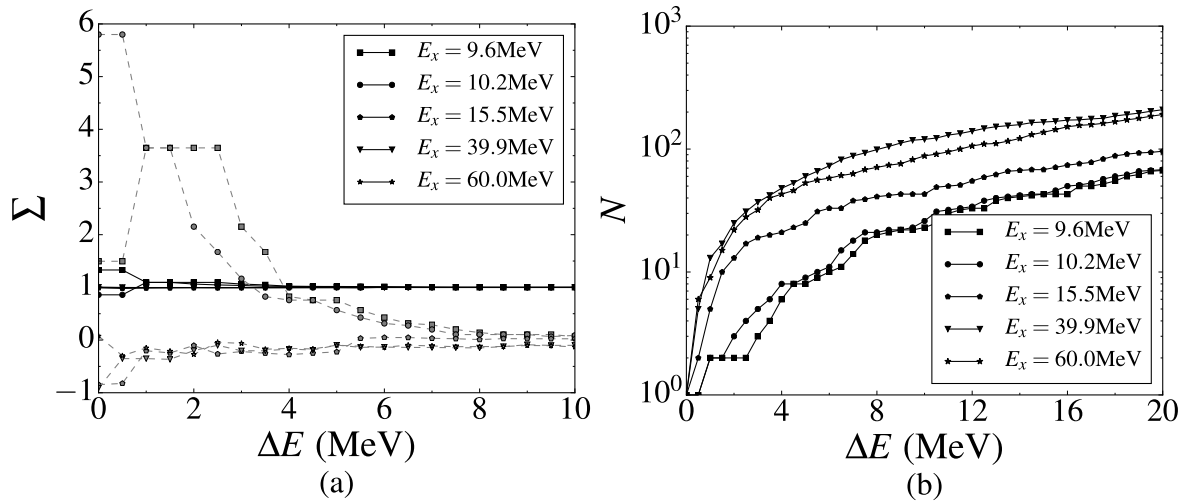


FIGURE 4.6 – (a) Averaged contribution of the RPA components from the diagonal (4.8) (solid dark lines) and off-diagonal (4.9) (dashed gray lines) terms of the for 3^- states of ^{56}Ni . (b) The number of states averaged within the bin of excitation energy interval ΔE .

4.3 Leading-Particle Analysis

Proceeding with our analysis we focus on the leading particle model, i.e., the hypothesis that just one nucleon stays in the continuum during the reaction. In Figure (4.7) we show the average energy of the fast (leading) and slow particles after a nucleon-nucleon collision in nuclear matter as a function of the incident energy of the primary nucleon. The collision was assumed to be isotropic in the nucleon pair center of mass (KIKUCHI; KAWAI, 1968). Above an incident energy of 50 MeV, the averaged values are well approximated by

$$E_{high} = \frac{3}{4}(E_i - \langle E_{hole} \rangle) \quad \text{and} \quad E_{low} = \frac{1}{4}(E_i - \langle E_{hole} \rangle) \quad (4.10)$$

where the average hole energy is $\langle E_{hole} \rangle = 2E_F/7$ with E_F being the non-relativistic Fermi energy. The widths of the energy distributions are about $E_i/7$. The final phase space, in arbitrary units, also shown as a function of incident energy, represents a measure of the collision probability.

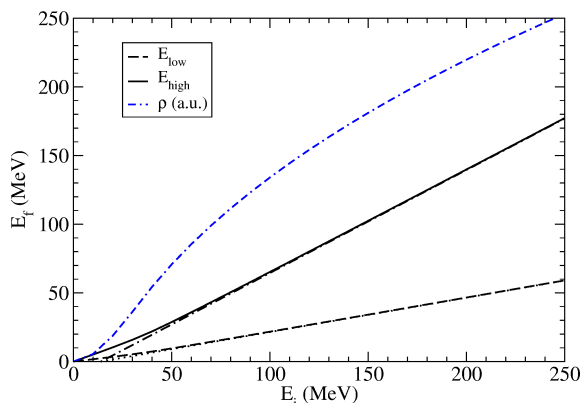


FIGURE 4.7 – Average energy of the fast (leading) and slow final particles in a nucleon-nucleon collision in nuclear matter as a function of the incident particle energy. The phase space final volume, in arbitrary units, is also shown as a function of initial energy.

For 60 MeV incident particle energy, the resulting primary particle energy after a collision is about 30 ± 9 MeV and that of the slow particle about 10 ± 9 MeV. They are both probably in continuum states. If we take into account the phase space volumes we see that it is approximately 7 times more probable that the second collision will be induced by the 30 MeV particle rather than the 10 MeV one. We can also say that a collision induced by the 30 MeV particle with another nucleon produces a new primary particle with average energy of 12 ± 4 MeV, which would still be in the continuum states. This problem is even more serious for higher energy incident particle showing that the leading particle, assumption is limited to only low incident projectile energies.

A collision induced by a first fast particle would result in one more continuum particle, which would have enough energy to create even more continuum particles. For energies

above 30 MeV the probability of the slow particle still being in the continuum should be taken into account and for higher energy incident particles the other particles created after each collision with the Fermi sea should also be considered.

We next intend to extend the multi-step direct model present in Sec.(2.4.2.2) to include more than one continuum particle. For this, we have in mind the Blann and Chadwick's semi-classical model. Quantum models take into account either the possibility of the incident particle being captured in a bound state of the nucleus through creation of a p-h pair that initiates the compound multi-step reaction or a multi-step direct reaction initiated by a p-h pair in which only the primary particle remains unbound (in continuum). The semi-classical model of Blann and Chadwick takes both possibilities into consideration as well the possibility in which the second particle of the p-h pair is also in the continuum.

To describe the excited nuclear states within the chain of p-h states, the $np - nh$ response function is used for the n^{th} reaction stage. The applications of Feshbach, Kerman and Koonin have only used a response function of non-interaction p-h states (BONETTI *et al.*, 1994; KONING; CHADWICK, 1997). Tamura, Udagawa and Lenske have used an interacting response function in a random phase approximation and add a contribution from collective low energy states (TAMURA *et al.*, 1982; RAMSTRÖM *et al.*, 2004). Our results shown in Sec.(4) reinforces the analogy with the semi-classical model of Blann e Chadwick (BLANN; CHADWICK, 1998) that we use as a guide in this project. That is, except in the case of low-energy collective modes, the particles and holes of an excited state are well approximated by independent distributions in energy of each of the particle and hole pair at the unperturbed energy of each. We suggest the use a Gaussian distribution for (2.115) with the $\sigma(E_m)$ dependence which has not been used so far in the literature.

For the extension to higher energy incident particle energies we intend to work in the eikonal approximation (GLAUBER, 1959; WALLACE, 1971; BUUCK; MILLER, 2014). Although this approximation is widely used for elastic scattering, projectile fragmentation and multiple scattering, it is normally used for only one particle or subsystem in a primary particle context.

5 Extension of the Quantum Formalism

In this section we present the formalism developed for inclusion of more particles in the continuum. This extension, is made in a high energy approximation using the eikonal wave function for unbound particle states. For pedagogical reasons, we start with elastic scattering and finish with a general expression for n particles in the continuum. In what follows k_i stands for initial and k_f final particle wave numbers, respectively.

5.1 Elastic scattering

The elastic scattering amplitude is

$$\begin{aligned}
 f_{el}(\mathbf{k}_f, \mathbf{k}_i) &= -\frac{1}{4\pi} \int d^3r e^{-i\mathbf{k}_f \cdot \mathbf{r}} \frac{2\mu}{\hbar^2} U(z, \mathbf{b}) \psi_{k_i}^{(+)}(z, \mathbf{b}) \\
 &= -\frac{1}{4\pi} \int d^3r e^{i\mathbf{q} \cdot \mathbf{r}} \frac{2\mu}{\hbar^2} U(z, \mathbf{b}) \exp\left[-\frac{i}{\hbar v} \int_{-\infty}^z U(z', \mathbf{b}) dz'\right] \\
 &\approx \frac{k}{2\pi i} \int d^2b e^{i\mathbf{q} \cdot \mathbf{b}} \left(\exp\left[-\frac{i}{\hbar v} \int_{-\infty}^{\infty} U(z, \mathbf{b}) dz\right] - 1 \right) \\
 &= \frac{k}{i} \int b db J_0(qb) (e^{2i\delta(b)} - 1)
 \end{aligned} \tag{5.1}$$

where $\mathbf{q} = \mathbf{k}_i - \mathbf{k}_f$ is the transferred angular momentum. The phase shift is defined as

$$\delta(b) = -\frac{1}{2\hbar v} \int_{-\infty}^{\infty} U(z, \mathbf{b}) dz = -\frac{1}{\hbar v} \int_0^{\infty} U(z, \mathbf{b}) dz, \tag{5.2}$$

where the last equality follows from the assumption that $U(z, \mathbf{b}) = U(-z, \mathbf{b})$.

Here, since $|\mathbf{k}_f| = |\mathbf{k}_i| = k$, we take

$$q = |\mathbf{k}_i - \mathbf{k}_f| = 2k \sin(\theta/2), \tag{5.3}$$

where θ is the scattering angle. The differential elastic cross section is then

$$\frac{d\sigma_{el}}{d\Omega} = |f_{el}(\mathbf{k}_f, \mathbf{k}_i)|^2. \quad (5.4)$$

A possible choice for the optical potential is the $t\rho$ approximation. The forward-angle nucleon-nucleon t-matrix is often parameterized as

$$t_{n_1 n_2}(\mathbf{q} = 0) = -\frac{2\pi\hbar^2}{\mu} f_{n_1 n_2}(\mathbf{q} = 0) = -\frac{\hbar v}{2} \sigma_{n_1 n_2}^T (\alpha_{n_1 n_2} + i) \quad (5.5)$$

where $f_{n_1 n_2}$ is the $n_1 - n_2$ scattering amplitude ($n_{1,2} = n, p$) and $\sigma_{pp}^T = \sigma_{nn}^T$ and σ_{pn}^T are the proton-proton, neutron-neutron and proton-neutron total cross sections. The $\alpha_{n_1 n_2}$ quantities stands for the ratio between the imaginary and the real part of the proton-nucleon scattering amplitude. In this case, we take for the proton-target optical potential

$$U(\mathbf{r}) = -\frac{\hbar v}{2} [\sigma_{pp}^T (i + \alpha_{pp}) \rho_p(\mathbf{r}) + \sigma_{pn}^T (i + \alpha_{pn}) \rho_n(\mathbf{r})] \quad (5.6)$$

The total cross sections $\sigma_{n_1 n_2}^T$ as well as the factors $\alpha_{n_1 n_2}$ are energy dependent. Both parameters are given for higher projectile energies in Table 5.1 and for lower incident energies in Table 5.2. Interpolation is performed whenever energies differ from these are used. We assume that the cross sections and factors $\alpha_{n_1 n_2}$ present in the optical potential also contain the effects of Pauli blocking in the nuclear medium. The position dependent quantities $\rho_p(\mathbf{r})$ and $\rho_n(\mathbf{r})$ are the target proton and neutron densities. These are often approximated as Z/A and N/A times the total nucleon density, $\rho_m(\mathbf{r})$, where Z and N are the proton and neutron number of the nucleus of mass number $A = Z + N$.

E [MeV]	σ_{pp}^T [mb]	α_{pp}	σ_{pn}^T [mb]	α_{pn}
100	33.2	1.87	72.7	1.00
150	26.7	1.53	50.2	0.96
200	23.6	1.15	42.0	0.71
325	24.5	0.45	36.1	0.16
425	27.4	0.47	33.2	0.25
550	36.9	0.32	35.5	-0.24
650	42.3	0.16	37.7	-0.35
800	47.3	0.06	37.9	-0.20
1000	47.2	-0.09	39.2	-0.46
2200	44.7	-0.17	42.0	-0.50

TABLE 5.1 – Parameters for nucleon-nucleon scattering necessary in the $t\rho$ potential approximation (RAY, 1979).

E [MeV]	$\langle \sigma_{pp}^T \rangle$ [mb]	$\langle \alpha_{pp} \rangle$
30	196.0	0.87
38	146.0	0.89
40	135.0	0.90
49	104.0	0.94
85	61.0	1.00

TABLE 5.2 – Lower energies parameters, averaged over pp and pn scattering, necessary in the $t\rho$ potential approximation (LENZI *et al.*, 1988).

The proton elastic scattering phase shift in the $t\rho$ approximation is given by

$$\begin{aligned} \delta(b) &= \frac{1}{2} \sigma_{pp}^T (i + \alpha_{pp}) \int_0^\infty \rho_p(z, \mathbf{b}) dz + \frac{1}{2} \sigma_{pn}^T (i + \alpha_{pn}) \int_0^\infty \rho_n(z, \mathbf{b}) dz \\ &\approx \frac{1}{2} \left[\sigma_{pp}^T (i + \alpha_{pp}) \frac{Z}{A} + \sigma_{pn}^T (i + \alpha_{pn}) \frac{N}{A} \right] \int_0^\infty \rho_m(z, \mathbf{b}) dz. \end{aligned} \quad (5.7)$$

Figure 5.1 shows in the right panel the dependence of the $t\rho$ parameters on energy and in the left panel some examples of the optical potential obtained for different incoming projectile energies with ^{90}Zr as the target nucleus.

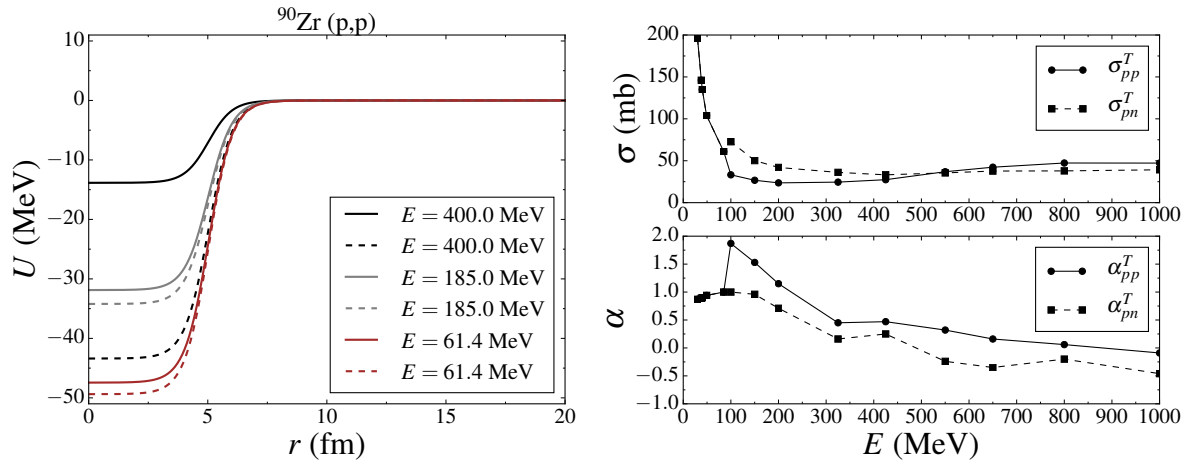


FIGURE 5.1 – Left panel: Optical potential for different nucleon induced reaction energies at ^{90}Zr . Right panel: The parameters for the $t\rho$ optical potential as a function of energy.

5.1.1 Proton Elastic Scattering

We start the numerical calculations with proton elastic scattering on two target nuclei ^{90}Zr and ^{208}Pb . Figures (5.2-5.3) present differential cross sections for incoming protons of different energies. We have employed $r_0 = 1.25$ fm and $a_0 = 0.65$ fm for the density ρ_m , providing good comparison with experimental data. For Figure (5.2) we consider an

incident proton energy of $E = 185$ MeV for two potentials, one including only $t\rho$ approximation and another with the $t\rho$ potential plus the Coulomb interaction. The Coulomb field becomes more important for backward scattering (highly deflected particles), and as expected, the more complete interaction reproduces the data better. Figure (5.3) presents several cases for different incident projectile energies. At higher incident energies, the calculated cross sections are very close to the experimental data. For lower energies, the eikonal approximation starts to lose its validity as can be seen in the $E = 61.4$ MeV case. Although our results do not follow exactly the distributions, we find the eikonal approximation together with the potential to be in good agreement with the data down to 60 MeV incoming particle energy.

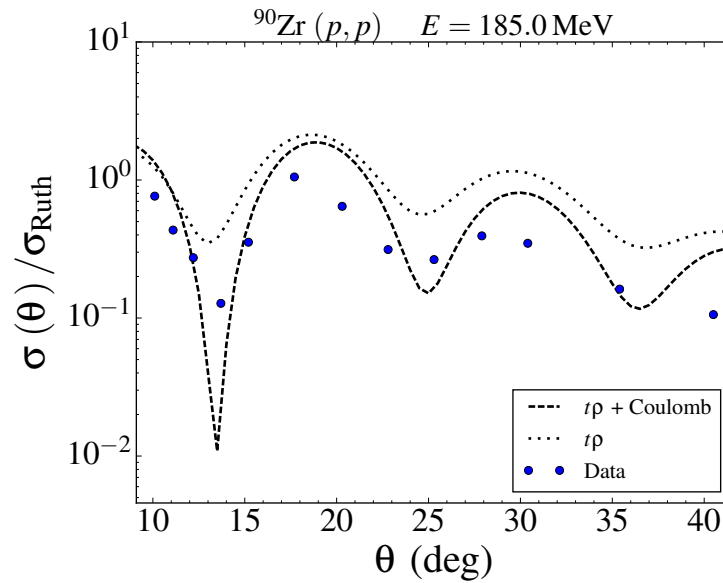


FIGURE 5.2 – Differential cross section normalized to the Rutherford cross sections for $^{90}\text{Zr}(p,p)$ elastic scattering (with and without the Coulomb potential). The incident proton energy is $E = 185$ MeV. The parameters of WS function are $r_0 = 1.25$ fm and $a_0 = 0.65$ fm. The data filled circles represent the experimental values, see Table 5.3 for references.

Reaction	Proton Incident Energy E (MeV)
$^{90}\text{Zr}(p,p)$	61.4 (FULMER <i>et al.</i> , 1969)
	80, 135, 160 (NADASEN <i>et al.</i> , 1981)
	156 (COMPARAT <i>et al.</i> , 1974)
	185 (HAGBERG; SUNDQVIST, 1971)
	400 (LEE <i>et al.</i> , 1988)
$^{208}\text{Pb}(p,p)$	318, 800 (HINTZ <i>et al.</i> , 1988)

TABLE 5.3 – Data sets for the proton elastic cross sections.

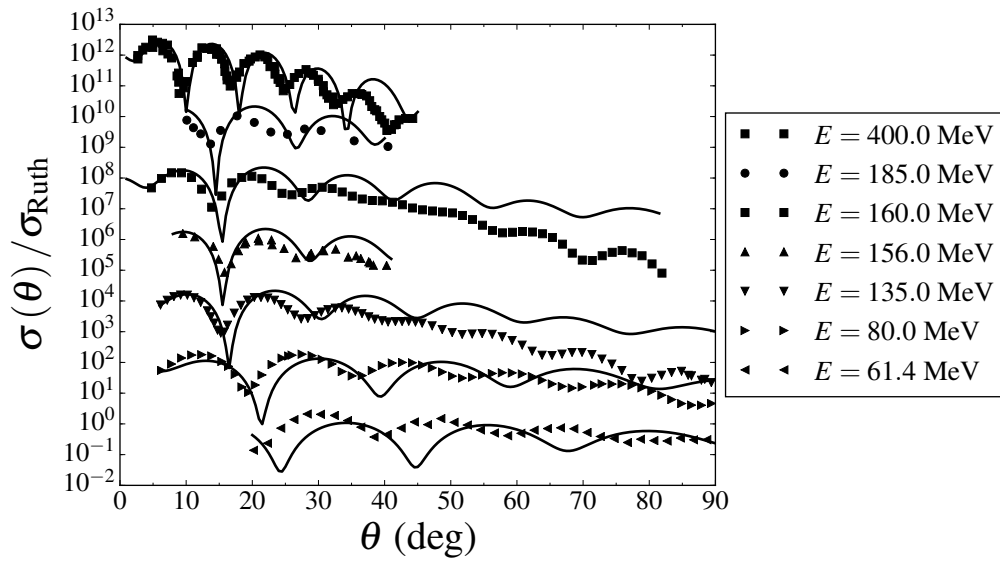


FIGURE 5.3 – Differential cross section normalized to the Rutherford cross sections for $^{90}\text{Zr}(p,p)$ at different energies. The experimental data are shown as symbols and the references are given in Table 5.3. The parameters of the potential are the same as Fig. 5.2. In order to present all cases, the cross sections were shifted by a constant factor starting from the bottom.

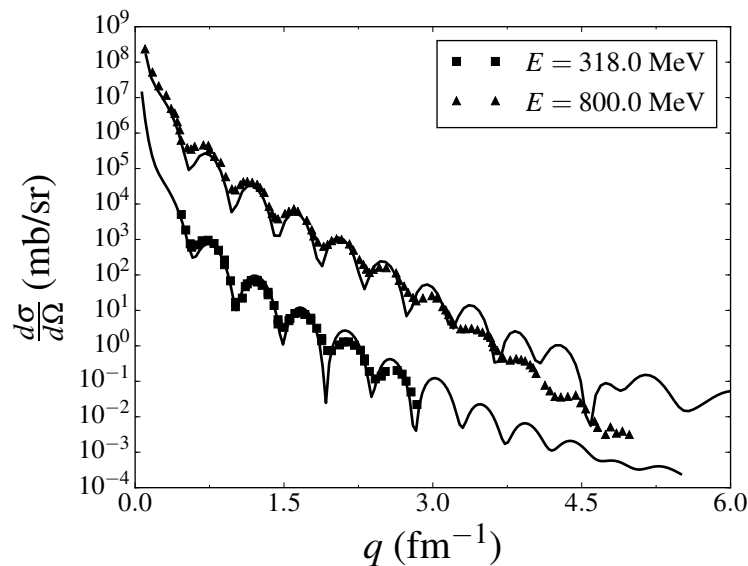


FIGURE 5.4 – Proton elastic scattering cross section from a ^{208}Pb target for different incident energies. Experimental data are shown as symbols (see Table 5.3 for references). Both the data and the calculation at 800 MeV were shift.

5.2 One-step inelastic scattering

The one-step DWBA amplitude of a nucleon-induced reaction has the general form

$$T_{DWBA} = \int d^3r \psi_{k_f}^{(-)*}(\mathbf{r}) \left\langle B \left| \sum_{j=1}^A V(\mathbf{r} - \mathbf{r}_j) \right| A \right\rangle \psi_{k_i}^{(+)}(\mathbf{r}) \quad (5.8)$$

where we have written the nucleon-nucleus interaction as a sum of nucleon-nucleon interactions $V(\mathbf{r} - \mathbf{r}')$. We now proceed to compute the transition matrix element $\langle \vec{k}_f; ph | T | \vec{k}_i \rangle$, where

$$|ph\rangle = a_p^\dagger a_h |A\rangle, \quad (5.9)$$

with p and h standing for states above and below Fermi level, respectively ($a_h \rightarrow$ destroys one particle below E_F – creates a hole). The state $|A\rangle$ is the initial state of the nucleus and the necessary expression of the matrix elements are derived in Appendix A.2.

Any individual interaction can be written as

$$\langle \mathbf{k}_f; ph | T | \mathbf{k}_i \rangle = \int d^3r d^3r' \psi_{k_f}^{(-)*}(\mathbf{r}) \psi_p^*(\mathbf{r}') V(\mathbf{r} - \mathbf{r}') \psi_h(\mathbf{r}') \psi_{k_i}^{(+)}(\mathbf{r}), \quad (5.10)$$

where ψ_h is an occupied orbital in the initial nucleus (a hole state after the collision) and ψ_p is an unoccupied orbital or continuum state of the initial nucleus. There are three possibilities for the final state:

1. One of the two particles remains in the continuum while the second occupies a previously unoccupied bound state of the nucleus. This is the situation assumed in all multi-step direct models and corresponds to the amplitude given above.
2. At sufficiently high incident energy, both of the final particles can be in the continuum. The DWBA amplitude will then be

$$\langle \mathbf{k}_{f_1}, \mathbf{k}_{f_2}; h | T | \mathbf{k}_i \rangle = \int d^3r d^3r' \psi_{k_{f_1}}^{(-)*}(\mathbf{r}) \psi_{k_{f_2}}^{(-)*}(\mathbf{r}') V(\mathbf{r} - \mathbf{r}') \psi_h(\mathbf{r}') \psi_{k_i}^{(+)}(\mathbf{r}). \quad (5.11)$$

3. At extremely low energy, both of the particles can occupy previously unoccupied bound states of the nucleus. In this case, we would say that the incident nucleon was absorbed. The corresponding DWBA amplitude is

$$\langle p_1 p_2 h | T | \mathbf{k}_i \rangle = \int d^3r d^3r' \psi_{p_1}^*(\mathbf{r}) \psi_{p_2}^*(\mathbf{r}') V(\mathbf{r} - \mathbf{r}') \psi_h(\mathbf{r}') \psi_{k_i}^{(+)}(\mathbf{r}). \quad (5.12)$$

To simplify the development of the possible amplitudes, we will assume that the nucleon-nucleon interaction can be well represented by a contact interaction,

$$V(\mathbf{r} - \mathbf{r}') \approx V_0 \delta(\mathbf{r} - \mathbf{r}') . \quad (5.13)$$

For the first case above, in which only one of the particles is in the continuum after the interaction, we have for the eikonal scattering amplitude,

$$\begin{aligned} \langle \mathbf{k}_f; ph | T^{(1)} | \mathbf{k}_i \rangle &= \int d^3r \psi_{\mathbf{k}_f}^{(-)*}(z, \mathbf{b}) V_0 \psi_p^*(z, \mathbf{b}) \psi_h(z, \mathbf{b}) \psi_{\mathbf{k}_i}^{(+)}(z, \mathbf{b}) \\ &= V_0 \int d^3r e^{i\mathbf{q}\cdot\mathbf{r}} \psi_p^*(z, \mathbf{b}) \psi_h(z, \mathbf{b}) \\ &\times \exp \left[-\frac{i}{\hbar v_f} \int_z^\infty U_f(z', \mathbf{b}) dz' - \frac{i}{\hbar v_i} \int_{-\infty}^z U_i(z', \mathbf{b}) dz' \right], \end{aligned} \quad (5.14)$$

rewriting the phases

$$\begin{aligned} \langle \mathbf{k}_f; ph | T^{(1)} | \mathbf{k}_i \rangle &= V_0 \int d^2b e^{i\mathbf{q}\cdot\mathbf{b}} e^{i(\delta_i(b) + \delta_f(b))} \\ &\times \int_{-\infty}^\infty dz \psi_p^*(z, \mathbf{b}) \psi_h(z, \mathbf{b}) \\ &\times \exp \left[iq_z z + \frac{i}{\hbar v_f} \int_0^z U_f(z', \mathbf{b}) dz' - \frac{i}{\hbar v_i} \int_0^z U_i(z', \mathbf{b}) dz' \right] \end{aligned} \quad (5.15)$$

with $\mathbf{q} = \mathbf{k}_i - \mathbf{k}_f$. We rewrite this as

$$\begin{aligned} \langle \mathbf{k}_f; ph | T^{(1)} | \mathbf{k}_i \rangle &= V_0 \int d^2b e^{i\mathbf{q}\cdot\mathbf{b}} e^{i(\delta_i(b) + \delta_f(b))} \\ &\times \int_{-\infty}^\infty dz \psi_p^*(z, \mathbf{b}) \psi_h(z, \mathbf{b}) \exp [iq_z z - i\phi_f(z, \mathbf{b}) + i\phi_i(z, \mathbf{b})] \end{aligned} \quad (5.16)$$

where

$$\phi_m(z, \mathbf{b}) = -\frac{1}{\hbar v_m} \int_0^z U_m(z', \mathbf{b}) dz' . \quad (5.17)$$

We note that

$$\lim_{z \rightarrow \infty} \phi_m(z, \mathbf{b}) = \delta_m(b) . \quad (5.18)$$

The amplitude of the second case above, in which both final state nucleons are in the

continuum, takes the form

$$\begin{aligned}
\langle \mathbf{k}_{f_1}, \mathbf{k}_{f_2}; h | T^{(1)} | \mathbf{k}_i \rangle &= V_0 \int d^3 r \psi_{k_{f_1}}^{(-)*}(z, \mathbf{b}) \psi_{k_{f_2}}^{(-)*}(z, \mathbf{b}) \psi_h(z, \mathbf{b}) \psi_{k_i}^{(+)}(z, \mathbf{b}) \\
&= V_0 \int d^2 b e^{i\mathbf{q}\cdot\mathbf{b}} e^{i(\delta_i(b) + \delta_{f_1}(b) + \delta_{f_2}(b))} \\
&\quad \times \int_{-\infty}^{\infty} dz \psi_h(z, \mathbf{b}) \exp [iq_z z - i\phi_{f_1}(z, \mathbf{b}) - i\phi_{f_2}(z, \mathbf{b}) + i\phi_i(z, \mathbf{b})] .
\end{aligned} \tag{5.19}$$

where we now have $\mathbf{q} = \mathbf{k}_i - \mathbf{k}_{f_1} - \mathbf{k}_{f_2}$.

The final amplitude, in which the interaction de-excites the incoming projectile to a bound state and there is no outgoing wave, can be written as

$$\langle p_1 p_2 h | T^{(1)} | \mathbf{k}_i \rangle = V_0 \int d^2 b e^{i\delta_i(b)} \int_{-\infty}^{\infty} dz \psi_{p_1}^*(z, \mathbf{b}) \psi_{p_2}^*(z, \mathbf{b}) \psi_h(z, \mathbf{b}) \exp [ik_z z + i\phi_i(z, \mathbf{b})] . \tag{5.20}$$

5.3 Two-step inelastic scattering

The very simplest two-step amplitude will have only one particle in the continuum after each of the two interactions. For a specific intermediate state \mathbf{k}_m, p_1, h_1 , we can write this as

$$\begin{aligned}
\langle \mathbf{k}_f; p_2 h_2, p_1 h_1 | T^{(2)} | \mathbf{k}_i \rangle &= \int d^3 r d^3 r' \psi_{k_f}^{(-)*}(z, \mathbf{b}) \psi_{p_2}^*(z, \mathbf{b}) \psi_{h_2}(z, \mathbf{b}) \\
&\quad \times G_m^{(+)}(z, \mathbf{b}; z', \mathbf{b}') \psi_{p_1}^*(z, \mathbf{b}) \psi_{h_1}(z, \mathbf{b}) \psi_{k_i}^{(+)}(z', \mathbf{b}') .
\end{aligned} \tag{5.22}$$

Which gives by introducing eikonal waves

$$\begin{aligned}
\langle \mathbf{k}_f; p_2 h_2, p_1 h_1 | T^{(2)} | \mathbf{k}_i \rangle &= V_0^2 \int d^2 b e^{i\mathbf{q}\cdot\mathbf{b}} e^{i(\delta_i(b) + \delta_f(b))} \left(\frac{-i}{\hbar v_m} \right) \\
&\quad \times \int_{-\infty}^{\infty} dz \psi_{p_2}^*(z, \mathbf{b}) \psi_{h_2}(z, \mathbf{b}) \\
&\quad \quad \quad \times \exp [i(k_m - k_f)_z z - i\phi_f(z, \mathbf{b}) + i\phi_m(z, \mathbf{b})] \\
&\quad \times \int_{-\infty}^z dz' \psi_{p_1}^*(z', \mathbf{b}) \psi_{h_1}(z', \mathbf{b}) \\
&\quad \quad \quad \times \exp [i(k_i - k_m)_z z' - i\phi_m(z', \mathbf{b}) + i\phi_i(z', \mathbf{b})] .
\end{aligned} \tag{5.23}$$

We begin to see a pattern here. Let us define the quantity

$$W_{lph,m}(z, \mathbf{b}) = V_0 \psi_p^*(z, \mathbf{b}) \psi_h(z, \mathbf{b}) \exp [i(k_m - k_l)_z z - i\phi_l(z, \mathbf{b}) + i\phi_m(z, \mathbf{b})] . \quad (5.24)$$

Then for the one-step inelastic amplitude above, with only one particle in the continuum, we have

$$\langle \mathbf{k}_f; ph | T^{(1)} | \mathbf{k}_i \rangle = \int d^2b e^{i\mathbf{q}\cdot\mathbf{b}} e^{i(\delta_i(b)+\delta_f(b))} \int_{-\infty}^{\infty} dz W_{fph,i}(z, \mathbf{b}) , \quad (5.25)$$

and for the two-step inelastic amplitude with only one particle in the continuum, we can write

$$\begin{aligned} \langle \mathbf{k}_f; p_2h_2, p_1h_1 | T^{(2)} | \mathbf{k}_i \rangle &= -i \int d^2b e^{i\mathbf{q}\cdot\mathbf{b}} e^{i(\delta_i(b)+\delta_f(b))} \\ &\times \int_{-\infty}^{\infty} dz W_{fp_2h_2,m}(z, \mathbf{b}) \frac{1}{\hbar v_m} \int_{-\infty}^z dz' W_{mp_1h_1,i}(z', \mathbf{b}) . \end{aligned} \quad (5.26)$$

The same final state of the two-step amplitude can be reached through other intermediate states, in particular through the state in which the particle-hole states are excited in the order p_2h_2 and then p_1h_1 . We can generalize the definition of W to the two-particle final state amplitude by defining

$$W_{lmh,n}(z, \mathbf{b}) = V_0 \psi_h(z, \mathbf{b}) \exp [i(k_n - k_l - k_m)_z z - i\phi_l(z, \mathbf{b}) - i\phi_m(z, \mathbf{b}) + i\phi_n(z, \mathbf{b})] . \quad (5.27)$$

We then have for the one-step amplitude with two particles in the continuum

$$\langle \mathbf{k}_{f_1}, \mathbf{k}_{f_2}; h | T^{(1)} | \mathbf{k}_i \rangle = \int d^2b e^{i\mathbf{q}\cdot\mathbf{b}} e^{i(\delta_i(b)+\delta_{f_1}(b)+\delta_{f_2}(b))} \int_{-\infty}^{\infty} dz W_{f_1f_2h,i}(z, \mathbf{b}) . \quad (5.28)$$

An example of a two-step process in which the first step excites two-particles to the continuum but the second inelastically scatters one of the two without exciting another particle to the continuum would then be given by

$$\begin{aligned} \langle \mathbf{k}_{f_1}, \mathbf{k}_{f_2}; p_2h_2, h_1 | T^{(2)} | \mathbf{k}_i \rangle_1 &= V_0^2 \int d^3r d^3r' \psi_{\mathbf{k}_{f_2}}^{(-)*}(z, \mathbf{b}) \psi_{p_2}^*(z, \mathbf{b}) \psi_{h_2}(z, \mathbf{b}) \\ &\times G_m^{(+)}(z, \mathbf{b}; z', \mathbf{b}') \psi_{\mathbf{k}_{f_1}}^{(-)*}(z', \mathbf{b}') \psi_{h_1}(z', \mathbf{b}') \psi_{\mathbf{k}_i}^{(+)}(z', \mathbf{b}') \\ &= -i \int d^2b e^{i\mathbf{q}\cdot\mathbf{b}} e^{i(\delta_i(b)+\delta_{f_1}(b)+\delta_{f_2}(b))} \\ &\times \int_{-\infty}^{\infty} dz W_{f_2p_2h_2,m}(z, \mathbf{b}) \frac{1}{\hbar v_m} \int_{-\infty}^z dz' W_{f_1mh_1,i}(z', \mathbf{b}) . \end{aligned} \quad (5.29)$$

The other amplitude of this type rescatters the first continuum particle,

$$\begin{aligned} \langle \mathbf{k}_{f_1}, \mathbf{k}_{f_2}; p_2 h_2, h_1 | T^{(2)} | \mathbf{k}_i \rangle_2 &= -i \int d^2 b e^{i\mathbf{q}\cdot\mathbf{b}} e^{i(\delta_i(b)+\delta_{f_1}(b)+\delta_{f_2}(b))} \\ &\times \int_{-\infty}^{\infty} dz W_{f_1 p_2 h_2, m'}(z, \mathbf{b}) \\ &\times \frac{1}{\hbar v_m} \int_{-\infty}^z dz' W_{m' f_2 h_1, i}(z', \mathbf{b}) . \end{aligned} \quad (5.30)$$

The full amplitude of this type is the sum of the two. The coherence/incoherence between such modes is one of the points we plan to study in the future.

There is also a two-step process in which the first step inelastically scatters the incident particle while the second step excites an additional particle to the continuum. This is given by

$$\begin{aligned} \langle \mathbf{k}_{f_1}, \mathbf{k}_{f_2}; h_2, p_1 h_1 | T^{(2)} | \mathbf{k}_i \rangle &= -i \int d^2 b e^{i\mathbf{q}\cdot\mathbf{b}} e^{i(\delta_i(b)+\delta_{f_1}(b)+\delta_{f_2}(b))} \\ &\times \int_{-\infty}^{\infty} dz W_{f_1 f_2 h_2, m}(z, \mathbf{b}) \\ &\times \frac{1}{\hbar v_m} \int_{-\infty}^z dz' W_{m p_1 h_1, i}(z', \mathbf{b}) . \end{aligned} \quad (5.31)$$

There are three two-step amplitudes that result in three particles in the continuum. We can reduce these to expressions of the type

$$\begin{aligned} \langle \mathbf{k}_{f_1}, \mathbf{k}_{f_2}, \mathbf{k}_{f_3}; h_2, h_1 | T^{(2)} | \mathbf{k}_i \rangle_1 &= -i \int d^2 b e^{i\mathbf{q}\cdot\mathbf{b}} e^{i(\delta_i(b)+\delta_{f_1}(b)+\delta_{f_2}(b)+\delta_{f_3}(b))} \\ &\times \int_{-\infty}^{\infty} dz W_{f_2 f_3 h_2, m}(z, \mathbf{b}) \\ &\times \frac{1}{\hbar v_m} \int_{-\infty}^z dz' W_{m f_1 h_1, i}(z', \mathbf{b}) , \end{aligned} \quad (5.32)$$

and

$$\begin{aligned} \langle \mathbf{k}_{f_1}, \mathbf{k}_{f_2}, \mathbf{k}_{f_3}; h_2, h_1 | T^{(2)} | \mathbf{k}_i \rangle_2 &= -i \int d^2 b e^{i\mathbf{q}\cdot\mathbf{b}} e^{i(\delta_i(b)+\delta_{f_1}(b)+\delta_{f_2}(b)+\delta_{f_3}(b))} \\ &\times \int_{-\infty}^{\infty} dz W_{f_1 f_3 h_2, m}(z, \mathbf{b}) \\ &\times \frac{1}{\hbar v_m} \int_{-\infty}^z dz' W_{m f_2 h_1, i}(z', \mathbf{b}) , \end{aligned} \quad (5.33)$$

and

$$\begin{aligned} \langle \mathbf{k}_{f_1}, \mathbf{k}_{f_2}, \mathbf{k}_{f_3}; h_2, h_1 | T^{(2)} | \mathbf{k}_i \rangle_3 &= -i \int d^2b e^{i\mathbf{q}\cdot\mathbf{b}} e^{i(\delta_i(b)+\delta_{f_1}(b)+\delta_{f_2}(b)+\delta_{f_3}(b))} \\ &\times \int_{-\infty}^{\infty} dz W_{f_1 f_2 h_2, m}(z, \mathbf{b}) \\ &\times \frac{1}{\hbar v_m} \int_{-\infty}^z dz' W_{m f_3 h_1, i}(z', \mathbf{b}) . \end{aligned} \quad (5.34)$$

With these, we have all of the one and two-step amplitudes that excite particles to the continuum. We can write the two-step amplitudes that de-excite particles to the bound states using the quantity

$$W_{p_1 p_2 h, m}(z, \mathbf{b}) = V_0 \psi_{p_1}^*(z, \mathbf{b}) \psi_{p_2}^*(z, \mathbf{b}) \psi_h(z, \mathbf{b}) \exp[ik_{mz}z + i\phi_m(z, \mathbf{b})] . \quad (5.35)$$

We have the two-step absorption amplitude of a single particle in the continuum,

$$\langle p_2 p_3 h_2, p_1 h_1 | T^{(2)} | \mathbf{k}_i \rangle = -i \int d^2b e^{i\delta_i(b)} \int_{-\infty}^{\infty} dz W_{p_2 p_3 h_2, m}(z, \mathbf{b}) \frac{1}{\hbar v_m} \int_{-\infty}^z dz' W_{m p_1 h_1, i}(z', \mathbf{b}) , \quad (5.36)$$

as well as the more interesting amplitude, in which one of two outgoing particles is absorbed,

$$\begin{aligned} \langle \mathbf{k}_f; p_1 p_2 h_2, h_1 | T^{(2)} | \mathbf{k}_i \rangle &= -i \int d^2b e^{i\mathbf{q}\cdot\mathbf{b}} e^{i(\delta_i(b)+\delta_f(b))} \\ &\times \int_{-\infty}^{\infty} dz W_{p_1 p_2 h_2, m}(z, \mathbf{b}) \frac{1}{\hbar v_m} \int_{-\infty}^z dz' W_{m f h_1, i}(z', \mathbf{b}) , \end{aligned} \quad (5.37)$$

with $\mathbf{q} = \mathbf{k}_i - \mathbf{k}_f$.

5.4 Differential energy-angular distributions

As stated above, the elastic angular distribution is given by

$$\frac{d\sigma_{el}}{d\Omega} = |f_{el}(\mathbf{k}_f, \mathbf{k}_i)|^2 . \quad (5.38)$$

We can put this into the general framework we will use to calculate other energy-angular distributions by defining

$$\langle \mathbf{k}_f | T_{el} | \mathbf{k}_i \rangle = -4\pi \frac{\hbar^2}{2\mu} f_{el}(\mathbf{k}_f, \mathbf{k}_i) . \quad (5.39)$$

We obtain the elastic differential cross section from the T-matrix element as

$$\begin{aligned}
d\sigma_{el} &= \frac{2\pi}{\hbar v_i} \frac{d^3 k_f}{(2\pi)^3} |\langle \mathbf{k}_f | T_{el} | \mathbf{k}_i \rangle|^2 \delta(E_f - E_i) \\
&= \frac{\mu}{\hbar^2 k_i} \frac{k_f^2 dk_f d\Omega_f}{(2\pi)^2} |\langle \mathbf{k}_f | T_{el} | \mathbf{k}_i \rangle|^2 \delta(E_f - E_i) \\
&= \left(\frac{\mu}{\hbar^2} \frac{1}{2\pi} \right)^2 \frac{k_f}{k_i} d\Omega_f |\langle \mathbf{k}_f | T_{el} | \mathbf{k}_i \rangle|^2 \delta(E_f - E_i) dE_f.
\end{aligned} \tag{5.40}$$

If we now integrate over the final energy and use the fact that $k_f = k_i$, we find

$$\frac{d\sigma_{el}}{d\Omega_f} = \left(\frac{\mu}{2\pi\hbar^2} \right)^2 |\langle \mathbf{k}_f | T_{el} | \mathbf{k}_i \rangle|^2 = |f_{el}(\mathbf{k}_f, \mathbf{k}_i)|^2. \tag{5.41}$$

For an inelastic amplitude with only one final particle in the continuum, we obtain a similar expression

$$d\sigma_{i \rightarrow f} = \left(\frac{\mu}{\hbar^2} \frac{1}{2\pi} \right)^2 \frac{k_f}{k_i} d\Omega_f |\langle \mathbf{k}_f | T_{el} | \mathbf{k}_i \rangle|^2 \delta(E_f + \varepsilon^* - E_i) dE_f, \tag{5.42}$$

where ε^* is the final excitation energy of the target nucleus. We find in this case,

$$\frac{d\sigma_{i \rightarrow f}}{d\Omega_f} = \left(\frac{\mu}{2\pi\hbar^2} \right)^2 \frac{k_f}{k_i} |\langle \mathbf{k}_f | T_{i \rightarrow f} | \mathbf{k}_i \rangle|^2. \tag{5.43}$$

When there are two final particles in the continuum, the expression for the energy-angular distribution becomes

$$\begin{aligned}
d\sigma_{i \rightarrow f} &= \frac{2\pi}{\hbar v_i} \frac{d^3 k_{f_1}}{(2\pi)^3} \frac{d^3 k_{f_2}}{(2\pi)^3} |\langle \mathbf{k}_{f_1}, \mathbf{k}_{f_2} | T_{i \rightarrow f} | \mathbf{k}_i \rangle|^2 \delta(E_{f_1} + E_{f_2} + \varepsilon^* - E_i) \\
&= 2\pi \frac{\mu}{\hbar^2 k_i} \frac{k_{f_1}^2 dk_{f_1} d\Omega_{f_1}}{(2\pi)^3} \frac{k_{f_2}^2 dk_{f_2} d\Omega_{f_2}}{(2\pi)^2} |\langle \mathbf{k}_{f_1}, \mathbf{k}_{f_2} | T_{i \rightarrow f} | \mathbf{k}_i \rangle|^2 \delta(E_{f_1} + E_{f_2} + B(A, 1) + \varepsilon^* - E_i) \\
&= \frac{1}{(2\pi)^5} \left(\frac{\mu}{\hbar^2} \right)^3 \frac{k_{f_1} k_{f_2}}{k_i} dE_{f_1} d\Omega_{f_1} dE_{f_2} d\Omega_{f_2} |\langle \mathbf{k}_{f_1}, \mathbf{k}_{f_2} | T_{i \rightarrow f} | \mathbf{k}_i \rangle|^2 \\
&\quad \times \delta(E_{f_1} + E_{f_2} + B(A, 1) + \varepsilon^* - E_i),
\end{aligned} \tag{5.44}$$

where $B(A, 1)$ is the binding energy in the target nucleus of the additional nucleon in the continuum. Integrating over E_{f_2} , for example, then furnishes

$$\frac{d\sigma_{i \rightarrow f}}{dE_{f_1} d\Omega_{f_1} d\Omega_{f_2}} = \frac{1}{(2\pi)^5} \left(\frac{\mu}{\hbar^2} \right)^3 \frac{k_{f_1} k_{f_2}}{k_i} |\langle \mathbf{k}_{f_1}, \mathbf{k}_{f_2} | T_{i \rightarrow f} | \mathbf{k}_i \rangle|^2, \tag{5.45}$$

where E_{f_2} is constrained by energy conservation.

In the general case of n particles in the continuum, we have

$$\begin{aligned}
d\sigma_{i \rightarrow f} &= \frac{2\pi}{\hbar v_i} \prod_{j=1}^n \frac{d^3 k_{f_j}}{(2\pi)^3} |\langle \mathbf{k}_{f_1} \dots \mathbf{k}_{f_n} | T_{i \rightarrow f} | \mathbf{k}_i \rangle|^2 \delta \left(\sum_{j=1}^n E_{f_j} + B(A, n-1) + \varepsilon^* - E_i \right) \\
&= 2\pi \frac{\mu}{\hbar^2 k_i} \prod_{j=1}^n \frac{k_{f_j}^2 dk_{f_j} d\Omega_{f_j}}{(2\pi)^3} |\langle \mathbf{k}_{f_1} \dots \mathbf{k}_{f_n} | T_{i \rightarrow f} | \mathbf{k}_i \rangle|^2 \delta \left(\sum_{j=1}^n E_{f_j} + B(A, n-1) + \varepsilon^* - E_i \right) \\
&= \frac{1}{(2\pi)^{3n-1}} \left(\frac{\mu}{\hbar^2} \right)^{n+1} \frac{\prod_{j=1}^n k_{f_j}}{k_i} \prod_{j=1}^n (dE_{f_j} d\Omega_{f_j}) |\langle \mathbf{k}_{f_1} \dots \mathbf{k}_{f_n} | T_{i \rightarrow f} | \mathbf{k}_i \rangle|^2 \\
&\quad \times \delta \left(\sum_{j=1}^n E_{f_j} + B(A, n-1) + \varepsilon^* - E_i \right), \tag{5.46}
\end{aligned}$$

where $B(A, n-1)$ is the binding energy of $n-1$ nucleons in the nucleus of mass A (and charge Z). Integrating over any one of the final particle energies then furnishes a differential flux distribution in terms of the n solid angles $d\Omega_j$ and the $n-1$ remaining energies E_j , with the integrated particle energy constrained by energy conservation.

Contributions to the absorption cross section have no emitted particles. These take the form

$$d\sigma_{abs} = \frac{2\pi}{\hbar v_i} |\langle T_{i \rightarrow f} | \mathbf{k}_i \rangle|^2 \delta(\varepsilon^* - E_i - B(A+1, 1)), \tag{5.47}$$

where $B(A+1, 1)$ is the binding energy of the incident nucleon in the compound nucleus formed through its absorption.

5.5 One-step Cross Sections

In the following sections the final formulas and the numerical results for one particle emission are presented. The simple single particle energies are obtained with the model described in Appendix A.3 and the wave functions are taken from the the quantum harmonic oscillator basis.

5.5.1 One particle in continuum

One may note that, in fact, for the first step there are three different particle-hole excitations,

$$\frac{d^2 \sigma^{(1)}}{d\Omega dE_f} = \frac{d^2 \sigma_{\pi\pi}^{(1)}}{d\Omega dE_f} + \frac{d^2 \sigma_{\nu\nu}^{(1)}}{d\Omega dE_f} + \frac{d^2 \sigma_{\pi\nu}^{(1)}}{d\Omega dE_f}, \tag{5.48}$$

where π (proton) and ν (neutron) represent the nature of the particle-hole excitation. For the moment we work with the first two types that do not involve charge exchange, the $\pi\pi$ and $\nu\nu$ particle-hole states.

The one-step double differential cross-section is obtained with

$$\frac{d^2\sigma_{f\leftarrow i}}{d\Omega dE_{k_f}} = \left(\frac{\mu}{2\pi\hbar^2}\right)^2 \frac{k_f}{k_i} \sum_{ph} \rho(E_x) \left| \left\langle \vec{k}_f; ph \left| T^{(1)} \right| \vec{k}_i \right\rangle \right|^2 \delta(E_i - E_f - E_x), \quad (5.49)$$

with each particle-hole excitation being weighted by a Breit-Wigner distribution

$$\rho(E_x) = \frac{1}{\pi} \frac{\gamma}{(E_x - E_{ph})^2 + \frac{\gamma^2}{4}} N(E_{ph}) dE_{ph}, \quad (5.50)$$

where $E_{ph} = E_p - E_h$ and $N(E_{ph})$ are the the p-h energy and density of states, respectively.

The excitation energy is obtained from the projectile energy loss $E_x = E_f - E_i$.

It is common to have, for low-excitation energies, cross-sections data for well defined total angular momenta and parity. For this reason, we compute the cross section for each total coupling angular momentum J (l for spinless case) and parity π . For high excitation energy values, the sum of all J and π contributions are computed.

One then has for nucleon inelastic scattering (with no spin interaction)

$$\frac{d^2\sigma_{f\leftarrow i}}{d\Omega dE_{k_f}} = \left(\frac{\mu}{2\pi\hbar^2}\right)^2 \frac{k_f}{k_i} \sum_{n_p n_h} \rho(E_x) \left| \left\langle \vec{k}_f; j_p n_p j_h n_h \left| T^{(1)} \right| \vec{k}_i \right\rangle \right|^2 \delta(E_i - E_f - E_x), \quad (5.51)$$

with

$$\begin{aligned} \sum_{n_p n_h} \left| \left\langle \vec{k}_f; j_p n_p j_h n_h \left| T \right| \vec{k}_i \right\rangle \right|^2 &= \sum_{lm} (l_p j_p | Y_l | l_h j_h)^2 \\ &\times \left| \int d^3r \psi_{k_f}^{(-)*}(\vec{r}) \phi_{pl_p j_p}(r) Y_{l-m}(\hat{r}) \phi_{hl_h j_h}(r) \psi_{k_i}^{(+)}(\vec{r}) \right|^2 \end{aligned} \quad (5.52)$$

where $(l_p j_p | Y_l | l_h j_h)$ is the reduced matrix element given in terms of 3- and 6-j symbols by

$$\begin{aligned} (l_p j_p | Y_l | l_h j_h) &= (-1)^{n_p + \sigma} \left[\frac{(2l_p + 1)(2l_h + 1)(2l + 1)(2j_h + 1)}{4\pi} \right]^{1/2} \\ &\times \begin{pmatrix} l_p & l_h & l \\ 0 & 0 & 0 \end{pmatrix} \begin{Bmatrix} j_p & l & j_h \\ l_h & \sigma & l_p \end{Bmatrix} \end{aligned}$$

The transition matrix elements with single particle states from a quantum harmonic os-

cillator basis becomes

$$\begin{aligned} & \int dr^3 \psi_{kf}^{(-)*}(\vec{r}) \phi_{pl_p j_p}(r) Y_{l-m}(\hat{r}) \phi_{hl_h j_h}(r) \psi_{ki}^{(+)}(\vec{r}) = \\ & V_0 \int b db e^{i(\delta_i(b) + \delta_f(b))} \int d\phi e^{-i|q_x|b \cos \phi} e^{im\phi} \\ & \times \int_{-\infty}^{\infty} dz g_{n_h, l_h}(\sqrt{b^2 + z^2}) P_l^m(\cos(\frac{z}{\sqrt{b^2 + z^2}})) g_{n_p, l_p}(\sqrt{b^2 + z^2}) \\ & \times \exp[iq_z z - i\phi_f(z, b) + i\phi_i(z, b)], \end{aligned}$$

and

$$\begin{aligned} & \int dr^3 \psi_{kf}^{(-)*}(\vec{r}) \phi_{pl_p j_p}(r) Y_{l-m}(\hat{r}) \phi_{hl_h j_h}(r) \psi_{ki}^{(+)}(\vec{r}) = \\ & V_0 2\pi i^m \int b db e^{i(\delta_i(b) + \delta_f(b))} J_m((k_i + k_f)b \sin(\theta/2)) \\ & \times \int_{-\infty}^{\infty} dz g_{n_h, l_h}(\sqrt{b^2 + z^2}) P_l^{-m}(\cos(\frac{z}{\sqrt{b^2 + z^2}})) g_{n_p, l_p}(\sqrt{b^2 + z^2}) \\ & \times \exp[iq_z z - i\phi_f(z, b) + i\phi_i(z, b)] \end{aligned} \quad (5.53)$$

after ϕ integration.

The phases are given by ¹

$$\delta_m(b) = 2\eta \ln(k_m b) + \frac{1}{2} \left[\sigma_{pp}^T(i + \alpha_{pp}) \frac{Z}{A} + \sigma_{pn}^T(i + \alpha_{pn}) \frac{N}{A} \right]_m \int_0^\infty \rho_n(\sqrt{z'^2 + b^2}) dz', \quad (5.54)$$

where

$$\eta = \frac{Ze^2\mu}{\hbar^2 k_m}, \quad (5.55)$$

and

$$\phi_m(z, b) = \frac{1}{2} \left[\sigma_{pp}^T(i + \alpha_{pp}) \frac{Z}{A} + \sigma_{pn}^T(i + \alpha_{pn}) \frac{N}{A} \right]_m \int_0^z \rho_n(\sqrt{z'^2 + b^2}) dz', \quad (5.56)$$

5.5.1.1 Low energy excitation

We start the inelastic calculations with a low energy excited state, the first 3^- excitation of ^{90}Zr . Fig.5.5 shows the RPA modes contributing to this excited state. We see on the left panel that only two components (red and blue dots) carry most of the information with several other components making small contributions to the strength (right panel on log scale). We can now use only the two components that most contribute to the state and compare to the full (all p-h components) results and to the experimental

¹For simplicity, we now only take into consideration the Coulomb contribution to the first phase δ . If we study a neutron-induced reaction, the Z/A and N/A are exchanged and the Coulomb potential is zero.

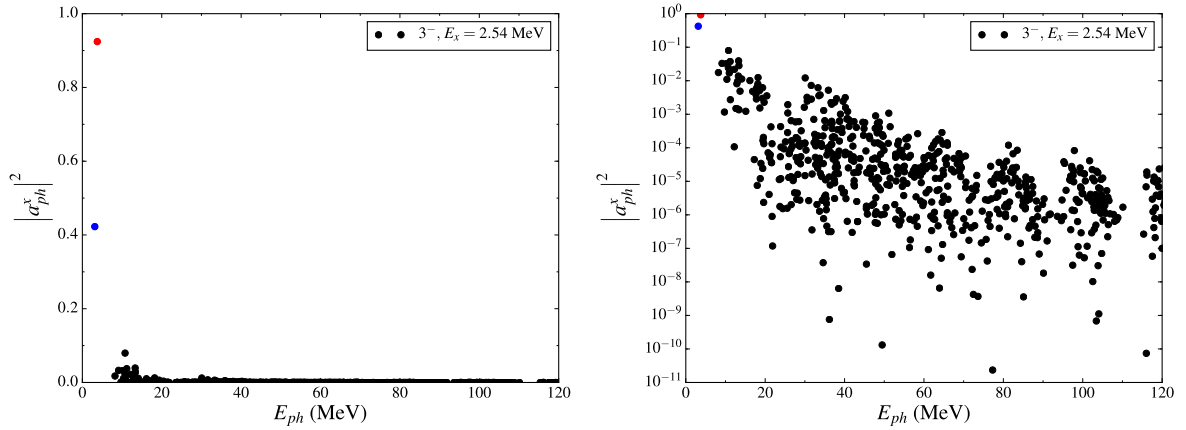


FIGURE 5.5 – Particle-hole mode contributions to the first 3^- excited state of ^{90}Zr . On the left two components are more pronounced but only contribute with 70 % of the strength. On the right panel, in log scale, many other modes make small contributions to complete the total strength.

data. The comparison is shown in Fig.5.6 for two proton incident energies. The results are reproduced rather well with the full particle hole basis (solid dark line). Applying a cut-off on the contributing modes reduces the strength of the cross sections, where the two most important contributions are still at least one order of magnitude below the experimental data. In addition, we also compare the results obtained with the simplified p-h basis and QHO to the ones obtained with all components present in the correspondent RPA state of Fig.5.5. For this, the single particle states from the HF mean field were also employed. The similarity of the results obtained indicate that the details of the single particle states are not critical in this approach, and the simplified model we use for the wave functions seems to be sufficient. The dotted line corresponds to the direct use of the RPA amplitudes a_{ph}^x instead of the Breit-Wigner distribution. In general, the shape of the angular distribution is related to the angular momentum coupling. But one of the reasons for our results not being perfectly comparable with the data is the randomness assumption assumed. The interference between different modes was neglected and a more refined approach is necessary.

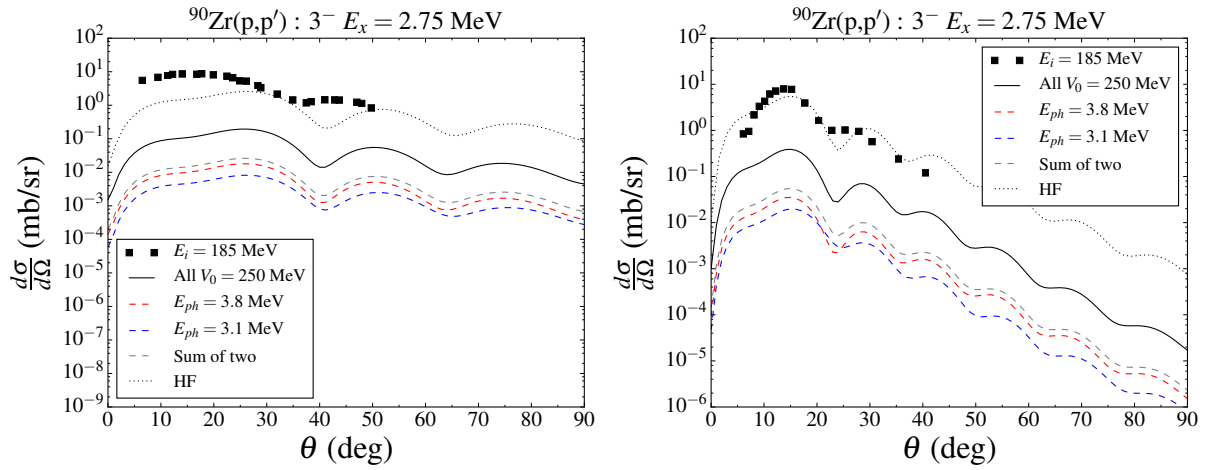


FIGURE 5.6 – Inelastic proton cross section for ^{90}Zr at 57.5 MeV (left panel) and 185 MeV (right panel). The dashed blue, red and gray lines represent the separate $E_{ph} = 3.1$ MeV, $E_{ph} = 3.8$ MeV particle hole contributions and the sum of these two components, respectively. The full dark solid line represent calculations performed with all p-h components. The dotted dark line is obtained with all p-h components of the RPA state with the single particle HF states employed.

5.5.1.2 Radial Transition Density of States

Cross sections can be obtained by using the transition density of a state given by (COLÒ *et al.*, 2013)

$$\delta_\nu(\vec{r}) = \langle \nu | \hat{\rho}(\vec{r}) | \tilde{0} \rangle = \delta\rho_\nu(r) Y_{JM}^*(\hat{r}), \quad (5.57)$$

where ν represents an RPA excited state. This quantity preserves the sign of each eigenvector component in a simple sum over all p-h components.

The differential cross section is directly obtained by squaring the transition matrix elements (see Appendix A.4 for details)

$$\frac{d\sigma^2}{dE_f d\Omega_f} \sim \left| T_{k_f \leftarrow k_i}^\nu \right|^2 \delta(E_i - E_f + E_\nu), \quad (5.58)$$

where

$$\begin{aligned} T_{k_f \leftarrow k_i}^\nu &= \sum_M 2\pi i^{-M} \sqrt{\frac{(2J+1)(J+M)!}{4\pi(J-M)!}} \int b db j_{-M}((k_i + k_f) \sin(\theta/2) b) e^{i(\delta_f(b) + \delta_i(b))} \\ &\quad \times \int dz \exp[iq_z z + \text{sign}(z)(-i\phi_f(z, b) + i\phi_i(z, b))] \\ &\quad \times \delta\rho_\nu\left(\sqrt{z^2 + b^2}\right) P_J^{-M}\left(\frac{z}{\sqrt{b^2 + z^2}}\right), \end{aligned} \quad (5.59)$$

is summed over the M projection values

$$M \rightarrow [-J, J] \rightarrow [-J, -J+1, \dots, 0, \dots, J-1, J].$$

We use the radial transition density $\delta_\nu(r)$ from the RPA code (COLÒ *et al.*, 2013) (with linear interpolation when necessary). In Figure 5.7, we show on the left panel the radial transition density δ_ν for the first excited energy 3^- state of ^{90}Zr . This function is a sum of the neutron and proton contributions and is necessary to obtain the cross section of Eq.5.58 shown on the right panel of Fig. 5.7. The cross section values are in good agreement with the data. The shift for the small energy case is a geometrical effect reflected by the target radius. We apply this approach at other energies for ^{208}Pb . The results compare well to the experimental data for all energies employed, as can be seen in Fig. 5.8. For both targets the excitation energy obtained with the RPA does not reproduce exactly the experimental value. Although a detailed study of the RPA excitation in this context is beyond the scope of this work, better results can be obtained with larger numerical bases and more computation time.

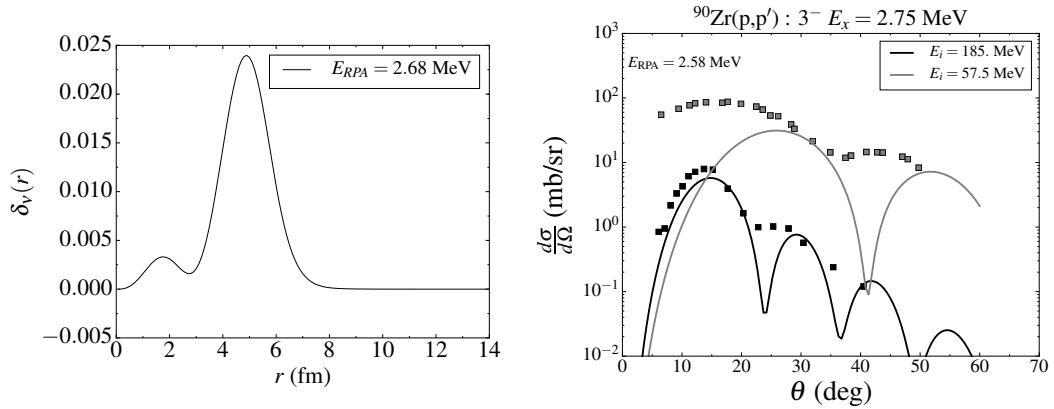


FIGURE 5.7 – Left panel: radial transition density δ_ν for the first excited energy 3^- state of ^{90}Zr . Right panel: Differential double cross section for proton scattering obtained with (5.58). Cross-section values of the right panel are shifted for visualization convenience.

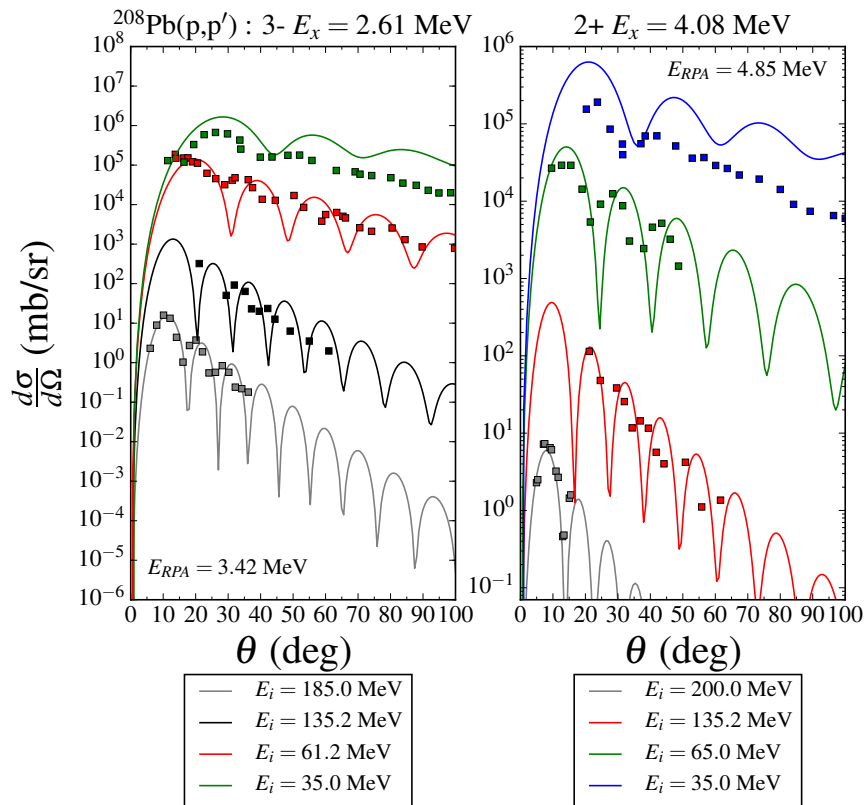


FIGURE 5.8 – Differential double cross section of proton inelastic scattering at 3^- (left panel) and 2^+ (right panel) excited states of ^{208}Pb . The values are shifted for visualization convenience.

The references for the cross-sections experimental data for 3^- , 2^+ excitations are given in Table 5.4.

Reaction	Excited State	Proton Incident Energy E (MeV)
$^{90}\text{Zr}(p,p')$	3^-	57.5 (MARTIN <i>et al.</i> , 1979), 185 (HAGBERG; SUNDQVIST, 1971)
$^{208}\text{Pb}(p,p')$	3^-	35 (WAGNER <i>et al.</i> , 1975), 61.2 (SCOTT <i>et al.</i> , 1977), 135.2 (ADAMS <i>et al.</i> , 1980), 185 (INGEMARSSON; FAGERSTRÖM, 1976)
$^{208}\text{Pb}(p,p')$	2^+	35 (WAGNER <i>et al.</i> , 1975), 65 (HAYAKAWA <i>et al.</i> , 1982), 135.2 (ADAMS <i>et al.</i> , 1980), 200 (MCDANIELS <i>et al.</i> , 1987)

TABLE 5.4 – Data sets for the proton inelastic cross sections for specific J^π excited target states.

5.5.1.3 Higher Excitation Energies

Figure 5.9 shows cross-sections results for higher excitation energies. The results shown are in good agreement with excitation energies up to 20 MeV, for larger values the discrete particle hole basis faces difficulties in feeding the excitation strength and a need for the second step of the reaction seems to appear. For higher excitation energy, the weighting/response of the p-h states make very small contributions if the energies of the pair E_{ph} are not large and comparable to E_x . For instance, at an excitation energy of 100 MeV, the angular distribution is a few orders of magnitudes below the expected experimental data. This is a case where higher modes of excitations, beyond a single particle-hole excitation take place.

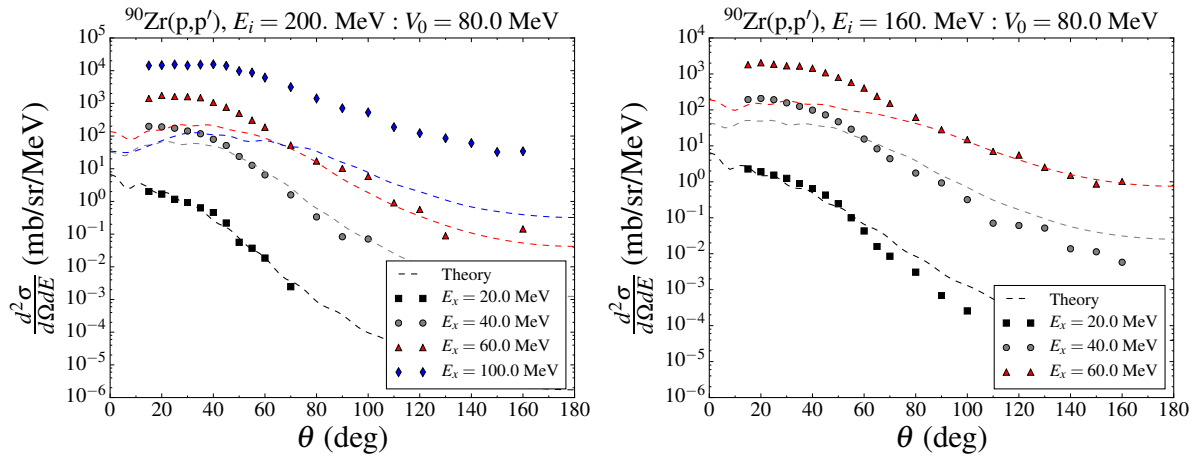


FIGURE 5.9 – Inelastic proton cross section from ^{90}Zr at different excitation energies for two incoming proton energies, 200 (left panel) and 160 MeV (right panel). Experimental data were taken from (RICHTER *et al.*, 1994).

5.5.1.4 Spin distributions

The total one-step cross-section is obtained from

$$\sigma_{E_i} = \int dE_{k_f} \int 2\pi d\theta \sin\theta \frac{d^2\sigma_{f\leftarrow i}}{d\Omega dE_{k_f}} \quad (5.60)$$

with $0 < E_f < E_i$.

As we compute the double differential cross-section for each angular momentum coupling J , we also have

$$\sigma_{E_i} = \sum_J \sigma^J. \quad (5.61)$$

The spin distribution can then be obtained as

$$P(J) = \frac{\sigma^J}{\sigma_{E_i}}. \quad (5.62)$$

Figs.5.10 shows the spin distribution for ^{90}Zr for different energy values. All distributions have the largest contribution from $J \sim 4$. One notes that these shift to the right as the incident energy increases is due to the larger excitation energies when adds more terms of larger angular momentum J (larger J usually means larger E_μ which only contributes for larger E_x due to the Breit-Wigner response function). The results obtained here are more restricted in value than the Wigner-like distribution formula usually assumed *ad hoc* in the context of the exciton model of pre-equilibrium emission

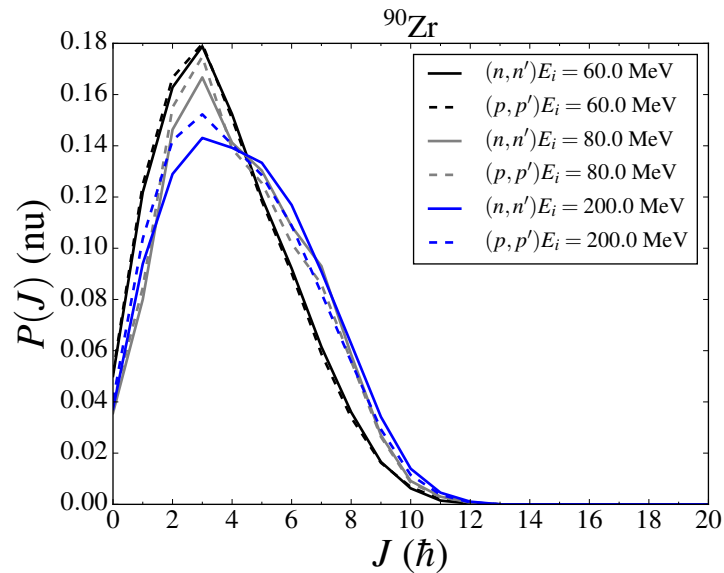


FIGURE 5.10 – Spin distribution (5.62) for nucleon induced reaction on ^{90}Zr .

5.5.2 Two particles in the continuum

For two particle emission, we have

$$\begin{aligned} \langle \vec{k}_{f_1}, \vec{k}_{f_2}; h | T^{(1)} | \vec{k}_i \rangle &= V_0 \int d^2b e^{i\vec{q}\cdot\vec{b}} e^{i(\delta_i(b)+\delta_{f_1}(b)+\delta_{f_2}(b))} \int_{-\infty}^{\infty} dz \psi_h(z, \vec{b}) \\ &\quad \times \exp \left[iq_z z - i\phi_{f_1}(z, \vec{b}) - i\phi_{f_2}(z, \vec{b}) + i\phi_i(z, \vec{b}) \right]. \end{aligned} \quad (5.63)$$

where $\vec{q} = \vec{k}_i - \vec{k}_{f_1} - \vec{k}_{f_2}$. In this case, two particles are being emitted and the angle between them has to be defined. In what follows we present two approaches: one for the case of a sum of the two momenta resulting in one momentum vector and one scattering angle (dependent continuum particles); and another case considering both as independent. The expressions then have two scattering angles, one for each of the continuum particles (independent continuum particles).

5.5.2.1 Dependent continuum particles

We can write the components of the transfer momentum vector as

$$\vec{q} = \vec{k}_i - \vec{k}_{f_1} - \vec{k}_{f_2} = \vec{k}_i - \vec{k}', \quad (5.64)$$

where $\vec{k}' = \vec{k}_{f_1} + \vec{k}_{f_2}$. Then,

$$\vec{q} \cdot \vec{b} = -k' b \sin \theta \cos \phi \quad (5.65)$$

and

$$q_z z = (k_i - k' \cos \theta) z, \quad (5.66)$$

with $k' = \sqrt{k_{f_1}^2 + k_{f_2}^2}$. We now have $\theta_{k_i k'}$, and the angle between k_{f_1} and k_{f_2} becomes arbitrary.

Considering the definition above, the expression for the transition amplitude becomes quite similar to the case of one particle in the continuum

$$\begin{aligned} \langle \vec{k}_{f_1}, \vec{k}_{f_2}; h | T^{(1)} | \vec{k}_i \rangle &= V_0 \int b db \int d\phi e^{-ik' b \sin \theta \cos \phi} e^{i(\delta_i(b)+\delta_{f_1}(b)+\delta_{f_2}(b))} \\ &\quad \times \int_{-\infty}^{\infty} dz \psi_h(z, b, \phi) \\ &\quad \times \exp \left[i(k_i - k' \cos \theta) z + \frac{i}{\hbar v_{f_1}} \int_0^z U_{f_1}(\sqrt{z'^2 + b^2}) dz' \right. \\ &\quad \left. + \frac{i}{\hbar v_{f_2}} \int_0^z U_{f_2}(\sqrt{z'^2 + b^2}) dz' - \frac{i}{\hbar v_i} \int_0^z U_i(\sqrt{z'^2 + b^2}) dz' \right]. \end{aligned}$$

and then,

$$\begin{aligned}
\left\langle \vec{k}_{f_1}, \vec{k}_{f_2}; h \left| T^{(1)} \right| \vec{k}_i \right\rangle_{n', l', m'} &= V_0 2\pi i^{m'} \int b db J_{(m')}(k_f b \sin \theta) e^{i(\delta_i(b) + \delta_{f_1}(b) + \delta_{f_2}(b))} \\
&\times \int_{-\infty}^{\infty} dz g_{n', l'}(\sqrt{b^2 + z^2}) P_{l'}^{m'}\left(\frac{z}{\sqrt{b^2 + z^2}}\right) \\
&\times \exp \left[i(k_i - k' \cos \theta) z + \frac{i}{\hbar v_{f_1}} \int_0^z U_{f_1}(\sqrt{z'^2 + b^2}) dz' \right. \\
&\left. + \frac{i}{\hbar v_{f_2}} \int_0^z U_{f_2}(\sqrt{z'^2 + b^2}) dz' - \frac{i}{\hbar v_i} \int_0^z U_i(\sqrt{z'^2 + b^2}) dz' \right].
\end{aligned} \tag{5.67}$$

5.5.2.2 Independent continuum particles

We can write the transferred momentum vector as

$$\vec{q} = \vec{k}_i - \vec{k}_{f_1} - \vec{k}_{f_2}; \quad \vec{b} = (b \cos \phi, b \sin \phi), \tag{5.68}$$

then with a $x - z$ scattering process and assuming the incoming momentum $\vec{k}_i = (0, 0, k_i)$, see Fig. 5.11, the components of \vec{q} are

$$q_z = k_i - k_{f_1} \cos \theta_1 - k_{f_2} \cos \theta_2, \quad q_x = k_{f_1} \sin \theta_1 - k_{f_2} \sin \theta_2, \quad q_y = 0. \tag{5.69}$$

Considering the definition above, the expression for the transition amplitude becomes

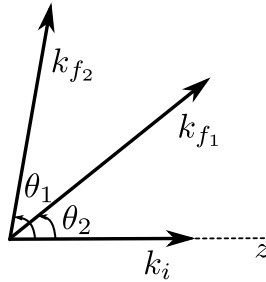


FIGURE 5.11 – Scattering angle representation for two continuum particles.

similar to that of one particle in continuum case

$$\begin{aligned}
\langle \vec{k}_{f_1}, \vec{k}_{f_2}; h | T^{(1)} | \vec{k}_i \rangle &= V_0 \int b db \int d\phi e^{-ib \cos \phi (k_{f_1} \sin \theta_1 - k_{f_2} \sin \theta_2)} e^{i(\delta_i(b) + \delta_{f_1}(b) + \delta_{f_2}(b))} \\
&\times \int_{-\infty}^{\infty} dz \psi_h(z, b, \phi) \\
&\times \exp \left[i(k_i - k_{f_1} \cos \theta_1 - k_{f_2} \cos \theta_2) z + \frac{i}{\hbar v_{f_1}} \int_0^z U_{f_1}(\sqrt{z^2 + b^2}) dz' \right. \\
&\left. + \frac{i}{\hbar v_{f_2}} \int_0^z U_{f_2}(\sqrt{z^2 + b^2}) dz' - \frac{i}{\hbar v_i} \int_0^z U_i(\sqrt{z^2 + b^2}) dz' \right].
\end{aligned}$$

and then,

$$\begin{aligned}
\langle \vec{k}_{f_1}, \vec{k}_{f_2}; h | T^{(1)} | \vec{k}_i \rangle_{n', l', m'} &= C_{l' m'} V_0 2\pi i^{m'} \int b db J_{(m')} (b(k_{f_1} \sin \theta_1 - k_{f_2} \sin \theta_2)) \\
&\times e^{i(\delta_i(b) + \delta_{f_1}(b) + \delta_{f_2}(b))} \int_{-\infty}^{\infty} dz g_{n', l'}(\sqrt{b^2 + z^2}) P_{l'}^{m'} \left(\frac{z}{\sqrt{b^2 + z^2}} \right) \\
&\times \exp \left[i(k_i - k_{f_1} \cos \theta_1 - k_{f_2} \cos \theta_2) z + \frac{i}{\hbar v_{f_1}} \int_0^z U_{f_1}(\sqrt{z^2 + b^2}) dz' \right. \\
&\left. + \frac{i}{\hbar v_{f_2}} \int_0^z U_{f_2}(\sqrt{z^2 + b^2}) dz' - \frac{i}{\hbar v_i} \int_0^z U_i(\sqrt{z^2 + b^2}) dz' \right].
\end{aligned} \tag{5.70}$$

where

$$C_{l' m'} = (-1)^{m'} \sqrt{\frac{(2l+1)(l-m')!}{4\pi(l+m')!}}, \tag{5.71}$$

with the same phases as for the one particle emission case.

Figure 5.12 shows a preliminary result for two particle emission within the independent angle description. The angular distribution of particle 1 is calculated for a fixed scattering angle of the second particle θ_2 . The difference in angle is found to cause, mainly, shifts in the cross section values.

5.5.3 No outgoing particle – absorption

Since $\vec{q} = \vec{k}_i$ and $\vec{k}_i \perp \vec{b}$

$$\begin{aligned}
\langle p_1 p_2 h | T^{(1)} | \vec{k}_i \rangle &= V_0 \int d^2 b e^{i\delta_i(b)} \int_{-\infty}^{\infty} dz \psi_{p_1}^*(z, \vec{b}) \psi_{p_2}^*(z, \vec{b}) \psi_h(z, \vec{b}) \\
&\times \exp \left[ik_{z,i} z + i\phi_i(z, \vec{b}) \right].
\end{aligned} \tag{5.72}$$

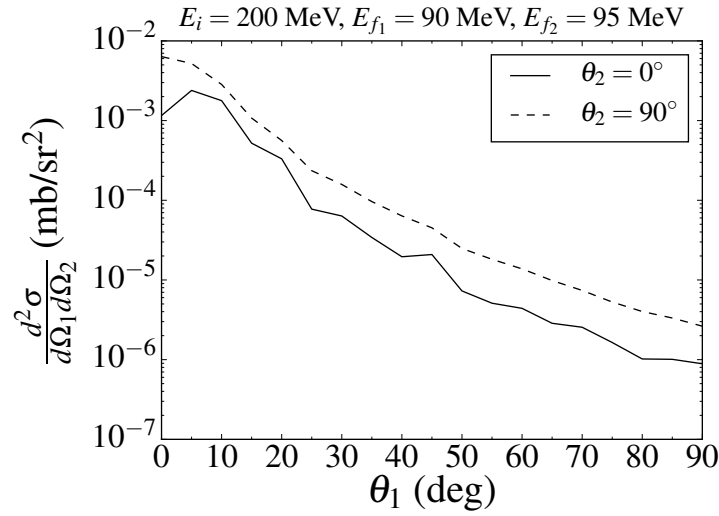


FIGURE 5.12 – Angular distribution for two proton emission from ^{90}Zr target with proton projectiles of $E_i = 200$ MeV. One of the emitted particles is maintained fixed for the calculations (preliminary results).

$$\begin{aligned}
 \langle p_1 p_2 h | T^{(1)} | \vec{k}_i \rangle &= V_0 \int b db \int d\phi e^{i\delta_i(b)} \\
 &\times \int_{-\infty}^{\infty} dz \psi_{p_1}^*(z, b, \phi) \psi_{p_2}^*(z, b, \phi) \psi_h(z, b, \phi) \\
 &\times \exp \left[ik_{z,i} z + -\frac{i}{\hbar v_i} \int_0^z U_i(\sqrt{z^2 + b^2}) dz' \right].
 \end{aligned}$$

$$\begin{aligned}
 \langle p_1 p_2 h | T^{(1)} | \vec{k}_i \rangle_{n_{p_1} l_{p_1} m_{p_1}, n_{p_2} l_{p_2} m_{p_2}, n' l' m'} &= V_0 \int b db e^{i\delta_i(b)} \int d\phi \int_{-\infty}^{\infty} dz \\
 &\times g_{n_1, l_1}(\sqrt{b^2 + z^2}) P_{l_1}^{m_1} \left(\frac{z}{\sqrt{b^2 + z^2}} \right) e^{-im_1 \phi} \\
 &\times g_{n_2, l_2}(\sqrt{b^2 + z^2}) P_{l_2}^{m_2} \left(\frac{z}{\sqrt{b^2 + z^2}} \right) e^{-im_2 \phi} \\
 &\times g_{n', l'}(\sqrt{b^2 + z^2}) P_{l'}^{m'} \left(\frac{z}{\sqrt{b^2 + z^2}} \right) e^{im' \phi} \\
 &\times \exp \left[ik_{z,i} z - \frac{i}{\hbar v_i} \int_0^z U_i(\sqrt{z^2 + b^2}) dz' \right].
 \end{aligned}$$

which reads to ²

$$\begin{aligned}
\left\langle p_1 p_2 \hbar \left| T^{(1)} \right| \vec{k}_i \right\rangle_{n_{p_1} l_{p_1} m_{p_1}, n_{p_2} l_{p_2} m_{p_2}, n' l' m'}^{m' = m_{p_1} + m_{p_2}} &= 2\pi V_0 \int b db e^{i\delta_i(b)} \int_{-\infty}^{\infty} dz \\
&\times g_{n_1, l_1} \left(\sqrt{b^2 + z^2} \right) P_{l_1}^{m_1} \left(\frac{z}{\sqrt{b^2 + z^2}} \right) \\
&\times g_{n_2, l_2} \left(\sqrt{b^2 + z^2} \right) P_{l_2}^{m_2} \left(\frac{z}{\sqrt{b^2 + z^2}} \right) \\
&\times g_{n', l'} \left(\sqrt{b^2 + z^2} \right) P_{l'}^{m'} \left(\frac{z}{\sqrt{b^2 + z^2}} \right) \\
&\times \exp \left[ik_{z,i} z - \frac{i}{\hbar v_i} \int_0^z U_i \left(\sqrt{z'^2 + b^2} \right) dz' \right].
\end{aligned} \tag{5.73}$$

² Let $M = m' - m_{p_1} - m_{p_2}$, then

$$\int_0^{2\pi} e^{i\phi M} d\phi = 0,$$

for M integer and $M \neq 0$. For $M = 0$

$$\int_0^{2\pi} e^0 d\phi = 2\pi,$$

implying $m' = m_{p_1} + m_{p_2}$.

6 Conclusion and Outlook

In this thesis, we have covered various topics related to nuclear reaction. Some of the tools and technics were briefly describe and a more profound discussion of preequilibrium processes was given. We also studied the eikonal approximation which is very useful for high energy processes in which we have focused this work. It replaces the many terms needed in partial wave expansion by an integral over the impact parameter. This wave function was used to represent particles that remains in the continuum during the preequilibrium processes of a nuclear reaction.

We have deduced an extension to the MS quantum theory in analogy with the Blann and Chadwick model. For consistency with the flux loss due to the optical potential, one part of the flux of the second stage should be responsible for absorption to a bound state of one of the particles in the continuum through creation of a p-h pair. We have taken into account channels in which the continuum particles create a new p-h pair with a bound particle or a new p-h pair with an unbound (continuum) particle. In this way, after the second nucleon-nucleon collision there is the possibility of 0, 1, 2, or three particles to be in the continuum.

Elastic scattering of proton projectiles was calculated as test of the $t\rho$ optical potential, which is easily implemented that produced good results at different energies, especially at higher energeties. A more detailed analysis was performed for the one particle emission of the first step of the reaction. For this, we studied the response function of particle-hole excitations in the RPA approach. We have found the more energetic states to be incoherent in energy and the statistical assumptions justified resulting in a Breit-Wiger shape of the p-h strength function independent of the total angular momentum. This distribution provides the weights for each necessary p-h transition matrix elements in the cross section formula. We have shown that the single particle states represented by a quantum harmonic oscillator basis compares very well to the results obtained with states from the Hartree-Fock mean field. This is expected since many p-h states contribute to the cross section, which smooths out particular details of the orbital wave functions.

The low-energy excited states present effects from coherence of the state components involved. Under some limit, the statistical assumptions employed have provided relative good results for proton inelastic scattering from 3^- excited state of ^{90}Zr . The angular

distributions at these energies have a very structured and detailed shape of oscillation requiring a more sophisticated model to reproduce them. For instance, as we have shown, good results can be obtained with the radial transition density of states where the coherence of the components is preserved.

For more energetic reactions the description proposed here is in a good agreement with the data up to 30,40 MeV of excitation. Beyond these values, more steps and excitations of a different nature take part in the reaction. We recall the simplicity of raising particles to the continuum or adding bound states components in this approach, which facilitates the study of multiple emission and absorption. The $t\rho$ optical potential employed together with the eikonal phase shifts have served as an important simplification of the scattering dynamics allowing the study of one-step components of preequilibrium reactions.

As a continuation of this work, we intend to analyze in detail multiple continuum particles as well as the second step of a pre-equilibrium reaction. Also of interest, is the implementation of more realistic interactions such as São Paulo potential or the Koning-Delaroche optical potentials. We also intend to perform calculations including more detailed models of nuclear excitation in comparison with existing models at both low and high excitation energies. We plan to analyze in more detail the different possible excitations varying the number of particles in the continuum over 0, 1,2 for the first and over 0,1,2 and 3 for the second step of the reaction. We expect to see coherence among different configurations of final states with more than one emission (when a is firstly excited and secondly b, or the opposite). We recall that the works by Tamura, Udagawa and Lenske have preserved this coherence in the spatial propagation but have assumed incoherence in averages over nucleus states. In contrast to this, papers from Nishioka, Weidenmüller and Yoshida have affirmed that at low excitation energies, the statistics of states is not yet sufficient for the microscopic structure to be incoherent in average. We intend to extend our investigation of the phase of states involved in those transitions carefully as a function of excitation energy in order to understand better the limits of such coherence.

Appendix A - Tool Box

A.1 Momentum Direction and System of Reference

Assume a nonelastic case $k \neq k'$ and without loss of generality let the scattering be in the xz -plane. Defining the transferred momentum $\vec{q} \equiv \vec{k}_i - \vec{k}_f$, we want to calculate in cylindrical coordinates

$$\vec{q} \cdot \vec{r} = \vec{q} \cdot \vec{b} + \vec{q} \cdot z \hat{z} \quad (\text{A.1})$$

The two simplest options for z -axis reference are represented in Figure (A.1). In case (a) z -axis is placed along the incident particle momentum, while in (b) along the bisector of the scattering angle direction ($\rightarrow \vec{k} + \vec{k}'$). The second case (b) is somewhat closer to a classical trajectory and reproduces better backward scattering particles (GLAUBER, 1959).

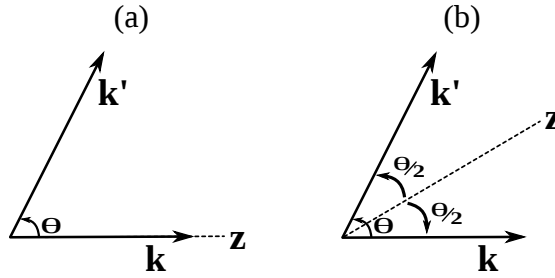


FIGURE A.1 – The two options for z -axis definition: (a) z -axis is placed on incident particle momentum direction \vec{k} and (b) z -axis on the bisector of the scattering angle θ . Note that in the second case $\hat{z} \rightarrow \vec{k} + \vec{k}'$.

- (a) The transferred momentum vector \mathbf{q} has the components, with $\mathbf{k} \perp \mathbf{b} \rightarrow \mathbf{k} = (0, 0, k)$ (note that $k \neq k'$)

$$q_z = k - k' \cos \theta \quad q_x = -k' \sin \theta \quad q_y = 0, \quad (\text{A.2})$$

such that

$$\vec{q} \cdot \vec{b} = (-k' \sin \theta \hat{x}, k - k' \cos \theta \hat{z}) \cdot (b \cos \phi \hat{x}, b \sin \phi \hat{y}) = -k' b \sin \theta \cos \phi. \quad (\text{A.3})$$

and

$$\vec{q} \cdot z\hat{z} = q_z z = (k - k' \cos \theta) z. \quad (\text{A.4})$$

- (b) The transferred momentum vector \mathbf{q} has the components (note that $k \neq k'$ and $\mathbf{k} = (-k \sin(\theta/2), 0, k \cos(\theta/2))$ ¹ and $\mathbf{k}' = (k' \sin(\theta/2), 0, k' \cos(\theta/2))$)

$$q_z = k_z - k'_z = (k - k') \cos(\theta/2) \quad (\text{A.5})$$

$$q_x = -k \sin(\theta/2) - k' \sin(\theta/2) = -(k + k') \sin(\theta/2) \quad (\text{A.6})$$

$$q_y = 0 \quad (\text{A.7})$$

then,

$$\vec{q} \cdot \vec{b} = -(k + k') \sin(\theta/2) b \cos \phi, \quad (\text{A.8})$$

and

$$\vec{q} \cdot z\hat{z} = (k - k') \cos(\theta/2) z. \quad (\text{A.9})$$

A.2 Transition matrix elements

We want to evaluate the matrix element

$$\langle k_f | \langle ph | V | A \rangle | k_i \rangle \quad (\text{A.10})$$

where

$$\begin{aligned} |A\rangle &= |HF\rangle \\ |ph\rangle &= a_\alpha^\dagger h_\beta^\dagger |HF\rangle \\ |k_i\rangle &= d_i^\dagger |\tilde{0}\rangle \\ |k_f\rangle &= d_f^\dagger |\tilde{0}\rangle \end{aligned} \quad (\text{A.11})$$

Here the particle-creation operator is denoted by a^\dagger . Our Fock space consists of three types of creation operators (plus of the annihilation operators):

1. The hole-creation operator h_α^\dagger creating a hole state below the Fermi surface.
2. The particle-creation operator b_α^\dagger creating a bound particle state above the Fermi surface.
3. The particle-creation operator d_α^\dagger creating a scattering state (corresponding to an incoming/outgoing nucleon). In this case the index α should be seen as a more general label of a state.

¹ k_x has a minus sign due to the x-axis orientation

For a simpler notation we also define the vacuum

$$|\phi_0\rangle = |HF\rangle|\tilde{0}\rangle. \quad (\text{A.12})$$

We consider here the case where the particle-hole pair corresponds to bound states. The other cases need some more considerations. Furthermore, V should take the form:

$$V = \frac{1}{4} \sum_{\alpha'\beta'\gamma'\delta'} \bar{v}_{\alpha'\beta'\gamma'\delta'} c_{\alpha'}^\dagger c_{\beta'}^\dagger c_{\delta'} c_{\gamma'}, \quad (\text{A.13})$$

where $\bar{v}_{\alpha'\beta'\gamma'\delta'} = v_{\alpha'\beta'\gamma'\delta'} - v_{\alpha'\beta'\delta'\gamma'}$ with

$$v_{\alpha'\beta'\gamma'\delta'} = \int \phi_{\alpha'}^\dagger(\mathbf{x}_1) \phi_{\beta'}^\dagger(\mathbf{x}_2) v(\mathbf{x}_1, \mathbf{x}_2) \phi_{\gamma'}(\mathbf{x}_1) \phi_{\delta'}(\mathbf{x}_2) d\mathbf{x}_1 d\mathbf{x}_2. \quad (\text{A.14})$$

Here \mathbf{x}_k denotes in general both dependence on spatial coordinates and spin, i.e., in general one has both integration and summation over spin projection (but as long as we use a spin-independent interaction this is not important). Moreover, the summations in (A.13) runs over all three classes of operators discussed above. In this way, the index α' can represent a particle state, a hole state or a scattering state.

Consider now the expression

$$\langle k_f | \langle ph|V|A\rangle | k_i \rangle = \frac{1}{4} \sum_{\alpha'\beta'\gamma'\delta'} \bar{v}_{\alpha'\beta'\gamma'\delta'} \langle \phi_0 | d_f h_\beta a_\alpha c_{\alpha'}^\dagger c_{\beta'}^\dagger c_{\delta'} c_{\gamma'} d_i^\dagger | \phi_0 \rangle. \quad (\text{A.15})$$

For a non-zero result the number of creation operators of each type must match the number of annihilation operators. This leads to the following:

1. First consider the incoming and outgoing nucleons. We need first annihilate the nucleon in the state $|k_i\rangle$. Thus, either δ' or γ' must represent a scattering state, i.e. $c_{\gamma'} \rightarrow d_{\gamma'}$ or $c_{\delta'} \rightarrow d_{\delta'}$. Similarly, we need to create a nucleon in the state $|k_f\rangle$. Similarly, α' or β' must label a scattering state.
2. For the target part we need to create a hole and a particle. Then, either δ' or γ' is a hole index. Thus, $c_{\delta'} \rightarrow h_{\delta'}^\dagger$ or $c_{\gamma'} \rightarrow h_{\gamma'}^\dagger$.
3. In summary, two of the operators will act on the incoming/outgoing nucleons and the other ones on the target.

Therefore,

$$\begin{aligned}
\langle \phi_0 | d_f h_\beta a_\alpha c_{\alpha'}^\dagger c_{\beta'}^\dagger c_{\delta'} c_{\gamma'} d_i^\dagger | \phi_0 \rangle &= \langle \phi_0 | d_f h_\beta a_\alpha c_{\alpha'}^\dagger c_{\beta'}^\dagger c_{\delta'} c_{\gamma'} d_i^\dagger | \phi_0 \rangle \\
&+ \langle \phi_0 | d_f h_\beta a_\alpha c_{\alpha'}^\dagger c_{\beta'}^\dagger c_{\delta'} c_{\gamma'} d_i^\dagger | \phi_0 \rangle + \langle \phi_0 | d_f h_\beta a_\alpha c_{\alpha'}^\dagger c_{\beta'}^\dagger c_{\delta'} c_{\gamma'} d_i^\dagger | \phi_0 \rangle \\
&+ \langle \phi_0 | d_f h_\beta a_\alpha c_{\alpha'}^\dagger c_{\beta'}^\dagger c_{\delta'} c_{\gamma'} d_i^\dagger | \phi_0 \rangle = - \langle \phi_0 | d_f h_\beta a_\alpha d_{\alpha'}^\dagger d_{\beta'}^\dagger h_{\delta'}^\dagger d_{\gamma'}^\dagger d_i^\dagger | \phi_0 \rangle \\
&- \langle \phi_0 | d_f h_\beta a_\alpha d_{\alpha'}^\dagger d_{\beta'}^\dagger h_{\delta'}^\dagger d_{\gamma'}^\dagger d_i^\dagger | \phi_0 \rangle - \langle \phi_0 | d_f h_\beta a_\alpha d_{\alpha'}^\dagger d_{\beta'}^\dagger d_{\delta'}^\dagger h_{\gamma'}^\dagger d_i^\dagger | \phi_0 \rangle \\
&- \langle \phi_0 | d_f h_\beta a_\alpha d_{\alpha'}^\dagger d_{\beta'}^\dagger d_{\delta'}^\dagger h_{\gamma'}^\dagger d_i^\dagger | \phi_0 \rangle,
\end{aligned} \tag{A.16}$$

where in the last step we replaced the generic c-operators by the appropriate particle-, hole- or scattering operators, so that the contractions don't vanish. The minus signs are due to $C_{\delta'} = -h_\delta^\dagger$ in the first and second terms and $C_{\gamma'} = -h_\gamma^\dagger$ in the last ones (see (SUHONEN, 2007)).

Then, by inserting the results of the contractions (leading to Dirac delta functions) and the phases (corresponding to even or odd number of crossings) we obtain

$$\begin{aligned}
\langle \phi_0 | d_f h_\beta a_\alpha c_{\alpha'}^\dagger c_{\beta'}^\dagger c_{\delta'} c_{\gamma'} d_i^\dagger | \phi_0 \rangle &= - (-1)^2 \delta_{\alpha',f} \delta_{\beta',\alpha} \delta_{\gamma',i} \delta_{\delta',\beta} - (-1)^1 \delta_{\alpha',\alpha} \delta_{\beta',f} \delta_{\gamma',i} \delta_{\delta',\beta} \\
&- (-1)^3 \delta_{\alpha',f} \delta_{\beta',\alpha} \delta_{\gamma',\beta} \delta_{\delta',i} - (-1)^2 \delta_{\alpha',\alpha} \delta_{\beta',f} \delta_{\gamma',\beta} \delta_{\delta',i} \\
&= -\delta_{\alpha',f} \delta_{\beta',\alpha} \delta_{\gamma',i} \delta_{\delta',\beta} + \delta_{\alpha',\alpha} \delta_{\beta',f} \delta_{\gamma',i} \delta_{\delta',\beta} \\
&+ \delta_{\alpha',f} \delta_{\beta',\alpha} \delta_{\gamma',\beta} \delta_{\delta',i} - \delta_{\alpha',\alpha} \delta_{\beta',f} \delta_{\gamma',\beta} \delta_{\delta',i},
\end{aligned} \tag{A.17}$$

and thus

$$\begin{aligned}
\langle k_f | \langle ph | V | HF \rangle | k_i \rangle &= \frac{1}{4} \sum_{\alpha' \beta' \gamma' \delta'} \bar{v}_{\alpha' \beta' \gamma' \delta'} (-\delta_{\alpha',f} \delta_{\beta',\alpha} \delta_{\gamma',i} \delta_{\delta',\beta} + \delta_{\alpha',\alpha} \delta_{\beta',f} \delta_{\gamma',i} \delta_{\delta',\beta} \\
&+ \delta_{\alpha',f} \delta_{\beta',\alpha} \delta_{\gamma',\beta} \delta_{\delta',i} - \delta_{\alpha',\alpha} \delta_{\beta',f} \delta_{\gamma',\beta} \delta_{\delta',i}) \\
&= \frac{1}{4} (-\bar{v}_{f\alpha i \beta} + \bar{v}_{\alpha f i \beta} + \bar{v}_{f\alpha \beta i} - \bar{v}_{\alpha f \beta i}) = \bar{v}_{f\alpha \beta i}.
\end{aligned} \tag{A.18}$$

The matrix elements are

$$\begin{aligned}
\bar{v}_{f\alpha \beta i} &= v_{f\alpha \beta i} - v_{f\alpha i \beta} \\
&= \int d^3 r d^3 r' \psi_{k_f}^{(-)*}(\vec{r}) \psi_p^*(\vec{r}') V(\vec{r} - \vec{r}') \psi_h(\vec{r}') \psi_{k_i}^{(+)}(\vec{r}) \\
&- \int d^3 r d^3 r' \psi_{k_f}^{(-)*}(\vec{r}) \psi_p^*(\vec{r}') V(\vec{r} - \vec{r}') \psi_{k_i}^{(+)}(\vec{r}') \psi_h(\vec{r})
\end{aligned} \tag{A.19}$$

Since the overlap of the second term of the expression (A.19) is usually small, we focus on the first term alone

$$\langle k_f | \langle ph | V | HF \rangle | k_i \rangle = \int d^3r d^3r' \psi_{k_f}^{(-)*}(\vec{r}) \psi_p^*(\vec{r}') V(\vec{r} - \vec{r}') \psi_h(\vec{r}') \psi_{k_i}^{(+)}(\vec{r}), \quad (\text{A.20})$$

where $\alpha \equiv p$ and $\beta \equiv h$.

We can interpret $\langle k_f | \langle ph | V | HF \rangle | k_i \rangle$ as :

1. $|HF\rangle|k_i\rangle$ The incident nucleon k_i interacts with the target nucleus $|HF\rangle$ (in its ground state)
2. The interaction is represented by the two body potential $V(\vec{r} - \vec{r}')$, with prime coordinates (nucleons within the nucleus) and nonprime ones for the incident and outgoing projectile motion. We assume the projectile-target interaction only excites one particle-hole state of the target nucleus $\langle ph|$. This is only valid for high-energy excitation (or high projectile energy
3. The final state is then, the scattered projectile $\langle k_f|$ and the particle-hole state $\langle ph|$. We here don't make distinctions between bound and unbound particles of the p-h pair).
4. At the end we will sum over ph states each being weighted by a defined distribution.

Representing the target nucleus excitation by a linear combination of p-h states, i.e, $\sum_{\alpha\beta} a_{\alpha\beta} |\alpha\beta\rangle$ we can make use of what we did above to end up with the following transition matrix.

$$\begin{aligned} \sum_{\alpha\beta} \langle k_f | \langle \alpha\beta | V | HF \rangle | k_i \rangle &= \sum_{\alpha\beta} a_{\alpha\beta} \bar{v}_{f\alpha\beta i} \\ &= \sum_{\alpha\beta} a_{\alpha\beta} \int d^3r d^3r' \psi_{k_f}^{(-)*}(\vec{r}) \psi_p^*(\vec{r}') V(\vec{r} - \vec{r}') \psi_h(\vec{r}') \psi_{k_i}^{(+)}(\vec{r}) \end{aligned} \quad (\text{A.21})$$

We obtain the transition matrix for the cross section by

$$\left| \sum_{\alpha\beta} \langle k_f | \langle \alpha\beta | V | HF \rangle | k_i \rangle \right|^2 = \sum_{\alpha'\beta'} a_{\alpha'\beta'}^\dagger \bar{v}_{f\alpha'\beta' i}^\dagger \sum_{\alpha\beta} a_{\alpha\beta} \bar{v}_{f\alpha\beta i} \quad (\text{A.22})$$

Now if we consider an average over a small range of residual excitation energy only contributions with $\alpha'\beta' = \alpha\beta$ survive, which gives

$$\left| \sum_{\alpha\beta} \langle k_f | \langle ph | V | HF \rangle | k_i \rangle \right|^2 = \sum_{\alpha\beta} |a_{\alpha\beta}|^2 |\bar{v}_{f\alpha\beta i}|^2. \quad (\text{A.23})$$

The amplitudes $a_{\alpha\beta}$ can be replaced by a distribution

$$|a_{\alpha\beta}|^2 = \rho(E_{\alpha\beta}, E_x). \quad (\text{A.24})$$

where ρ represents the strength function of each p-h mode.

A.3 Single Particle Energy Model

We follow Chapter 3 of Jouni's book (SUHONEN, 2007). The single particle energies are the eigenvalues of the following matrix

$$H_{\nu'\nu} = \int_0^\infty r^2 dr g_{\nu'l}(r) g_{\nu l}(r) \left[\frac{\hbar^2}{2m_n} \left(\frac{4\nu + 2l + 3}{b^2} - \frac{r^2}{b^2} \right) + v_{WS}(r) + v_C(r) + \frac{1}{2} [j(j+1) - l(l+1) - \frac{3}{4}] \hbar^2 v_{LS}(r) \right] \quad (\text{A.25})$$

where ν stands for the principal QHO quantum number. The orbital and total angular momentum are represented by l and j , respectively. We assume the Wood-Saxon potential,

$$v_{WS}(r) = \frac{-V_0}{1 + \exp[(r - R_0)/a_0]}, \quad (\text{A.26})$$

where the target radius and nuclear diffusiveness are

$$R_0 = r_0 A^{1/3} \text{ fm, and } a_0 = 0.67 \text{ fm,} \quad (\text{A.27})$$

with $r_0 = 1.27$ fm. The potential strength is

$$V_0 = 51 \pm \frac{3(N - Z)}{A} \text{ MeV,} \quad (\text{A.28})$$

+ for proton and – for neutron states. The spin-orbit interaction is

$$v_{LS}(r) = v_{LS}^0 r_0^2 \frac{1}{r} \left[\frac{d}{dr} \frac{1}{1 + \exp[(r - R_0)/a]} \right], \quad (\text{A.29})$$

with

$$v_{LS}^0 = 0.44 V_0 \text{ MeV.} \quad (\text{A.30})$$

For charged particles, the Coulomb repulsion is

$$\frac{Ze^2}{2R_0} \left[3 - \left(\frac{r}{R_0} \right)^2 \right] \text{ for } r \leq R_0 \quad \text{and} \quad Ze^2/r \text{ for } r > R_0. \quad (\text{A.31})$$

The harmonic oscillator parameter

$$b = \frac{197.33}{\sqrt{940 \times \hbar\omega}} \text{ fm} \quad (\text{A.32})$$

is taken following the Blomqvist-Molinari formula (BLOMQVIST; MOLINARI, 1968)

$$\hbar\omega = (45A^{-1/3} - 25A^{-2/3}) \text{ MeV}. \quad (\text{A.33})$$

As a numerical test we compute the single particle proton energies for ^{16}O Table A.1 and ^{20}Ca Table A.2. These, were found to have good agreement with the values found in (SUHONEN, 2007). In addition Figure A.2, shows the number of proton p-h states in

nlj	$E_{nlj}(\text{MeV})$	$\nu = 0$	$\nu = 1$	$\nu = 2$	$\nu = 3$	$\nu = 4$	$\nu = 5$
0s _{1/2}	-26.445	1.000	-0.008	0.005	-0.016	-0.003	-0.002
0p _{3/2}	-14.653	0.999	-0.021	0.037	-0.028	0.001	-0.006
0p _{1/2}	-8.929	0.995	-0.044	0.077	-0.034	0.010	-0.010
0d _{5/2}	-3.099	0.988	-0.088	0.106	-0.063	0.023	-0.019
1s _{1/2}	-0.517	0.012	0.935	-0.258	0.206	-0.119	0.044
0d _{3/2}	4.819	0.874	-0.309	0.290	-0.192	0.124	-0.067

TABLE A.1 – Proton single particle energies for ^{16}O .

nlj	$E_{nlj}(\text{MeV})$
0s _{1/2}	-29.981
0p _{3/2}	-21.361
0p _{1/2}	-18.367
0d _{5/2}	-12.128
1s _{1/2}	-7.894
0d _{3/2}	-6.116
0f _{7/2}	-2.549
1p _{3/2}	1.101
1p _{1/2}	3.466
0f _{5/2}	6.110

TABLE A.2 – Proton single particle energies for ^{20}Ca .

form of a histogram for ^{56}Ni . The distribution is larger around 25-50 MeV providing a large basis for excitations at those energies.

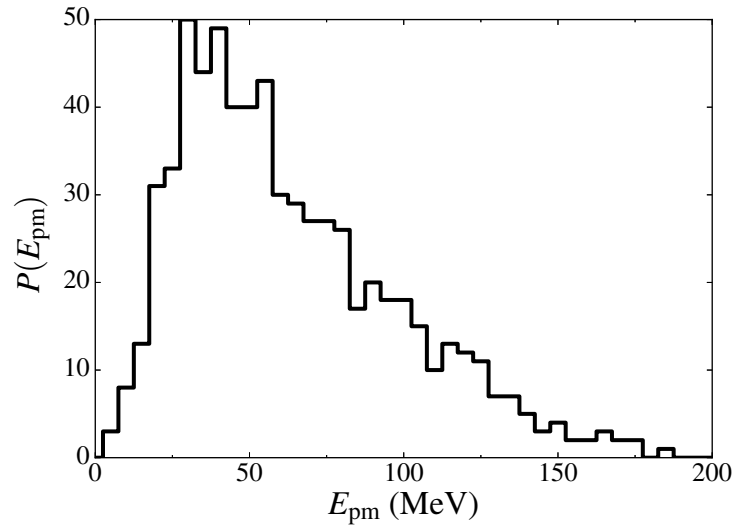


FIGURE A.2 – Number of p-h proton states for ^{56}Ni . Only bound or quasi-bound (below Coulomb plus Centrifugal barrier, see Appendix A.5) states are taken as possible particle orbitals.

A.4 Transition Density of States and Cross-Sections

The transition density of a state is given by (FESBACH, 1992; COLÒ *et al.*, 2013)

$$\delta_\nu(\vec{r}) = \langle \nu | \hat{\rho}(\vec{r}) | \tilde{0} \rangle = \delta\rho_\nu(r) Y_{JM}^*(\hat{r}), \quad (\text{A.34})$$

where ν is the excited energy index, J and M the total and its projection angular momentum, respectively. The spherical harmonic is given by

$$Y_{JM}^*(\hat{r}) = e^{-iM\phi} \sqrt{\frac{(2J+1)(J+M)!}{4\pi(J-M)!}} P_J^{-M}(\cos\theta), \quad (\text{A.35})$$

and the radial part of the transition density by

$$\delta\rho_\nu(r) = \frac{1}{\sqrt{2J+1}} \sum_{im} \left(X_{mi}^{(\nu)} + Y_{mi}^{(\nu)} \right) \langle m | |Y_J| | i \rangle \frac{u_m(r)u_i(r)}{r^2}, \quad (\text{A.36})$$

where u_m and u_i are single particle and hole states, respectively.

The transition matrix elements can be written as (FESBACH, 1992)

$$T_{k_f \leftarrow k_i}^\nu = \int d\vec{r} \psi_{k_f}^{(-)}(\vec{r}) \delta_\nu(\vec{r}) \psi_{k_i}^{(+)}(\vec{r}), \quad (\text{A.37})$$

where ν stands for the excited state at a given J^π in our RPA framework.

With eikonal distorted waves we have,

$$\psi_{k_f}^{(-)}(\vec{r}) \psi_{k_i}^{(+)}(\vec{r}) = e^{i\vec{q}\cdot\vec{r}} \exp \left[-i \frac{\mu}{\hbar^2 k_f} \int_z^\infty U_f(\vec{b}, z) dz - i \frac{\mu}{\hbar^2 k_i} \int_{-\infty}^z U_i(\vec{b}, z) dz \right], \quad (\text{A.38})$$

and

$$\begin{aligned} T_{k_f \leftarrow k_i}^\nu &= \sum_M \int b db d\phi dz e^{i\vec{q}\cdot\vec{b}} \exp \left[i q_z z - i \frac{\mu}{\hbar^2 k_f} \int_z^\infty U_f(\vec{b}, z) dz - i \frac{\mu}{\hbar^2 k_i} \int_{-\infty}^z U_i(\vec{b}, z) dz \right] \\ &\quad \times \delta\rho_\nu \left(\sqrt{z^2 + b^2} \right) e^{-iM\phi} \sqrt{\frac{(2J+1)(J+M)!}{4\pi(J-M)!}} P_J^{-M} \left(\frac{z}{\sqrt{b^2 + z^2}} \right), \end{aligned} \quad (\text{A.39})$$

performing the angular integration ²

$$\begin{aligned} T_{k_f \leftarrow k_i}^\nu &= \sum_M 2\pi i^{-M} \sqrt{\frac{(2J+1)(J+M)!}{4\pi(J-M)!}} \int b db j_{-M}((k_i + k_f) \sin(\theta/2) b) \\ &\quad \times \int dz \exp \left[i q_z z - i \frac{\mu}{\hbar^2 k_f} \int_z^\infty U_f(\vec{b}, z) dz - i \frac{\mu}{\hbar^2 k_i} \int_{-\infty}^z U_i(\vec{b}, z) dz \right] \\ &\quad \times \delta\rho_\nu \left(\sqrt{z^2 + b^2} \right) P_J^{-M} \left(\frac{z}{\sqrt{b^2 + z^2}} \right), \end{aligned} \quad (\text{A.41})$$

we can organize the eikonal phases to give

$$\begin{aligned} T_{k_f \leftarrow k_i}^\nu &= \sum_M 2\pi i^{-M} \sqrt{\frac{(2J+1)(J+M)!}{4\pi(J-M)!}} \int b db j_{-M}((k_i + k_f) \sin(\theta/2) b) e^{i(\delta_f(b) + \delta_i(b))} \\ &\quad \times \int dz \exp [i q_z z + \text{sign}(z)(-i\phi_f(z, b) + i\phi_i(z, b))] \\ &\quad \times \delta\rho_\nu \left(\sqrt{z^2 + b^2} \right) P_J^{-M} \left(\frac{z}{\sqrt{b^2 + z^2}} \right), \end{aligned} \quad (\text{A.42})$$

where

$$\text{sign}(z) = \begin{cases} -1 & \text{if } z < 0 \\ 0 & \text{if } z = 0 \\ 1 & \text{if } z > 0 \end{cases}$$

²Assuming

$$\vec{q} \cdot \vec{b} = -(k_i + k_f) \sin(\theta/2) b \cos \phi \quad \vec{q} \cdot z \hat{z} = (k_i - k_f) \cos(\theta/2) z, \quad (\text{A.40})$$

The phases are given by ³

$$\delta_m(b) = 2\eta \ln(k_m b) + \frac{1}{2} \left[\sigma_{pp}^T(i + \alpha_{pp}) \frac{Z}{A} + \sigma_{pn}^T(i + \alpha_{pn}) \frac{N}{A} \right]_m \int_0^\infty \rho_n(\sqrt{z'^2 + b^2}) dz', \quad (\text{A.43})$$

and

$$\phi_m(z, b) = \frac{1}{2} \left[\sigma_{pp}^T(i + \alpha_{pp}) \frac{Z}{A} + \sigma_{pn}^T(i + \alpha_{pn}) \frac{N}{A} \right]_m \int_0^z \rho_n(\sqrt{z'^2 + b^2}) dz', \quad (\text{A.44})$$

The differential cross section is then be obtained by

$$\frac{d\sigma^2}{dE_f d\Omega_f} \sim \left| T_{k_f \leftarrow k_i}^\nu \right|^2 \delta(E_i - E_f + E_\nu). \quad (\text{A.45})$$

A.5 Particle States Bellow Barrier

When computing orbital particle states, one may find small positive energy values (they are positive but small in magnitude). Theses energies quasibound, i.e. they don't belong to continuum, they are sometimes called quasi-stationary or long-lived single-particle states. They are not in the continuum but localized within a barrier created by centrifugal force $l(l+1)r^2$ plus the Coulomb $1.44Z/r$ (in the case of proton states).

We can have an idea of whether a state is within this barrier or not by computing both centrifugal (v_{cf}) and Coulomb (v_c) heights:

$$v_{cf}(R) = \frac{\hbar^2}{2m_N} \frac{l(l+1)}{R^2} \approx 13.2A^{-2/3}l(l+1) \text{ MeV} \quad (\text{A.46})$$

$$v_C(R) = 1.44 \frac{Z}{R} \approx 1.15ZA^{-1/3} \text{ MeV}. \quad (\text{A.47})$$

The particle energy has then to be below the sum of both heights.

For example, consider the proton state $E_{0d_{3/2}} = 4.1 \text{ MeV}$ for ^{16}O . For this case one finds

$$v_{cf} = 12.47 \text{ MeV} \quad v_C = 3.65 \text{ MeV}.$$

The total height of the barrier is = 16.12 MeV, which is about four times the proton state energy. Therefore this proton state can be considered bounded in our calculations.

³We only take into consideration the coulomb part in the first phase. This is an approximation! If we study neutron induced reaction we have to make the potential charge independent, just replace Z/A by N/A and do the same for the neutron fraction.

Bibliography

ABRAMOWITZ, M.; STEGUN, I. A. **Handbook of Mathematical Functions with Formulas, Graphs, and Mathematical Tables**. Tenth printing, december 1972, with corrections. New York: Dover, 1964. 40

ADAMS, G.; BACHER, A.; EMERY, G.; JONES, W.; MILLER, D.; LOVE, W.; PETROVICH, F. Inelastic excitation of normal parity levels in 208pb by 135 mev protons. **Physics Letters B**, v. 91, n. 1, p. 23 – 26, 1980. ISSN 0370-2693. 91

AGASSI, D.; WEIDENMULLER, H.; MANTZOURANIS, G. The statistical theory of nuclear reactions for strongly overlapping resonances as a theory of transport phenomena. **Physics Reports**, v. 22, n. 3, p. 145–179, 1975. ISSN 03701573. 48

BERTRAND, F.; PEELLE, R. Complete hydrogen and helium particle spectra from 30- to 60-mev proton bombardment of nuclei with $A=12$ to 209 and comparison with the intranuclear cascade model. **Physical Review C**, v. 8, n. 3, p. 1045–1064, 1973. ISSN 05562813. ix, 19

BISPLINGHOFF, J. Configuration mixing in preequilibrium reactions: A new look at the hybrid-exciton controversy. **Physical Review C**, v. 33, n. 5, p. 1569–1580, 1986. ISSN 05562813. 46

BLANN, M. Hybrid model for pre-equilibrium decay in nuclear reactions. **Physical Review Letters**, v. 27, n. 6, p. 337–340, 1971. ISSN 00319007. 45

BLANN, M. Importance of the nuclear density distribution on pre-equilibrium decay. **Physical Review Letters**, v. 28, n. 12, p. 757–759, 1972. ISSN 00319007. 45

BLANN, M. A priori pre-equilibrium decay models. **Nuclear Physics A**, v. 213, n. 3, p. 570–588, 1973. ISSN 03759474. 45

BLANN, M. New precompound decay model. **Physical Review C**, v. 54, n. 3, p. 1341–1349, 1996. ISSN 05562813. 47

BLANN, M.; CHADWICK, M. New precompound decay model: Angular distributions. **Physical Review C**, v. 57, n. 1, p. 233–243, 1998. ISSN 05562813. 47, 71

BLANN, M.; VONACH, H. Global test of modified precompound decay models. **Physical Review C**, v. 28, n. 4, p. 1475–1492, 1983. ISSN 05562813. 46

BLOMQUIST, J.; MOLINARI, A. Collective 0^- vibrations in even spherical nuclei with tensor forces. **Nuclear Physics A**, v. 106, n. 3, p. 545 – 569, 1968. ISSN 0375-9474. 107

- BOHR, A. N.; MOTTELSON, B. R. **Nuclear Structure**. [S.l.]: World Scientific Pub Co Inc, 1998. v. 1. 60
- BONETTI, R.; CHADWICK, M. B.; HODGSON, P. E.; CARLSON, B. V.; HUSSEIN, M. S. The feshbach-kerman-koonin multistep compound reaction theory. **Physics Reports**, v. 202, n. 4, p. 171–231, 1991. ISSN 03701573. 49
- BONETTI, R.; KONING, A. J.; AKKERMANS, J.; HODGSON, P. The feshbach-kerman-koonin multistep direct reaction theory. **Physics Reports**, v. 247, n. 1, p. 1–58, 1994. ISSN 03701573. 49, 52, 71
- BORCHERS, R. R.; WOOD, R. M.; HOLBROW, C. H. Continuous neutron spectra from (p, n) reactions. **Nuclear Physics**, v. 88, n. 3, p. 689–696, 1966. ISSN 00295582. 44
- BORTFELD, T.; PAGANETTI, H.; KOOY, H. Mo-a-t-6b-01: Proton beam radiotherapy - the state of the art. **Medical Physics**, American Association of Physicists in Medicine, v. 32, n. 6Part13, p. 2048–2049, 2005. ISSN 2473-4209. 20
- BUUCK, M.; MILLER, G. A. Corrections to the eikonal approximation for nuclear scattering at medium energies. **Physical Review C**, v. 90, n. 2, p. 024606–1–024606–9, aug 2014. 37, 71
- CHABANAT, E.; BONCHE, P.; HAENSEL, P.; MEYER, J.; SCHAEFFER, R. A Skyrme parametrization from subnuclear to neutron star densities Part II. Nuclei far from stabilities. **Nuclear Physics A**, v. 635, n. 1-2, p. 231–256, may 1998. ISSN 03759474. 65
- CHABANAT, E.; BONCHE, P.; HAENSEL, P.; MEYER, J.; SCHAEFFER, R. Erratum to "A Skyrme parametrization from subnuclear to neutron star densities. (II)" Nuclei far from stabilities". **Nuclear Physics A**, v. 643, n. 4, p. 441, dec 1998. ISSN 03759474. 65
- CHIMANSKI, E. V.; CARLSON, B. V.; CAPOTE, R.; KONING, A. J. Quasiparticle nature of excited states in random-phase approximation. **Phys. Rev. C**, American Physical Society, v. 99, p. 014305, Jan 2019. Disponível em: <<https://link.aps.org/doi/10.1103/PhysRevC.99.014305>>. 65
- CLINE, C. K. The pauli exclusion principle in pre-equilibrium decay. **Nuclear Physics A**, v. 195, n. 2, p. 353–360, 1972. ISSN 03759474. 45
- CLINE, C. K.; BLANN, M. The pre-equilibrium statistical model: Description of the nuclear equilibration process and parameterization of the model. **Nuclear Physics A**, v. 172, n. 2, p. 225–259, 1971. ISSN 03759474. 45
- COHEN, B. L. **Concepts of Nuclear Physics**. [S.l.]: McGraw-Hill, 1971. 62, 63
- COLÒ, G.; CAO, L.; GIAI, N. V.; CAPELLI, L. Self-consistent RPA calculations with Skyrme-type interactions: the skyrme-rpa program. **Computer Physics Communications**, v. 184, n. 1, p. 142–161, jan 2013. 65, 89, 108
- COMPARAT, V.; FRASCARIA, R.; MARTY, N.; MORLET, M.; WILLIS, A. Proton-nucleus elastic scattering at 156 mev. **Nuclear Physics A**, v. 221, n. 2, p. 403 – 413, 1974. ISSN 0375-9474. 75

- DUPUIS, M. **Modèles de réactions directes et de pré-équilibre quantique pour la diffusion de nucléons sur des noyaux sphériques (Ph.D. Thesis)**. Tese (Doutorado) — Université de Bordeaux, 2006. 52
- DUPUIS, M. Microscopic description of elastic and direct inelastic nucleon scattering off spherical nuclei. **The European Physical Journal A**, v. 53, n. 5, p. 111, 2017. ISSN 1434-601X. 52
- DUPUIS, M.; KAWANO, T.; DELAROCHE, J. P.; BAUGE, E. Microscopic model approach to (n,xn) pre-equilibrium reactions for medium-energy neutrons. **Physical Review C**, v. 83, n. 1, 2011. ISSN 05562813. 52
- FESBACH, H. **Theoretical nuclear physics: Nuclear reactions**. [S.l.]: John Wiley and Sons, Inc., 1992. 108
- FESHACH, H.; KERMAN, A.; KOONIN, S. The statistical theory of multi-step compound and direct reactions. **Annals of Physics**, v. 125, n. 2, p. 429–476, 1980. ISSN 00034916. 48
- FULMER, C. B.; BALL, J. B.; SCOTT, A.; WHITEN, M. L. Elastic scattering of 61.4-mev protons. **Phys. Rev.**, American Physical Society, v. 181, p. 1565–1579, May 1969. 75
- GEIGER, H.; MARSDEN, E. On a diffuse reflection of the α -particles. **Proceedings of the Royal Society of London A: Mathematical, Physical and Engineering Sciences**, The Royal Society, v. 82, n. 557, p. 495–500, 1909. ISSN 0950-1207. 18
- GHOSHAL, S. N. An experimental verification of the theory of compound nucleus. **Phys. Rev.**, American Physical Society, v. 80, p. 939–942, Dec 1950. x, 42, 43
- GLAUBER, R. J. High-energy Collision Theory. In: **Lectures in Theoretical Physics**. New York: Interscience, 1959. p. 315–423. 29, 71, 101
- GRIFFIN, J. J. Statistical model of intermediate structure. **Physical Review Letters**, v. 17, n. 9, p. 478–481, 1966. ISSN 00319007. 43, 44
- HAGBERG, A. I. E.; SUNDQVIST, B. Scattering of 185 mev protons from 90 zr. **Physica Scripta**, v. 3, n. 6, p. 245, 1971. 75, 91
- HAYAKAWA, S. I.; FUJIWARA, M.; IMANISHI, S.; FUJITA, Y.; KATAYAMA, I.; MORINOBU, S.; YAMAZAKI, T.; ITAHASHI, T.; IKEGAMI, H. m_1 strength in ^{208}Pb from (p, p') and ($d, ^3\text{He}$) reactions. **Phys. Rev. Lett.**, American Physical Society, v. 49, p. 1624–1627, Nov 1982. Disponível em:
<<https://link.aps.org/doi/10.1103/PhysRevLett.49.1624>>. 91
- HEBBORN, C.; CAPEL, P. Analysis of corrections to the eikonal approximation. **Phys. Rev. C**, American Physical Society, v. 96, p. 054607, Nov 2017. Disponível em:
<<https://link.aps.org/doi/10.1103/PhysRevC.96.054607>>. 37
- HINTZ, N. M.; COOK, D.; GAZZALY, M.; FRANEY, M. A.; BARLETT, M. L.; HOFFMANN, G. W.; FERGERSON, R.; MCGILL, J.; PAULETTA, G.; BOUDRIE, R. L.; MCCLELLAND, J. B.; JONES, K. W. Energy dependence of neutron-proton matrix element ratios derived from 25–800 mev energy proton scattering. **Phys. Rev. C**, American Physical Society, v. 37, p. 692–709, Feb 1988. 75

- HOLBROW, C. H.; BARSCHALL, H. H. Neutron evaporation spectra. **Nuclear Physics**, v. 42, p. 264–279, 1963. ISSN 00295582. 44
- INGEMARSSON, A.; FAGERSTRÖM, B. Inelastic scattering of 185 mev protons from 208 pb. **Physica Scripta**, v. 13, n. 4, p. 208, 1976. 91
- KAMAL, A. **Nuclear Physics**. Berlin, Heidelberg: Springer Berlin Heidelberg, 2014. (Graduate Texts in Physics). ISBN 978-3-642-38654-1 978-3-642-38655-8. 19
- KIKUCHI, K.; KAWAI, M. Nuclear matter and nuclear reactions. **North-Holland**, North-Holland Pub. Co., 1968. 70
- KONING, A.; AKKERMANS, J. Randomness in multi-step direct reactions. **Annals of Physics**, v. 208, n. 1, p. 216 – 250, 1991. ISSN 0003-4916. 49, 54
- KONING, A.; AKKERMANS, J. Pre-equilibrium nuclear reactions: An introduction to classical and quantum-mechanical models. In: **Proceedings of the workshop on nuclear reaction data and nuclear reactors: Physics, design and safety**. [S.l.: s.n.], 1999. x, 44
- KONING, A.; CHADWICK, M. Microscopic two-component multistep direct theory for continuum nuclear reactions. **Physical Review C**, v. 56, n. 2, p. 970–994, 1997. ISSN 05562813. 52, 71
- KURT, G.; TUNG-MOW, Y. **Quantum Mechanics: Fundamentals**. second. New York: Springer -Verlag, 2003. 622 p. ISBN 0-387-95576-3. ix, 25, 40
- LEE, L.; DRAKE, T.; WONG, S.; FREKERS, D.; AZUMA, R.; BUCHMANN, L.; GALINDO-URIBARRI, A.; KING, J.; SCHUBANK, R.; ABEGG, R.; HELMER, R.; JACKSON, K.; MILLER, C.; YEN, S.; GERAMB, H. V. Intermediate energy proton scattering from 40ca, 90zr and 208pb. **Physics Letters B**, v. 205, n. 2, p. 219 – 222, 1988. ISSN 0370-2693. 75
- LENZI, S. M.; VITTURI, A.; ZARDI, F. Description of inelastic scattering between heavy ions in the glauber model. **Phys. Rev. C**, American Physical Society, v. 38, p. 2086–2093, Nov 1988. xiii, 74
- MARTIN, P.; GAILLARD, Y.; SAINTIGNON, P. de; PERRIN, G.; CHAUVIN, J.; DUHAMEL, G.; LOISEAUX, J. Excitation of low-lying levels and giant resonances in 90zr via 57.5 mev polarized proton inelastic scattering. **Nuclear Physics A**, v. 315, n. 3, p. 291 – 309, 1979. ISSN 0375-9474. 91
- MCDANIELS, D.; LISANTTI, J.; BERGQVIST, I.; SWENSON, L.; CHEN, X.; HOREN, D.; BERTRAND, F.; GROSS, E.; GLOVER, C.; SAYER, R.; BURKS, B.; HÄUSSER, O.; HICKS, K. Validity of collective model dwba analysis for intermediate energy proton scattering to low-lying states of 208pb. **Nuclear Physics A**, v. 467, n. 4, p. 557 – 574, 1987. ISSN 0375-9474. Disponível em:
<<http://www.sciencedirect.com/science/article/pii/0375947487903861>>. 91
- MERMOD, P.; BLOMGREN, J.; JOHANSSON, C.; ÖHRN, A.; ÖSTERLUND, M.; POMP, S.; BERGENWALL, B.; KLUG, J.; NILSSON, L.; OLSSON, N.; TIPPAWAN, U.; NADEL-TURONSKI, P.; JONSSON, O.; PROKOFIEV, A.; RENBERG, P.-U.;

- MAEDA, Y.; SAKAI, H.; TAMII, A.; AMOS, K.; CRESPO, R.; MORO, A. 95 meV neutron scattering on hydrogen, deuterium, carbon, and oxygen. **Phys. Rev. C**, American Physical Society, v. 74, p. 054002, Nov 2006. ix, 34, 36
- MITCHELL, G. E.; RICHTER, A.; WEIDENMÜLLER, H. A. Random matrices and chaos in nuclear physics: Nuclear reactions. **Reviews of Modern Physics**, v. 82, n. 4, p. 2845–2901, oct 2010. ISSN 0034-6861. 19
- NADASEN, A.; SCHWANDT, P.; SINGH, P. P.; JACOBS, W. W.; BACHER, A. D.; DEBEVEC, P. T.; KAITCHUCK, M. D.; MEEK, J. T. Elastic scattering of 80-180 meV protons and the proton-nucleus optical potential. **Phys. Rev. C**, American Physical Society, v. 23, p. 1023–1043, Mar 1981. Disponível em: <<https://link.aps.org/doi/10.1103/PhysRevC.23.1023>>. 75
- NISHIOKA, H.; VERBAARSCHOT, J. J. M.; WEIDENMÜLLER, H. A.; YOSHIDA, S. Statistical theory of precompound reactions: The multistep compound process. **Annals of Physics**, v. 172, n. 1, p. 67–99, 1986. ISSN 00034916. 48
- NISHIOKA, H.; WEIDENMÜLLER, H. A.; YOSHIDA, S. Statistical theory of precompound reactions: The multistep direct process. **Annals of Physics**, v. 183, n. 1, p. 166–187, 1988. ISSN 00034916. 48, 49, 53
- OBLOŽINSKÝ, P. Particle-hole state densities for statistical multi-step compound reactions. **Nuclear Physics A**, v. 453, n. 1, p. 127–140, 1986. ISSN 03759474. 49
- POMPEIA, C. A. S.; CARLSON, B. V.; GUIMARÃES, F. B. Configuration mixing in nucleon-induced pre-equilibrium reactions. **Proceedings of the Conference on Nuclear Data ND2007**, EDP Sciences, p. 07744, 2007. 47
- POMPEIA, C. S.; CARLSON, B. Configuration mixing in pre-equilibrium reactions. **Physical Review C**, v. 74, n. 5, 2006. ISSN 05562813. 48
- QAIM, S. Use of cyclotrons in medicine. **Radiation Physics and Chemistry**, v. 71, n. 3, p. 917 – 926, 2004. ISSN 0969-806X. 9th International Symposium on Radiation Physics (ISRP-9). 20
- QAIM, S. M. Nuclear data for production and medical application of radionuclides: Present status and future needs. **Nuclear Medicine and Biology**, v. 44, p. 31 – 49, 2017. ISSN 0969-8051. 20
- RAMSTRÖM, E.; LENSKE, H.; WOLTER, H. H. A multistep direct reaction approach for neutron-induced reactions at intermediate energy. **Nuclear Physics A**, v. 744, p. 108–124, 2004. ISSN 03759474. 52, 53, 71
- RAY, L. Proton-nucleus total cross sections in the intermediate energy range. **Phys. Rev. C**, American Physical Society, v. 20, p. 1857–1872, Nov 1979. xiii, 73
- RICHTER, W. A.; COWLEY, A. A.; HILLHOUSE, G. C.; STANDER, J. A.; KOEN, J. W.; STEYN, S. W.; LINDSAY, R.; JULIES, R. E.; LAWRIE, J. J.; PILCHER, J. V.; HODGSON, P. E. Preequilibrium (p,p') measurements and calculations for ⁹⁰Zr and neighboring nuclei for incident energies up to 200 meV. **Phys. Rev. C**, American Physical Society, v. 49, p. 1001–1011, Feb 1994. xii, 92

- ROWE, D. J. **Nuclear Collective Motion: Models and Theory**. [S.l.]: World Scientific, 2010. 63
- RUTHERFORD, E. The scattering of α and β particles by matter and the structure of the atom. **Philosophical Magazine Series 6**, v. 21, n. 125, p. 669–688, 1911. 18
- SATCHLER, G. R. **Direct Nuclear Physics**. [S.l.]: Oxford University Press, 1983. 50
- SATO, K.; YOSHIDA, S. Studies of nuclear second moments for pre-equilibrium nuclear reaction theories. **Zeitschrift für Physik A Atomic Nuclei**, v. 327, n. 4, p. 421–430, 1987. ISSN 09301151. 47
- SCOTT, A.; MATHUR, N.; PETROVICH, F. Low-lying normal parity excitations in the $^{208}\text{Pb}(p, p')^{208}\text{Pb}$ reaction at $E_p = 61.2$ mev. **Nuclear Physics A**, v. 285, n. 2, p. 222 – 234, 1977. ISSN 0375-9474. 91
- STANKIEWICZ, K.; MARCINKOWSKI, A.; HERMAN, M. Particle-hole state densities for calculation of the multi-step compound emission. **Nuclear Physics A**, v. 435, n. 1, p. 67–76, 1985. ISSN 03759474. 49
- SUHONEN, J. **From Nucleons to Nuclei: Concepts of Microscopic Nuclear Theory**. [S.l.]: Springer Verlag, Berlin, 2007. 104, 106, 107
- TAMURA, T.; UDAGAWA, T.; LENSKE, H. Multistep direct reaction analysis of continuum spectra in reactions induced by light ions. **Physical Review C**, v. 26, n. 2, p. 379–404, 1982. ISSN 05562813. 48, 52, 53, 71
- WAGNER, W. T.; CRAWLEY, G. M.; HAMMERSTEIN, G. R.; MCMANUS, H. High-resolution study of ^{208}Pb with 35-mev protons. **Phys. Rev. C**, American Physical Society, v. 12, p. 757–777, Sep 1975. 91
- WALLACE, S. J. Eikonal expansion. **Physical Review Letters**, v. 27, n. 9, p. 622–626, aug 1971. 71
- WEIDENMÜLLER, H. A.; MITCHELL, G. E. Random matrices and chaos in nuclear physics: Nuclear structure. **Reviews of Modern Physics**, American Physical Society, v. 81, n. 2, p. 539–589, may 2009. ISSN 0034-6861. 19
- WILLIAMS, F. C. Intermediate state transition rates in the griffin model. **Physics Letters B**, v. 31, n. 4, p. 184–186, 1970. ISSN 03702693. 45
- WOOD, R. M.; BORCHERS, R. R.; BARSCHALL, H. H. Neutrons from protons on isotopes of tin. **Nuclear Physics**, v. 71, n. 3, p. 529–545, 1965. ISSN 00295582. 44
- ZELEVINSKY, V.; VOLYA, A. **Physics of Atomic Nuclei**. [S.l.]: John Wiley & Sons, 2017. 63

FOLHA DE REGISTRO DO DOCUMENTO

1. CLASSIFICAÇÃO/TIPO TD	2. DATA 12 de fevereiro de 2019	3. DOCUMENTO Nº DCTA/ITA/TD-002/2019	4. Nº DE PÁGINAS 116
5. TÍTULO E SUBTÍTULO: Extension of the Quantum Formalism for Multistep Direct Nuclear Reactions			
6. AUTOR(ES): Emanuel Vicente Chimanski			
7. INSTITUIÇÃO(ÕES)/ÓRGÃO(S) INTERNO(S)/DIVISÃO(ÕES): Instituto Tecnológico de Aeronáutica – ITA			
8. PALAVRAS-CHAVE SUGERIDAS PELO AUTOR: Pré-equilíbrio; Multi-step; Reações nucleares			
9. PALAVRAS-CHAVE RESULTANTES DE INDEXAÇÃO: Reações nucleares; Equilíbrio; Modelos nucleares; Física nuclear; Física			
10. APRESENTAÇÃO: <input checked="" type="checkbox"/> Nacional <input type="checkbox"/> Internacional ITA, São José dos Campos. Curso de Doutorado. Programa de Pós-Graduação em Física. Área de Física Nuclear. Orientador: Prof. Dr. Brett Vern Carlson. Coorientador: Dr. Roberto Capote Noy. Defesa em 07/02/2019. Publicada em 2019.			
11. RESUMO: Reações nucleares de pré-equilíbrio ocorrem em uma escala de tempo intermediária entre as rápidas reações diretas e as lentas reações de evaporação do núcleo composto. Com o aumento da energia do projétil, as reações de pré-equilíbrio se apresentam como uma componente cada vez mais destacada nos espectros e distribuições angulares de reações nucleares sendo de importância especial em aplicações utilizando feixes energéticos de nucleons tais como, por exemplo, em terapia com feixe de prótons ou “accelerator-driven systems”. Embora seu estudo iniciou-se há mais de 50 anos atrás, devido a sua complexidade, ainda não existe uma descrição bem fundamentada delas. Os modelos quânticos propostos se limitam a processos de emissão de apenas uma partícula. Estes também utilizam hipóteses estatísticas e aproximações dificilmente justificáveis. Analisamos as primeiras duas etapas de uma reação de pré-equilíbrio e propomos uma extensão para o formalismo quântico para incluir até duas partículas no contínuo após a primeira colisão e até três após a segunda colisão, os números máximos de partículas permitido fisicamente. Estudamos em detalhe a coerência/incoerência entre excitações de estados de partícula-buraco de natureza diferente. Para isto, utilizamos os estados excitados na aproximação conhecida como “Random Phase Approximation”. A contribuição de cada componente de partícula-buraco foi determinada como sendo bem representada por uma distribuição do tipo Breit-Wigner. Também determinamos um comportamento universal para a largura desta distribuição. Além disso, verificamos a validade da suposição de aleatoriedade para estados de energia alta.			
12. GRAU DE SIGILO: <input checked="" type="checkbox"/> OSTENSIVO <input type="checkbox"/> RESERVADO <input type="checkbox"/> SECRETO			